FINAL REPORT

of the

HOT CORROSION MECHANISM STUDIES

Conducted for the

U.S. Naval Marine Engineering Laboratory
Annapolis, Maryland

Contract No. N-(600) (61533)-63219

by the

Research and Development Center
General Electric Company
Schenectady, New York

February 15, 1966

NEL-Sponsored
Report 1382.66
ASTIA AT 37 122
The Investigation Reported Herein
Was Conducted Under
Contract Number N600(61533)63219
for the
U. S. NAVY
MARINE ENGINEERING LABORATORY
Annapolis, Maryland
21402

FINAL REPORT

of the

HOT CORROSION MECHANISM STUDIES

Conducted for the

U.S. Naval Marine Engineering Laboratory
Annapolis, Maryland

Contract No. N-(600) (61533)-63219

by the

Research and Development Center
General Electric Company

Schenectady, New York

February 15, 1966

FOREWORD

This Final Report documents the results of the Hot Corrosion Mechanism Studies performed by the Research and Development Center of the General Electric Company under Contract No. N-(600)(61533)-63219 for the U.S. Naval Marine Engineering Laboratory, Annapolis, Maryland. The program was managed by R. W. Hardt, and leading technical contributors were A. U. Seybolt, J.R. Gambino, A. Beltran (Schenectady Materials and Processes Laboratory), and P.A. Bergman and M. Kaufman (Thomson Engineering Laboratory, West Lynn, Mass.). The program benefited from continual consultations with C.T. Sims (Schenectady Materials and Processes Laboratory), who is manager of a complementary program on Alloy Development, and with G.J. Danek, K. Zwilsky, and W. Wheatfield, all of the Marine Engineering Laboratory.

ABSTRACT

The occurrence and nature of "hot corrosion" was investigated. The elements nickel and cobalt, their binary alloys with chromium, and simple ternary alloys composed of third elements added to chromium-nickel and chromium-cobalt, were studied. Reaction kinetics of sulfate-induced oxidation were studied by thermal balance techniques. Hot corrosion severity at 1675°, 1750°, and 1900° F was determined for the prepared samples in burner rig tests that simulate actual engine environments. The nature of the corrosive attack was studied morphologically, largely by metallographic examinations.

Hot corrosion enhanced oxidation has been shown to follow sulfidation attack after sulfate reduction by the basis metal. The effects of sulfate concentrations, oxygen pressures, surface oxide film thicknesses, and temperatures were determined for elemental nickel, cobalt, and some of their alloys with chromium.

TABLE OF CONTENTS

APPENDICES

HOT CORROSION MECHANISM STUDIES

I. INTRODUCTION

A. Problem Occurrence

In the immediate post-war era, the late 1940's and early 1950's, the problem of "hot corrosion" of boiler combustion tubes was extensively studied. The occurrence of the especially deleterious form of corrosive attack was shown to correlate with the presence of condensed combustion reaction products, primarily molten vanadium oxide salts when residual fuel oils were used. Measures that have been applied in efforts to reduce the corrosive effects are:

1. fuel treatment, including additions to inhibiting (passivating) materials and removal of potentially corrosive elements by washing and/or fuel distillation,
2. decreased operating temperatures,
3. increased maintenance on scheduled shorter operating periods, and
4. improved alloys.

Means to alleviate the problem were found, and hot corrosion studies were, in large part, discontinued.

More recently, in the period 1960-65, attention has again been drawn to the "hot corrosion" problem, this time primarily associated with aircraft and naval gas turbine applications.

There is a paucity of data confirming the occurrence of catastrophic hot corrosion in actual operating components. Reasons for this are that most gas turbine power plants operate in environments not conducive to hot corrosion attack--that is, the combustion products for whatever reasons do not contain significant concentrations of condensable, inorganic, corrosive materials. Such environments include the high altitudes associated with distillate fuel-burning aircraft jet engines. Land-based gas turbines usually use natural gas or refined petroleum distillate as fuel and are usually not susceptible to hot corrosion attack.

The incidence of "hot corrosion" in gas turbines has been especially insidious. It appears with little visual warning and at sometimes catastrophic rate. In the past few years it has occurred with increased frequency, and is now considered a major problem. This coincided with an increase in the number of marine applications, higher temperatures, and with the utilization of higher strength nickel-base alloys which generally have relatively low chromium contents. This correlation of the appearance of "hot corrosion" to marine environments has deterred applications of gas turbine power in naval vessels.

Much effort has contributed to the present and yet incomplete understanding of "hot corrosion." Danek[1] in a report, "State-of-the-Art Survey on Hot Corrosion in Marine Gas-Turbine Engines," has prepared a concise review

of this work. One of the earlier more definitive studies of hot corrosion, reported in 1955 by Simons et al.[2] related hot corrosion to the reduction of sodium sulfate and subsequent sulfidation attack of the basis metal. In later studies, Bergman[3] related the corrosive attack to marine environments. In a succeeding study in which fuel sulfur concentrations and air-sea salt concentrations were varied, the dependence of hot corrosion on the coincident presence of both sea salt and sulfur was demonstrated, and the deposition of sodium sulfate was confirmed.

B. Investigation Plan

As one of two complementary Navy-supported programs, this Hot Corrosion Mechanism Study was conducted to determine and document in more detail the reactions that account for "Hot Corrosion." (The other program was intended to study the effectiveness of alloying and compositional variations on hot corrosion behavior.) It was therefore appropriate to direct the major part of this program in a systematic manner to result in improved understanding, rather than in an empirical way which might possibly provide an expeditious solution. Three types of investigations were planned and are reported in the following sections.

1. Reaction Kinetic Studies, largely by use of thermal gravimetric analysis techniques (T. G. A.). Although the T. G. A. Method does not simulate actual operating environmental conditions, the method provides relatively precise quantitative data expeditiously and economically.

2. Burner Rig Tests, in which simple metals and alloys can be compared under conditions designed to cause an accelerated corrosion at varying temperatures, in an environment that is intended to simulate actual engine environments in its effect on hot corrosion behavior.

3. Morphological Studies, generally consisting of metallographic analyses augmented by simple chemical and x-ray diffraction analyses. In addition to samples prepared in conducting the T. G. A. and Burner Rig Tests, many specimens prepared in special tests under varying condition serve to elucidate the nature of the hot salt oxidation attack.

In this program, a major difference from most previous studies was the emphasis upon simplicity. Especially in the earlier experiments, and generally during the course of the program, elemental cobalt or nickel specimens or simple, binary and ternary, alloy specimens of cobalt and nickel were specified.

II. PROGRAM REVIEW

A. Format

Experimental results and data obtained during this program are formally reported as Appendices to this report, each of which has been prepared by the principal contributors to the specified investigations. This section is therefore limited to a review of the detailed data adequate to allow comparative and integrated rationalization and interpretation.

B. Discussion of Results

1. Nickel

There has existed some doubt that sodium sulfate in itself constituted a corrosive medium toward nickel. Sykes and Shirley[4] found the salt innocuous toward heat-resistant steels, and early in this program the lack of intense attack in the absence of oxygen was noted in the thermogravimetric analyses conducted by Gambino (Appendix A). Seybolt in an independent but related study (Appendix B) unequivocally demonstrated the corrosive nature of sodium sulfate toward nickel, however. The corrosion consists of a sulfidation attack, largely concentrated at grain boundaries.

At temperatures high enough and in environments adequately concentrated with respect to available sulfur, molten nickel-nickel sulfide eutectic compositions develop. In the presence of oxygen, the nickel-nickel sulfide eutectic is preferentially oxidized.

As shown in Appendix A, Gambino used thermogravimetric (T.G.A.) methods to monitor the high-temperature oxidation of nickel in the presence of sodium sulfate and other salts. In the absence of surface oxide films, nickel was shown to oxidize initially at rates which were: (1) independent of sodium sulfate concentrations, (2) dependent upon oxygen pressures, (3) dependent upon temperature according to the Arrhenius equation, and (4) dependent upon the moisture content of the oxygen environment.

The high initial rates of oxidation of nickel in the presence of limited amounts of sodium sulfate shown by the T.G.A. studies (Appendix A) and the severity of the sulfidation attack of nickel by large excesses of sodium sulfate with or without oxygen present (as illustrated in Appendix B) indicate that these reactions do not rely on autocatalytic mechanisms, such as postulated by Simons et al.[2] since no accelerating periods are observed. Incubation periods have been observed, however, when oxide films were formed on the nickel specimens prior to exposure. In all cases studied, however, vigorous corrosion ultimately occurred, and no lasting protective quality can be ascribed to the oxide film on elemental nickel.

In the T.G.A. records of sample weight gains vs time, it was found that initial rates decrease significantly, and appear ultimately to approach rates for normal nickel oxidation. Moreover, the total amount of initial weight gain (accelerated oxidation) of sodium sulfate-coated nickel specimens exposed to a dry oxygen atmosphere is directly dependent upon the amount of sodium sulfate present (Fig. 3, Appendix A). The limited enhanced oxidation behavior, in contrast to that of Seybolt (Appendix B), indicates that the T.G.A. monitored rates exhibit an equilibrium in the reaction between sodium sulfate and nickel. This was proved by addition of sodium oxide to sodium sulfate on a nickel specimen; the oxidation rate was greatly diminished.

The correlation between the amount of nickel oxidation and the amount of sodium sulfate, e.g., the amount of available sulfur, indicates also that the available sulfur is expended during oxidation. In a dynamic combustion system

where sulfur-bearing fuels are burned, the "available sulfur" may be almost unlimited, however; the basic product of the sulfate corrosion (Na_2O), which has been shown to limit the reaction, is neutralized by combustion products (SO_2, SO_3).

2. Cobalt

In the monitoring of the oxidation rate of cobalt in the presence of sodium sulfate by T. G. A. methods, it was found that no significant reaction occurred. In a separate investigation, reported here as Appendix C, Beltran and Seybolt studied the hot corrosion of cobalt in crucible tests. Except for differences in temperatures which apparently reflect the higher melting points of the cobalt sulfides, the attack appeared identical in form to that of nickel. The contrasting results of crucible and T. G. A. exposures reflect the differences in experimental conditions, notably the difference in concentration of sodium sulfate. It must be concluded that:

(a) the attack of cobalt by sodium sulfate is completely analogous to that of nickel, and

(b) the equilibrium conditions are such that insignificant amounts of available sulfur (sulfide) exist in the T. G. A. samples thinly coated with the sulfate.

3. Chromium Additions

Seybolt and Beltran report in Appendices B and C on the attack of nickel-chromium and cobalt-chromium by sodium sulfate. Two important effects of chromium are suggested:

(a) the development of a contiguous, protecting chromium-rich surface oxide film, and

(b) the removal of diffused sulfur by formation of relatively stable and inert chromium sulfide.

T. G. A. studies (Fig. 27, Appendix A), indicate the large degree of improvement in hot corrosion resistance of 20% or higher chromium additions, but the relative importance of the two cited effects is not obvious. These kinetic data exhibit hot corrosion oxidation rates even lower than normal oxidation rates, resumably reflecting a protective effect of the enveloping molten salt. Chromium is clearly beneficial in imparting to nickel and cobalt improved hot corrosion resistance, although in environments containing excess sulfate severe attack does occur.

Similarly, Bergman shows in Appendix D (Figs. 4, 5, and 6) the beneficial effects of chromium additions to nickel in resisting hot corrosion in Burner Rig Tests. The required chromium content to provide hot corrosion resistance is shown to vary from 10% at 1675°F, to 15% at 1750°F, and 25% at 1900°F.

4. Alloying Additives

Several simple nickel and cobalt ternary alloys containing significant concentrations of chromium were prepared and tested by both T. G. A. methods

(Appendix A) and Burner Rig Tests (Appendix D). Large differences of the several additive elements on hot corrosion resistance were observed. In the T.G.A. tests, the deleterious effects of molybdenum and aluminum in nickel-chromium alloys are exhibited by high rates of oxidation measured as weight gain. In the Burner Rig Tests, conducted at three different temperatures and in a simulated application environment designed to accelerate hot corrosion attack, definitive comparisons of the several additive elements are possible by metallographic techniques. Comparison of the results of exposures to the three temperatures, 1650°, 1750°, and 1900°F, is instructive (Figs. 4, 5, and 6 in Appendix D). Whereas aluminum (erratically) and molybdenum exhibit a deleterious effect in nickel-chromium, increasing from slight at 1675°F, and moderate at 1750°F, to severe at 1900°F, tungsten is only slightly detrimental at 1750°F, but extremely so at 1900°F. Of the alloying elements studied, titanium and cobalt appear to degrade nickel-chromium least. Molybdenum and tungsten affect cobalt-chromium alloys similarly to their effect on nickel-chromium.

A developmental nickel-base alloy, PDRL-163,* was tested at 1675° and 1900°F for comparative purposes. At 1675°F it appeared to suffer moderately severe attack--as might be expected of an alloy containing significant amounts of alloying additives known to be deleterious--but at 1900°F, there was very little attack, simple logic to the contrary. Bergman notes the absence of spinel in the resulting oxidation products.

C. Conclusions

1. Both nickel- and cobalt-base alloys are susceptible to hot corrosion by direct sulfidation reactions with sodium sulfate.

2. Sulfidation attack of pure nickel and cobalt is primarily intergranular, and oxidation occurring subsequently, is preferentially at the sulfide-rich grain boundaries.

3. Chromium additions to both nickel and cobalt greatly improve hot corrosion resistances of the two metals.

4. Chromium is believed to be a beneficial addition because it is shown to: (a) allow a more resistant surface film to form, and/or (b) preferentially react with the sulfur present, changing the sulfide morphology and reducing the concentration of sulfur available for further attack.

5. Additions of other alloying elements to nickel- and cobalt-chromium alloys may degrade the hot corrosion resistances of the simple binaries.

6. Since ternary additions should not affect significantly the reactivity of chromium and sulfur, their detrimental effects must be related to the lack of a protective surface film formation.

7. The extent of sulfate-induced enhanced oxidation is governed by the amount of reactive sulfur present; as a corollary, during enhanced oxidation, the sulfur is expended, allowing redevelopment of oxidation resistance.

*International Nickel Company.

REFERENCES

1. G. J. Danek, "State-of-the-Art Survey on Hot Corrosion in Marine Gas-Turbine Engines," U. S. Navy Marine Engineering Laboratory Research and Development Rept. No. 32/65, Assignment 87, 111 (March 1965).

2. E. L. Simons, G. V. Browning, and H. A. Liebhafsky, "Sodium Sulfate in Gas Turbines," Corrosion, 11 (12), 505 (1955).

3. P. A. Bergman, "Saline Corrosion of Aircraft Gas Turbine Materials at Temperatures up to 2000F," General Electric Rept. No. R64SE10 (April 8, 1964).

4. C. Sykes and H. T. Shirley, "Scaling of Heat Resisting Steels, Influence of Combustible Sulfur and Oil-Fuel Ash Constituent," Iron Steel Inst. Special Rept. No. 43, 153 (1951).

APPENDIX A

THE ROLE OF SODIUM SULFATE IN THE ACCELERATED OXIDATION OF NICKEL

by

J. R. Gambino

General Electric Company
Schenectady, N. Y.

Submitted as a Topical Report
Related to the
Hot Corrosion Mechanism Study
Contract No. N-(600) (61533)-63219

Conducted for the
U. S. Naval Marine Engineering Laboratory
Annapolis, Md.

January 1966

APPENDIX A

THE ROLE OF SODIUM SULFATE IN THE ACCELERATED OXIDATION OF NICKEL

J.R. Gambino

I. INTRODUCTION

Metal components in the hot section of gas turbines operated in a marine environment are occasionally severely corroded.[1] The corrosion is typified by the formation of a voluminous oxide scale and the presence of sulfides at the corroding front. Salt deposits are invariably associated with this type of attack. As might be expected from these characteristics, the corrosion phenomena have been variously referred to as catastrophic oxidation, sulfidation, or hot corrosion depending on the viewpoint of the investigator. This type of corrosion has been duplicated[2] when both sodium chloride and sulfur-rich fuels are introduced in burner rig tests.

The work reported here is part of the "Hot Corrosion" mechanism study sponsored by the Naval Marine Engineering Laboratory with the expectation that knowledge of the mechanism would be helpful in designing* alloys resistant to hot corrosion. Because of the anticipated complexity of the hot corrosion process, it was felt that corrosion studies should be conducted on elemental metals, at least initially, thereby avoiding the superimposed chemical complexity of commercial alloy compositions. Since nickel-base alloys are reported to be more susceptible to hot corrosion than cobalt-base alloys, nickel was chosen for intensive study.

Most investigators agree that the deposition of sodium sulfate on the metal surface is a normal precursor† to hot corrosion. The sodium sulfate forms because sodium chloride is not stable in the presence of SO_2 or SO_3 at combustion temperatures, and according to Sulzer[3] should react exothermically as follows:

$$2\,NaCl + SO_2 + 1/2\,O_2 + H_2O \rightarrow Na_2SO_4 + 2\,HCl + 51\ kcal/mole. \qquad (1)$$

Therefore, the oxidation of nickel in the presence of thin surface coatings of sodium sulfate was chosen for initial study.

---

*A concurrent Navy sponsored program on alloy development, based primarily on improving strength characteristics of several corrosion-resistant alloys, is being conducted at the General Electric Company's Materials and Processes Laboratory, in Schenectady, and at the Thomson Engineering Laboratory in West Lynn, Mass.

†In residual fuel ash corrosion, low melting oxides also present can cause accelerated oxidation.

References to other investigation in this system could not be found in the literature. Simon et al.[4] conducted experiments that demonstrated that sodium sulfate alone* could cause accelerated oxidation of stainless steels under some conditions, however. From the results of this study, it was concluded that sodium sulfate is reduced locally to form a lower valent sulfur, which in turn reacts with the base metal to form a metal sulfide.

$$M + S \rightarrow MS \quad . \tag{2}$$

It was postulated that this sulfide reacts with sodium sulfate, generating more sulfur for further reaction with the base metal.

$$Na_2SO_4 + 3\ MS = 4\ S + 3\ MO + Na_2O \quad . \tag{3}$$

Since the sulfides sometimes form low melting eutectics, no protective oxide films form, and the reaction is more rapid than oxidation of the base metal. This reaction in a large excess of sodium is so rapid and exothermic that a localized thermal excursion is postulated as a significant factor in contributing to accelerated attack.

Autocatalysis results because more than one sulfur atom is produced per mole of sodium sulfate in reaction. These investigators were able to demonstrate that reducing conditions (exposure to hydrogen or electrolytic reduction) could initiate the reaction, and suggested that the base metal itself could act as the reducing agent if the film failure allowed contact with sodium sulfate.

Some observations on reactions in the nickel-oxygen-sodium sulfate system were made which might be helpful in further clarifying the role of sodium sulfate in "hot corrosion" reactions.

II. EXPERIMENTAL PROCEDURES

The weight change measurements were performed on two recording Cheverard thermobalances modified to allow signal readout with linear differential transformers. Coupons at room temperature were introduced into a heated furnace that had the desired gas or gases flowing through at a rate of 250 to 350 ml/min. Coupons, 0.75 by 1.25 inches, were usually sheared from commercial nickel sheet, 0.020 inch thick. Coupons were hand polished with 400- and 600-grit paper before coating or pretreatment.

A saturated solution of the salt to be applied was sprayed on coupons heated on a hot plate (surface temperature 250°C) using an airbrush. Such coatings were adherent and appeared uniform in the thicknesses used (up to 30 mg per coupon). One side of the coupon was coated and weighed; the opposite side was coated to within a few mg.

---

*In residual fuel ash corrosion, low melting oxides also present can cause accelerated oxidation.

When solid particles were added to the salt, brushing or dipping was used instead of spraying to apply the mixture, with a resultant loss of thickness and uniformity control.

Two types of nickel were used in this investigation. Spectroscopic analysis of the commercial nickel, nominally 99.5% pure, showed the following elements:

Nickel	Major constituent
Manganese	0.1% to 1.0%
Titanium	.01% to 0.1%
Silicon	.01% to .1%
Copper	.01% to .1%
Cobalt	.01% to .1%
Magnesium	.01% to .1%
Chromium	.001% to .01%

A higher purity nickel, nominally 99.99%, obtained from the Driver-Harris Company had the following impurities:

Nickel	Major constituent
Cobalt	0.01% to 0.1%
Iron	.01% to .1%
Copper	< .01%

The cobalt used had the following analysis:

Cobalt	Major constituent
Nickel	0.1% to 1.0%
Silver	< .001%
Silicon	< .001%
Copper	< .01%

In addition, a nickel - 1% chromium alloy was prepared by vacuum induction melting. The as-cast material was cut into coupons approximately the size of the nickel coupons.

III. RESULTS AND DISCUSSION

A. Oxidation Kinetics

Studies of corrosion kinetics have a well-known value in establishing mechanisms of corrosion phenomena. Kinetics should be especially useful in the hot corrosion study, which is likely be more complex than most other corrosion phenomena because of the several possible alternate and sequential reactions,

as well as the possibility of a molten metallic phase at the interface. Kinetic studies are useful in distinguishing or enumerating the different stages of the over-all corrosion process and establishing the boundaries of each stage. The rates of corrosion can be measured in each stage. Experiments can then be designed to determine the effect of various experimental parameters on the rates. The rate behavior itself, i.e., the mathematical equation best fitting the kinetic data, and their sequence, usually is instructive in verifying the type of reaction occurring. The rates and temperature behavior can be compared quantitatively with rates of related reaction and processes.

The weight change kinetics of a polished nickel coupon coated with sodium sulfate and exposed to dry oxygen at 900°C is shown in Fig. 1. A very rapid weight gain occurred in the first few minutes of exposure. Compared to oxidation of uncoated nickel for the same conditions, also shown in Fig. 1, sodium sulfate clearly induces accelerated corrosion.

The temperature dependence of oxidation was investigated. Nickel coated with sodium sulfate, exposed to dry oxygen at temperatures ranging from 750° to 940°C, changed weight as shown in Fig. 2. The behavior in the experiments conducted at 900°C above the melting point of sodium sulfate, 883°C, was identical to that observed at 850°C. At lower temperatures, where the initial weight changes occurred over a longer time, the initial oxidation rates had the normal dependence with temperature. Accelerated attack apparently can take place well below the melting point of sodium sulfate.

In the above experiments the coating weight was not always held constant. In another series of experiments the effect of coating weight on oxidation behavior was investigated. The weight change during exposure to dry oxygen at 825°C is shown in Fig. 3 for nickel coupons having different weights of sodium sulfate coating. Coating thickness had no noticeable effect on the initial oxidation rate as it might if transport through the sulfate were rate limiting. Coating thickness did have an effect on later oxidation stages. The severity of attack increased with increased coating thickness in the thickness range studied.

In other experiments the effect of water vapor on oxidation kinetics was studied. The weight change behavior at 805°C of a coated nickel coupon exposed to oxygen saturated with water at room temperature is shown in Fig. 4. A significant increase in the initial oxidation rate results from the presence of water vapor. A marked change in the duration of the initial oxidation behavior was caused by the water vapor also. This behavior had a curious dependence on temperature, exhibiting a maximum at about 800°C (Fig. 5).

Coated nickel coupons exposed to oxygen-argon gas mixtures at 805°C changed weight as shown in Fig. 6. At the lower oxygen pressures, where initial weight gain is obviously linear, the change from linear behavior occurs much later than at high oxygen pressures. At the high pressures, linear behavior is restricted to a short initial period and is sometimes difficult to identify. It will be assumed that all curves are initially linear for convenience in showing the dependence of these initial rates on oxygen pressure as in Fig. 7. Above 2% oxygen, the rate is more or less independent of oxygen pressure. At lower oxygen pressures, the rate increases proportionately* to oxygen pressure.

*Actual $r \approx PO_2^{3/4}$.

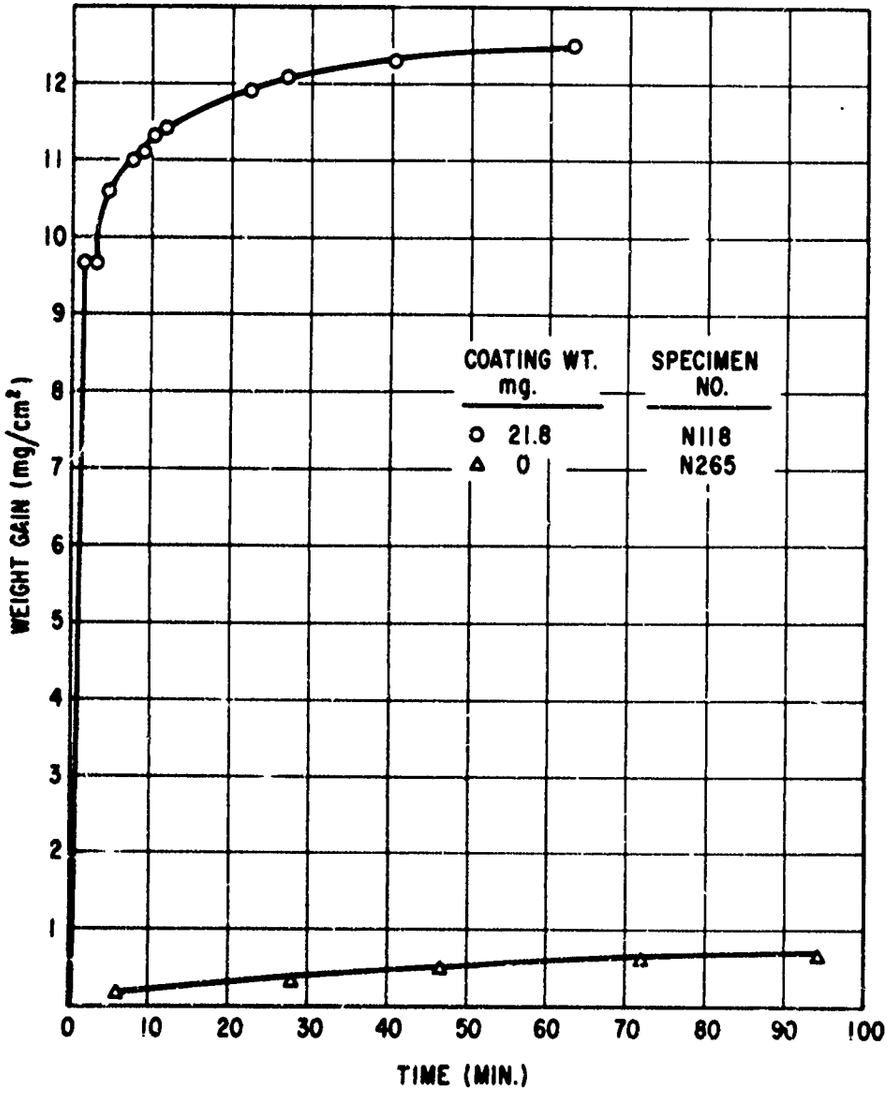

Fig. 1 Weight gain of nickel coated with sodium sulfate during exposure to dry oxygen at 900°C.

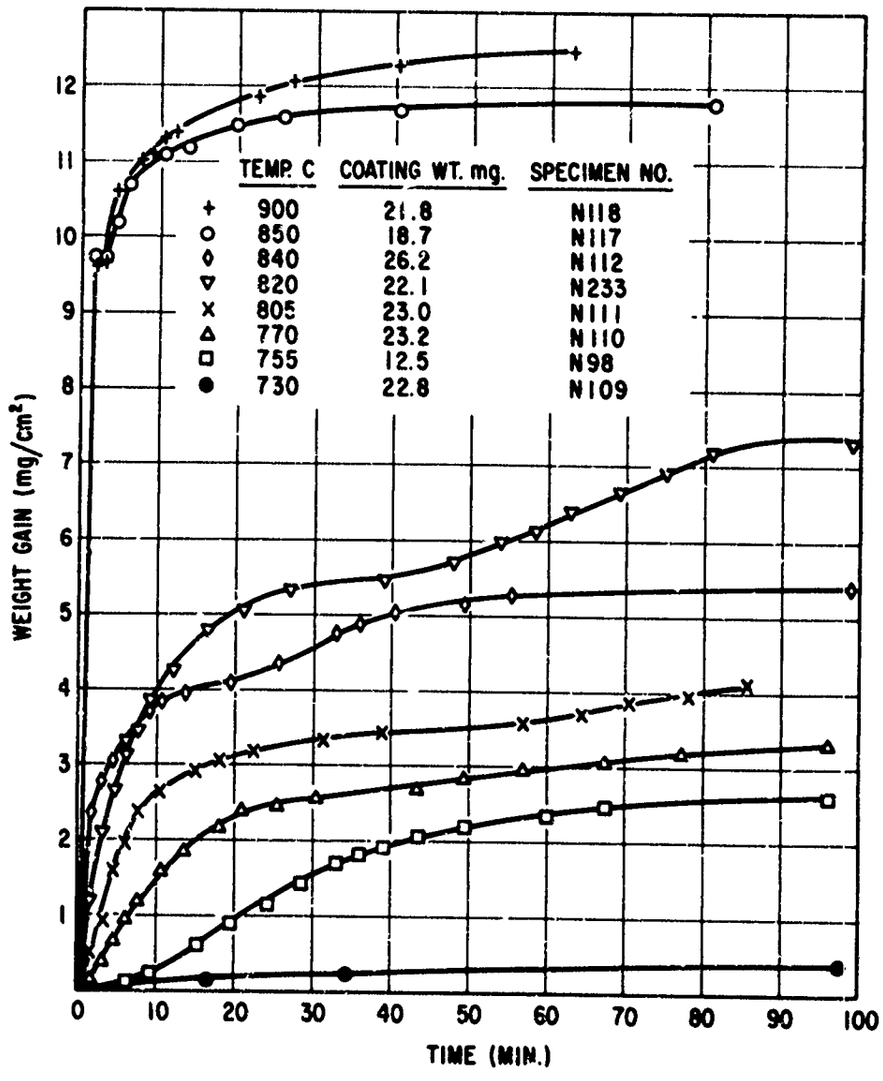

Fig. 2 Weight gain of nickel coated with sodium sulfate in dry oxygen at various temperatures.

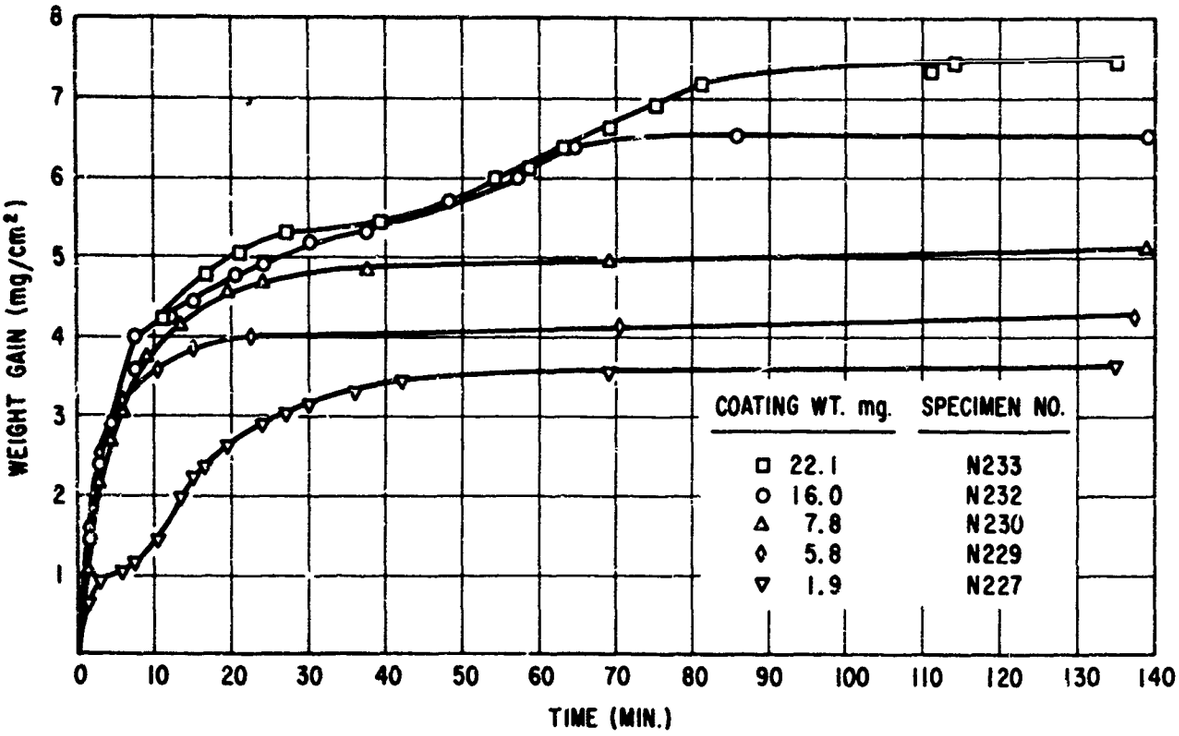

Fig. 3 Weight gain of nickel in dry oxygen at 825°C with sodium sulfate coatings of various thicknesses.

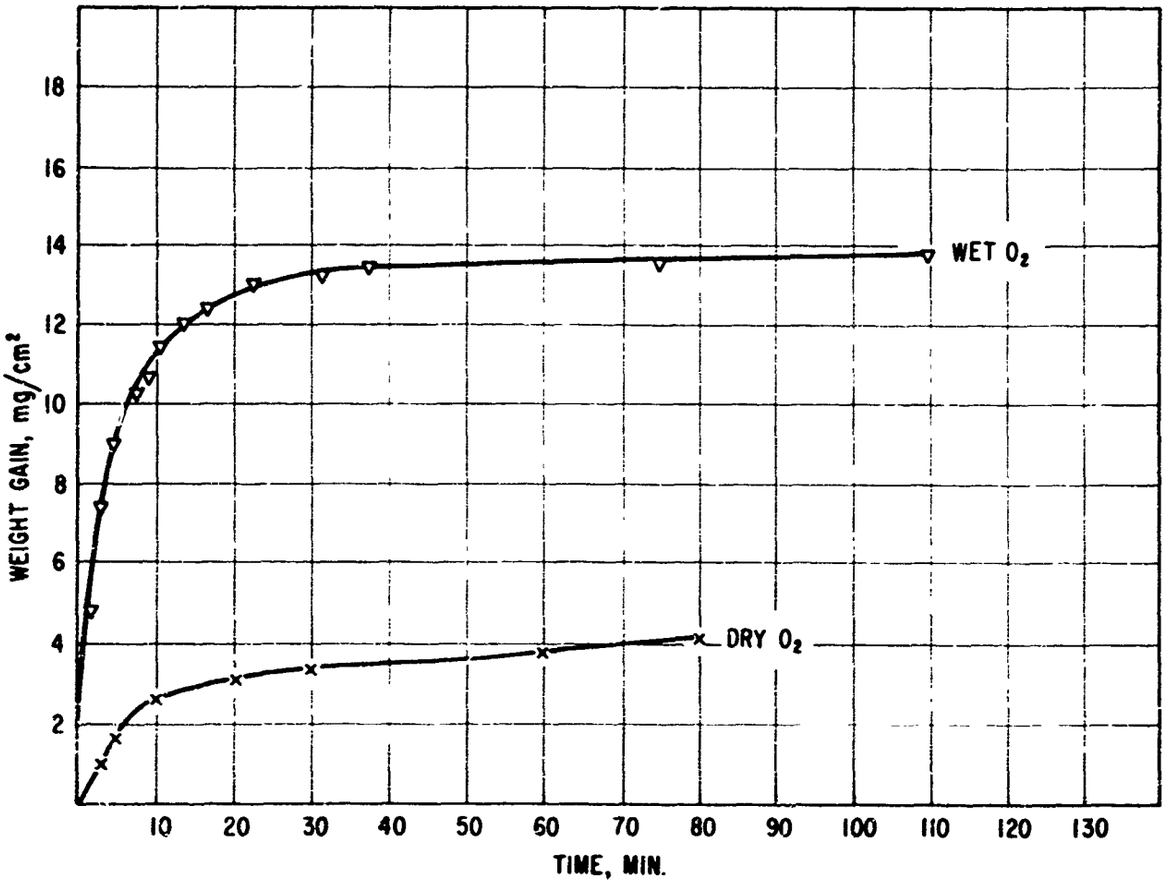

Fig. 4 Weight gain of nickel coated with sodium sulfate in wet oxygen at 805°C.

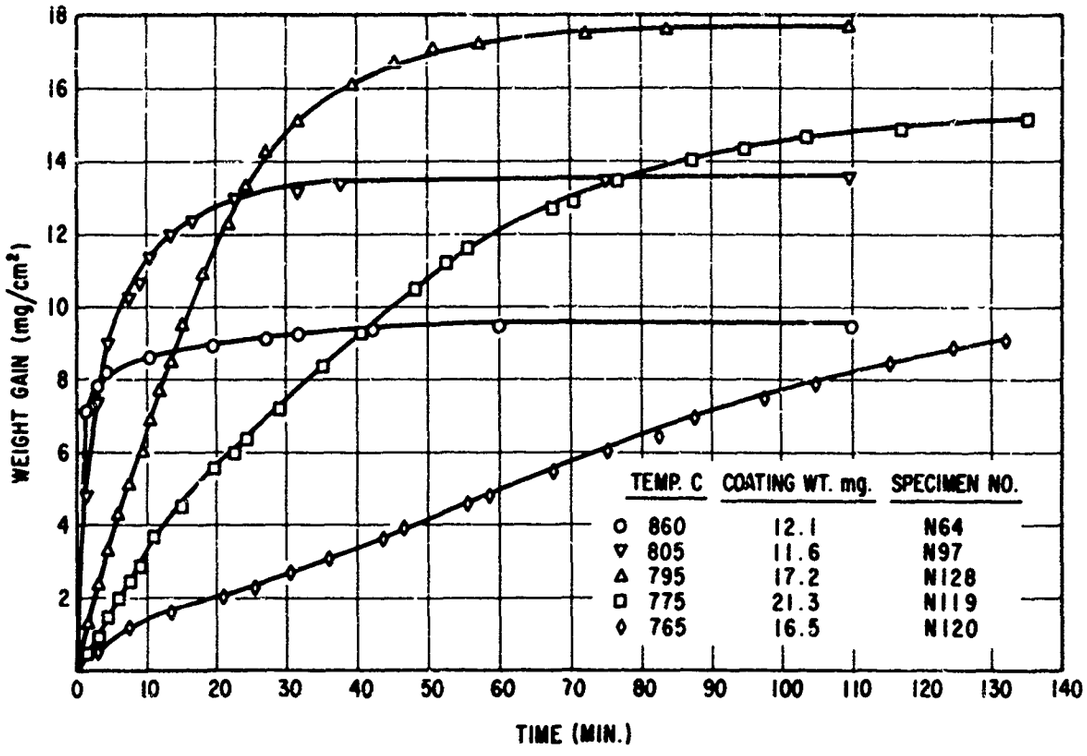

Fig. 5 Weight gain of nickel coated with sodium sulfate in wet oxygen at various temperatures.

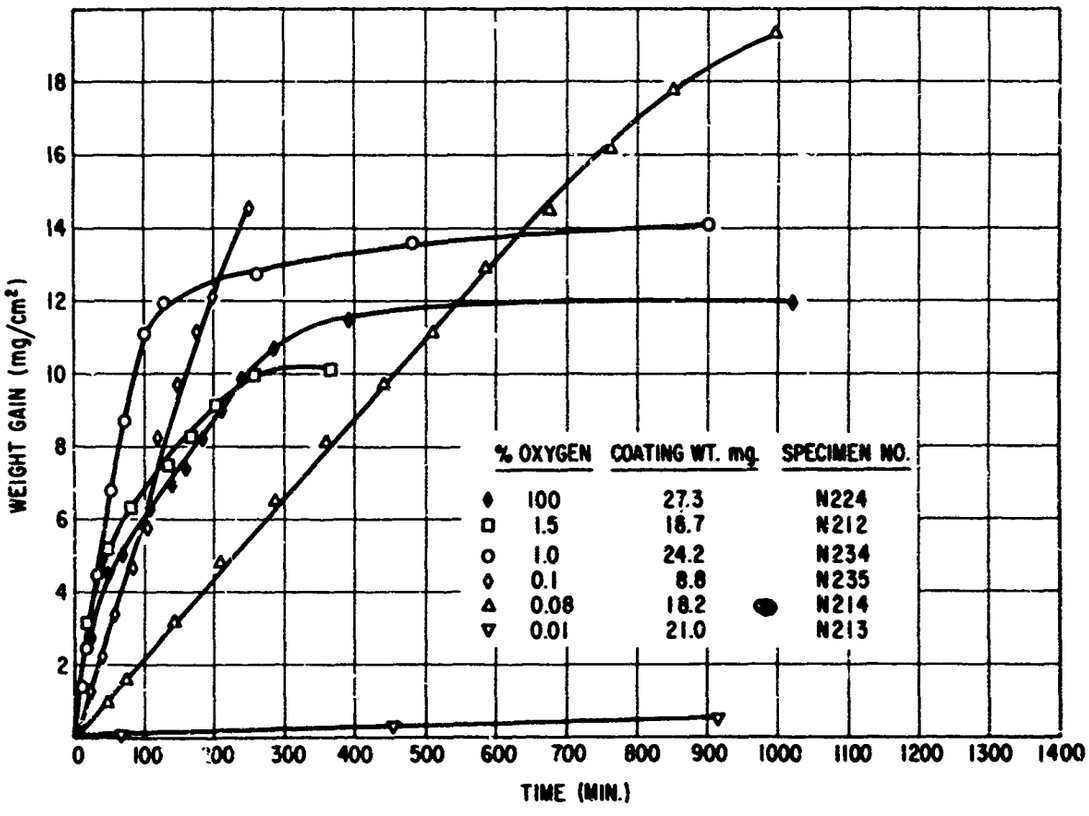

Fig. 6 Weight gain of nickel coated with sodium sulfate at different partial pressures of dry oxygen at 805°C.

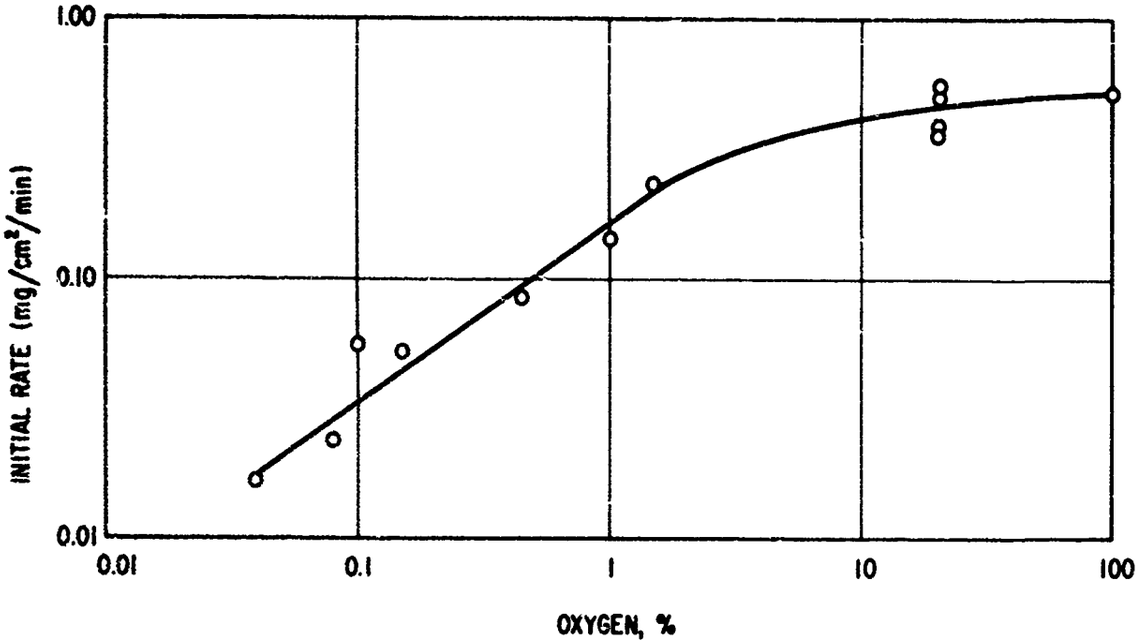

Fig. 7 The dependence of initial corrosion rate on oxygen partial pressure.

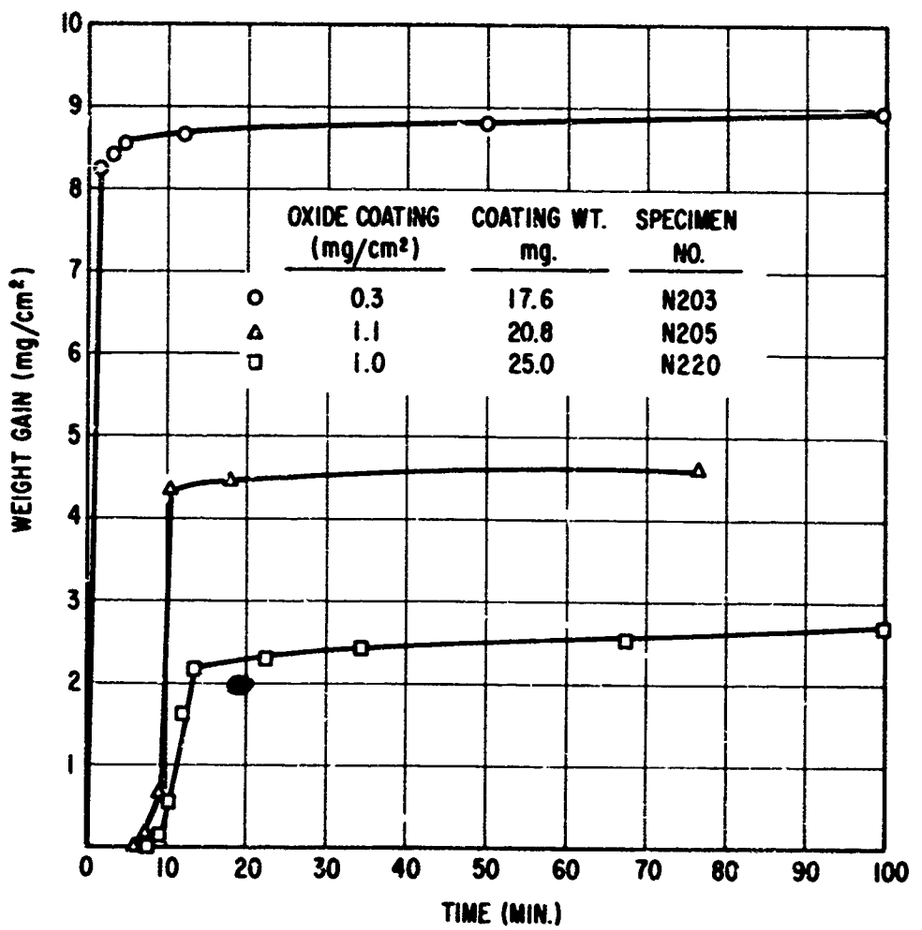

Fig. 8 The effects of preoxidizing nickel on corrosion in dry oxygen at 850°C.

These results suggest that transport of oxygen through the sulfate film is not rate controlling at the higher and usual oxygen pressures, and oxygen is readily available to the solid-liquid interface.

Some specimens were oxidized prior to coating with sodium sulfate. Preoxidation in air at 250°, 300°, 500°, and 600°C for 1 hour did not appear to influence weight gain kinetics in dry oxygen at 850°C. Exposure at 800°C for several hours did, however. Weight change curves are shown in Fig. 8 for 850°C exposure. An initial metal oxide film, 4000 Å thick (0.3 mg/cm^2), produced no detectable delay in the onset of accelerated oxidation; but increasing the oxide film weight further caused an increase in the incubation period preceding the initiation of accelerated corrosion. It is noteworthy that the oxide film was also penetrated at the lowest exposure temperature studied, 740°C.

B. Auxiliary Experiments

1. $NiO \cdot Na_2SO_4$

Nickel oxide powder was heated with sodium sulfate in an alumina or platinum crucible in room air at 900°C overnight. The product was analyzed by x-ray diffraction and nickel oxide was identified. The other peaks present could be accounted for by one or more of the sodium sulfate phases. It was concluded that no extensive chemical reaction takes place between nickel oxide and sodium sulfate under the test conditions used.

Nickel oxide single crystals (~0.3 gram) were immersed in liquid sodium sulfate (~1.0 gram) held in a platinum crucible at about 900°C. After 16 hours exposure the nickel content of the sodium sulfate was 0.1% to 1.0% (determined by semiqualitative spectrographic analysis of the melt). This approximate concentration was confirmed by weight loss measurements on crystals. In addition, the surfaces appeared etched. The results were about the same when nickel oxide single crystals were exposed to molten sodium chloride under the same conditions.

2. $Ni\text{-}Na_2SO_4$

A number of qualitative experiments were conducted to establish the products of the reaction between nickel and sodium sulfate. Such information is necessary to design meaningful kinetic studies in the system.

Nickel powder, mixed with sodium sulfate, in a 3:2 mole ratio, was heated in a nickel boat at 920°C overnight under argon. The major phases indicated by x-ray diffraction analyses were nickel and sodium sulfate. Several minor peaks could be taken as evidence of nickel oxide. Sulfate determination by the barium chloride method confirmed the presence of most (~90%) of the original sulfate. The pH measured could be accounted for by a sodium hydroxide concentration of 0.5%. Areas of the nickel boat, where the boat contacted the quartz furnace liner, had a golden-molten appearance typical of the nickel-nickel sulfide eutectic.

In another experiment in which sodium sulfate and nickel powder in a 7:10 mole ratio were heated in an alumina crucible under argon at 820°C overnight, the metal powder had coalesced into a single golden-molten mass typical of a nickel-nickel sulfide eutectic composition. Both nickel and sodium sulfate appeared to be the major phases based on x-ray examination. The experiment indicates that nickel can react readily with sodium sulfate. One possible explanation for the increased reactivity is that the alumina boat reacted with the sodium oxide formed and hence displaced the normal equilibrium in the system. Chemical analysis showed a slightly higher sodium hydroxide concentration (1%) and less sulfate remaining (~80%).

In similar experiments, it was determined that neither sulfite ion nor soluble nickel was formed in detectable quantities when nickel and sodium sulfate in a 1:2 mole ratio were mixed and heated overnight at 820°C in argon.

Polished nickel coupons were coated with sodium sulfate and heated under argon at 805°C for 1 hour. No weight change was observed. The heated coupons were boiled in water for 5 minutes, and (within experimental error) all of the sodium sulfate originally present was recovered in the soluble fraction. The coupon weight, after the soluble fraction was removed, was the same as the original coupon weight. Evidence of some attack can be detected in the photomicrograph shown in Fig. 9. No other phases were found by x-ray examination of the coupon surface.

A high-purity nickel coupon heated with a sodium sulfate coating at a higher temperature, 900°C, for a longer time--16 hours--exhibited a golden-molten phase localized largely at grain boundaries. No x-ray evidence of phases other than nickel was found at the surface.

The results of these experiments indicate that the probable reaction taking place is that suggested by Simon et al. and can be written:

$$9/2\ Ni + Na_2SO_4 \rightarrow 1/2\ Ni_3S_2 + Na_2O + 3\ NiO\ . \qquad (4)$$

The most noteworthy result of these studies, however, is that the reaction rates were very low. The low rates could result from the formation of a coherent oxide

Fig. 9 Sodium sulfate-coated nickel exposed to argon at 805°C for 60 minutes (N221). 100X

film acting as a reaction barrier. This seems unlikely based on the ease with which nickel oxide films were penetrated by sodium sulfate (see Fig. 8). An alternate explanation is that the reaction proceeds until an equilibrium concentration of sodium oxide is attained and does not continue until (1) a sulfide phase at the surface is eliminated by sulfur migration into the interior and (2) the equilibrium concentration of sodium oxide is lowered. Loss of sodium oxide from the system can occur by corrosion to sodium hydroxide in the presence of water vapor. This explanation is in accord with the available thermochemical data which indicate a substantially positive free energy change ($\Delta F = +27$ kcal at 800°C) for reaction (4) as written.

Alternate processes for the formation of nickel sulfide can be envisioned based on reacting impurities. Since manganese is the major impurity in the commerical nickel used, its possible reactions are considered. In contrast to the nickel reaction, the free energy change for the reduction reaction of sodium sulfate by manganese

$$Na_2SO_4 + 4\ Mn \rightarrow Na_2O + MnS + 3\ MnO \qquad (5)$$

is quite negative: $\Delta F \approx -105$ kcal.

If in addition the reaction between the sulfide and sulfate suggested by Simon et al.[4]

$$Na_2SO_4 + 3\ MnS \rightarrow Na_2O + 3\ MnO + 4\ S$$

$$4\ S + Ni \rightarrow NiS \qquad (6)$$

$$Na_2SO_4 + 3\ MnS + Ni \rightarrow Na_2O + 3\ MnO + NiS$$

takes place, nickel sulfidation could occur by this route. The free energy change for this reaction (6) is quite positive, however: $\Delta F \approx +90$. An aluminum impurity by contrast could be effective in this way since the free energy change of this reaction:

$$Na_2SO_4 + Al_2S_3 \rightarrow Na_2O + Al_2O_3 + 4\ S \qquad (7)$$

is nearly zero: $\Delta F \approx +7$.

When experiments were conducted to establish the phase equilibria quantitatively and the kinetics of this reaction, several experimental difficulties were encountered. In differential thermal analysis experiments, originally proposed to measure kinetics of this reaction, the nickel sulfide product reacted with the platinum-rhodium thermocouples. The formation of molten sulfides in general prevented the use of noble-metal containers. The dense alumina crucibles (triangle RR-Morganite) used seemed to be attacked by reactants and/or products, and affected the rate themselves.

3. $Na_2S + NiO$

Nickel oxide powder and sodium sulfide (as $Na_2S \cdot 9\ H_2O$) were mixed in a 1:4 mole ratio and heated in a nickel boat under argon for 1 hour at 820°C. Nickel metal with no nickel oxide was detected by x-ray diffraction of the product. The soluble fraction appeared to be all sulfates. The formation of sodium sulfide, by transient reducing conditions, could result in removal of nickel oxide films by this reaction.

C. Special Kinetic Experiments

The auxiliary experiments show that the originally proposed rapid and violent reaction of nickel and/or nickel sulfides with sodium sulfate does not occur in this system. Experiments were made to establish the reaction rate of sodium sulfate with nickel under oxidizing conditions. This was done by measuring the decrease in sodium sulfate during oxidation. In these experiments, nickel coupons coated with sodium sulfate were exposed to dry oxygen at 820°C for short times. The weight changes occurring during the exposure are shown in Fig. 10. These curves illustrate the degree of reproducibility obtained with the

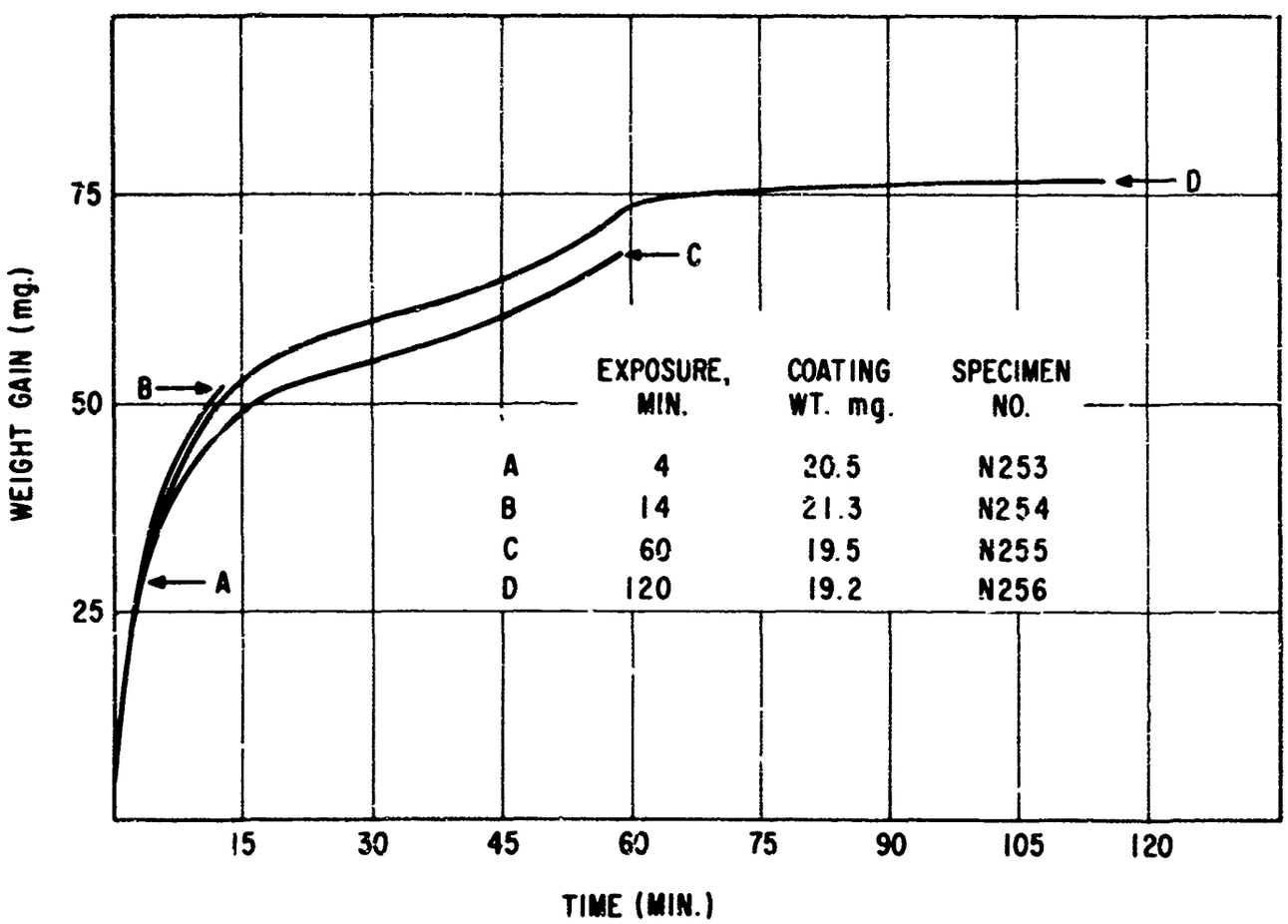

Fig. 10 Short time corrosion of nickel coated with sodium sulfate during exposure to dry oxygen at 820°C.

procedures used. The soluble material was removed from the exposed specimens and the sulfate content determined as shown below:

No.	Exposure Time (min)	Original Na_2SO_4 (mg)	Recovered Na_2SO_4 (mg)	% Recovered (approx)	pH (50 ml, H_2O)
N253	4	20.5	13	65	7.6
N254	14	21.3	14	65	8.4
N255	60	19.5	9	45	8.5
N256	120	19.2	9	45	8.7

The sodium sulfate content decreased and the basicity increased with exposure time. These results established that both nickel and sodium sulfate are available when the initial rapid oxidation ceases. Other experiments were conducted to further define the role of sodium sulfate in inducing accelerated oxidation.

In one experiment, a nickel coupon was reacted with a film of sodium sulfate for 1 hour at 800°C, and after the removal of soluble material from the surface, exposed to oxygen at 900°C. The weight gain was little, if any, larger than that observed when untreated nickel was exposed under the same conditions.

In other experiments, specimens were prereacted with sodium sulfate and subsequently exposed to oxygen without removal of the salt. This was accomplished by preheating coated specimens in an argon atmosphere before introducing oxygen. The weight change of two specimens heated for 10 and 15 minutes prior to dry oxygen exposure is shown in Fig. 11. The weight change of a coated coupon exposed without pretreatment is included for reference. The apparent difference caused by preheating in argon is a four- or fivefold increase in initial corrosion rate.

In another experiment, a coated nickel coupon was exposed to oxygen for 12 minutes at 850°C. Before the initial rapid oxidation stopped, the specimen was removed and washed to remove the sodium sulfate, and re-exposed under the same conditions. As shown in Fig. 12, oxidation almost ceased during the second exposure. In another experiment, a coated coupon was cooled during the initial oxidation and reheated without any noticeable effect on the rate.

These experiments establish that the presence of sodium sulfate is required to maintain accelerated oxidation. Also, the reaction product of sodium sulfate and nickel neither induces nor sustains accelerated oxidation. The sodium sulfate may be simply the source of sulfur for forming sulfides. To test this hypothesis the behavior of sulfided nickel was investigated.

Sulfided coupons (1 mg/cm^2 sulfur absorbed*) exposed to oxygen either coated or uncoated with sodium sulfate had the weight changes shown in Fig. 13. The sulfided specimens without coating exhibited a weight gain† not

*Presumably at the surface since formed in only a few minutes' exposure to hydrogen sulfide at 700°C.

†The loss of weight due to SO_3 evolution was not measured, however.

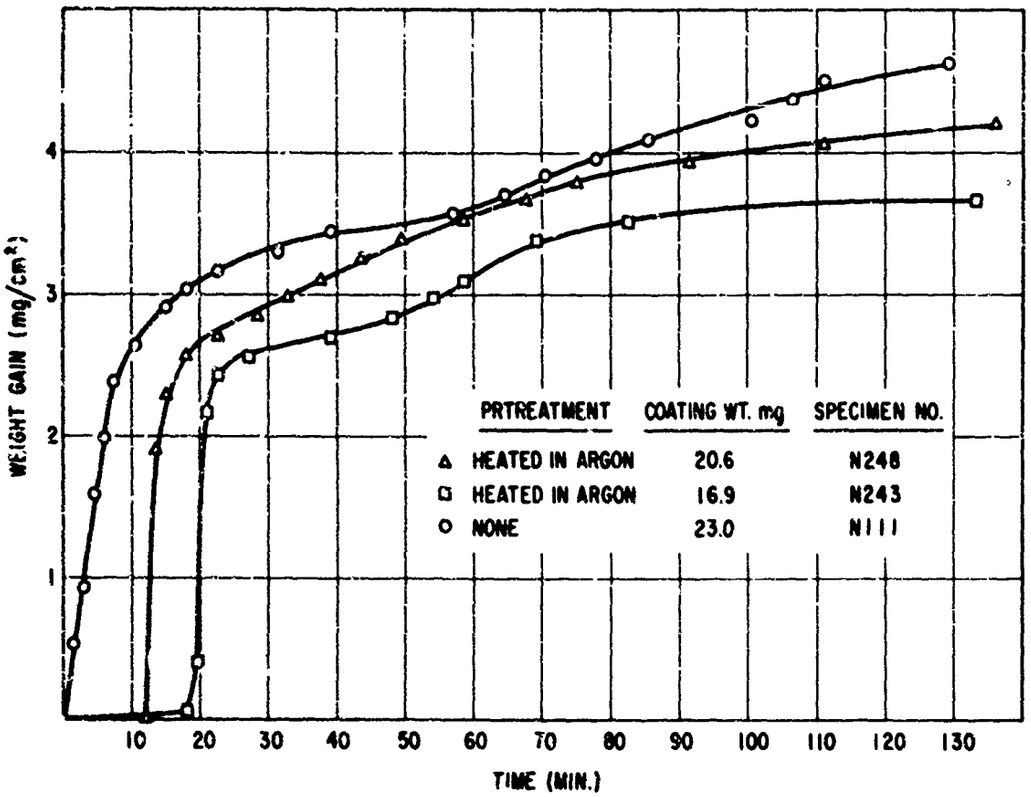

Fig. 11 The effect of prereacting sodium sulfate with nickel on its corrosion in dry oxygen at 805°C.

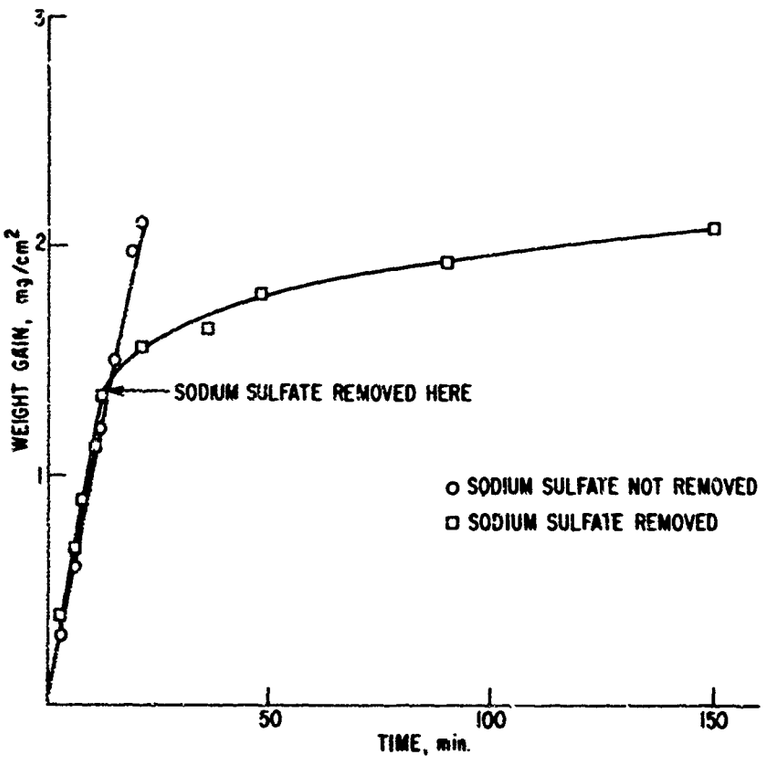

Fig. 12 The oxidation of high-purity nickel in dry oxygen at 850°C before and after sodium sulfate removal.

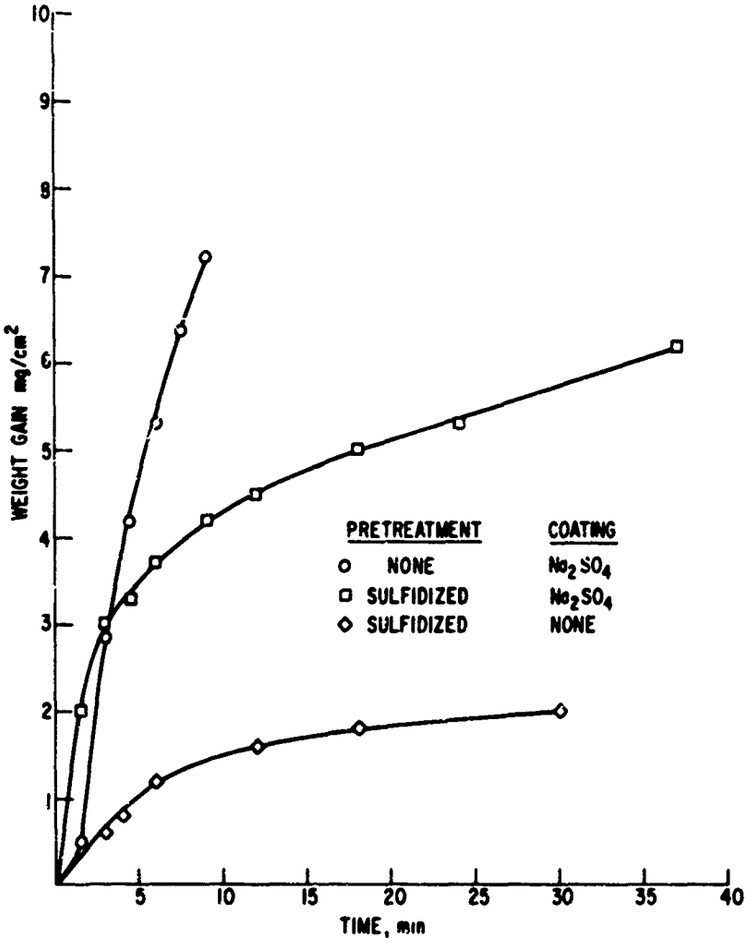

Fig. 13 Oxidation of pre-sulfidized high-purity nickel in dry oxygen at 900°C with and without a sodium sulfate coating.

much greater than untreated nickel. The initial oxidation rate of the coated specimen was somewhat higher than that of an untreated coupon.

In other work, (5) the oxidation of nickel under a molten borate layer was shown to be accelerated by introducing a noble metal probe extending from the air through the molten borate to the metal. Apparently, electron transfer through the borate was rate limiting. These results suggested to the authors (6, 7) that metal oxide coexisting with molten salts could act as the electron conductor in producing local cell action during "hot corrosion" of superalloys.

Two types of experiments were conducted to test this hypothesis. The first involved depositing sodium sulfate on a nickel coupon in a periodic array (accomplished by spraying through two different size screens). The uncoated nickel oxide exposed to oxygen and sulfate would constitute one-half of the cell suggested. When such specimens were exposed to dry oxygen at 850°C, weight gains shown in Fig. 14 were observed. The initial oxidation rate decreased, as might be expected if only a fraction of the surface were coated, however.

In the other experiment, oxides were added as powders to the sodium sulfate. The powders themselves could act as electronic conductors as well as increase the electronic conductivity of the melt by contributing ions by solution. Such additives had little effect on initial rates. The weight change when nickel oxide powder was added to film is shown in Fig. 15. If anything, the oxidation is depressed slightly.

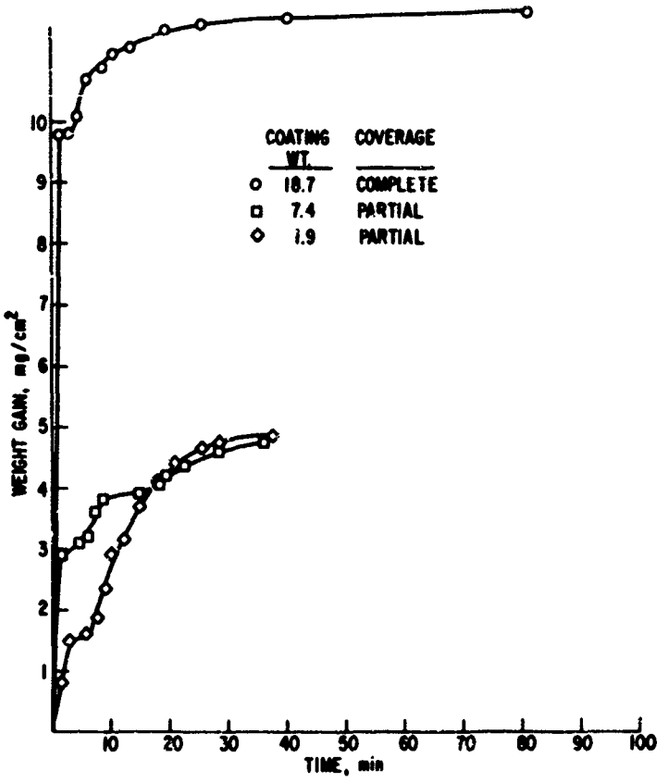

Fig. 14 Oxidation of nickel in dry oxygen at 850°C partially coated with sodium sulfate.

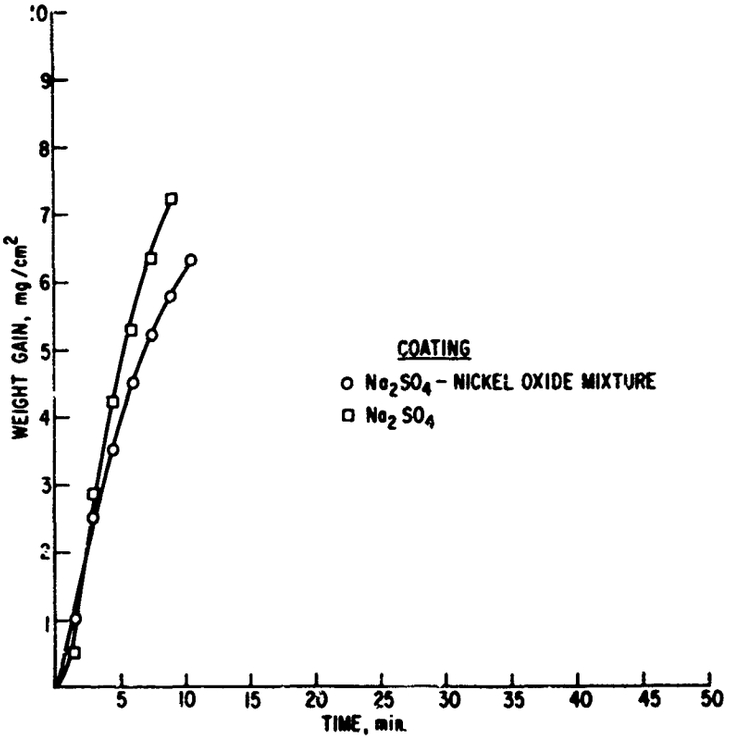

Fig. 15 Oxidation of high-purity nickel in dry oxygen at 900°C when coated with sodium sulfate-nickel oxide mixtures.

In most of the kinetics studies already described, the nickel used was commercially available sheet of nominal 99.5% purity. When high-purity nickel, 99.95%, was coated and exposed to wet or dry oxygen at various temperatures, the corrosion was less severe than that observed with commercial nickel as shown in Fig. 16. The enhancement of corrosion by water vapor was noted here also. These results indicate that the presence of impurities is not essential to accelerated oxidation, but has a large effect on the rates involved.

The oxidation of nickel was studied when the sodium sulfate was replaced by other salts. The weight change kinetics of nickel coated with sodium chloride when exposed to wet and dry air at 850°C are shown in Fig. 17. Corrosion is enhanced by sodium chloride, but is much less severe than that caused by the sulfate. Enhanced corrosion was not observed below the melting point. Corrosion is accelerated by the use of water vapor as in the sulfate system. Other data, not reported here, indicate that the pre-oxidation treatment leads to an incubation period similar to that observed with sodium sulfate. These results indicate that the sulfate ion is making an important contribution to accelerated oxidation.

The weight change kinetics of cobalt coated with sodium sulfate when exposed to dry oxygen is shown in Fig. 18. Normal oxidation of uncoated cobalt is included for reference. Sodium sulfate apparently has little or no effect on the normal oxidation of cobalt. The reason for the strikingly different effect of sodium sulfate in this system is not known. It does not stem from the absence of a molten eutectic phase, however, since no enhancement was noted at 900°C.

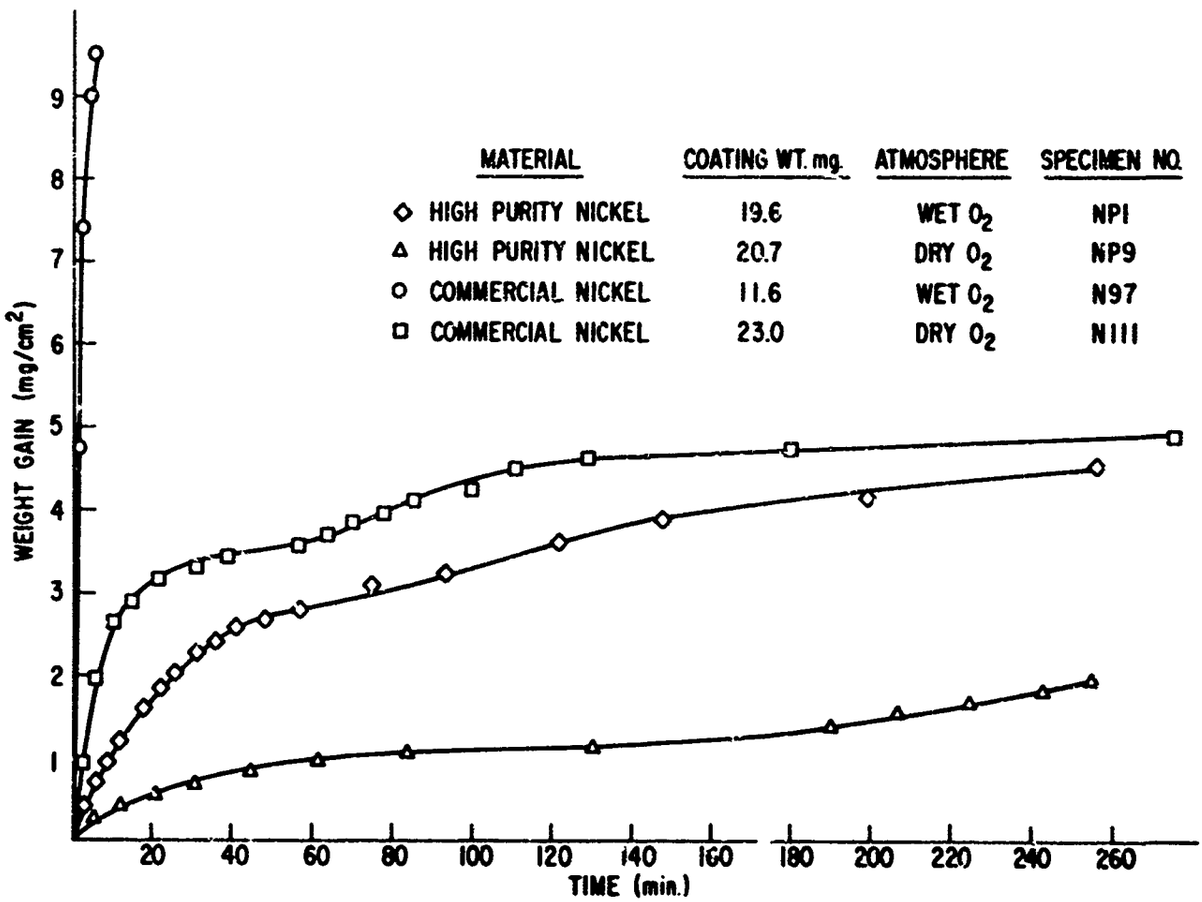

Fig. 16 Weight gain of high-purity nickel in wet and dry oxygen at 805°C.

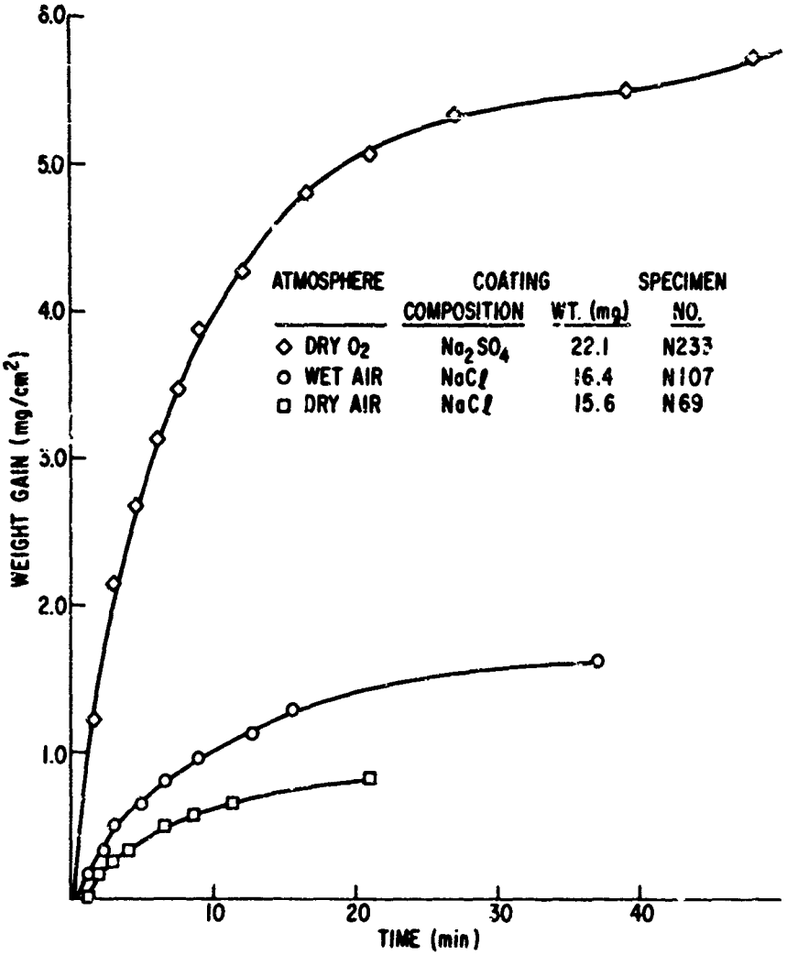

Fig. 17 Weight change of nickel coated with sodium chloride during exposure to wet or dry air at 850°C.

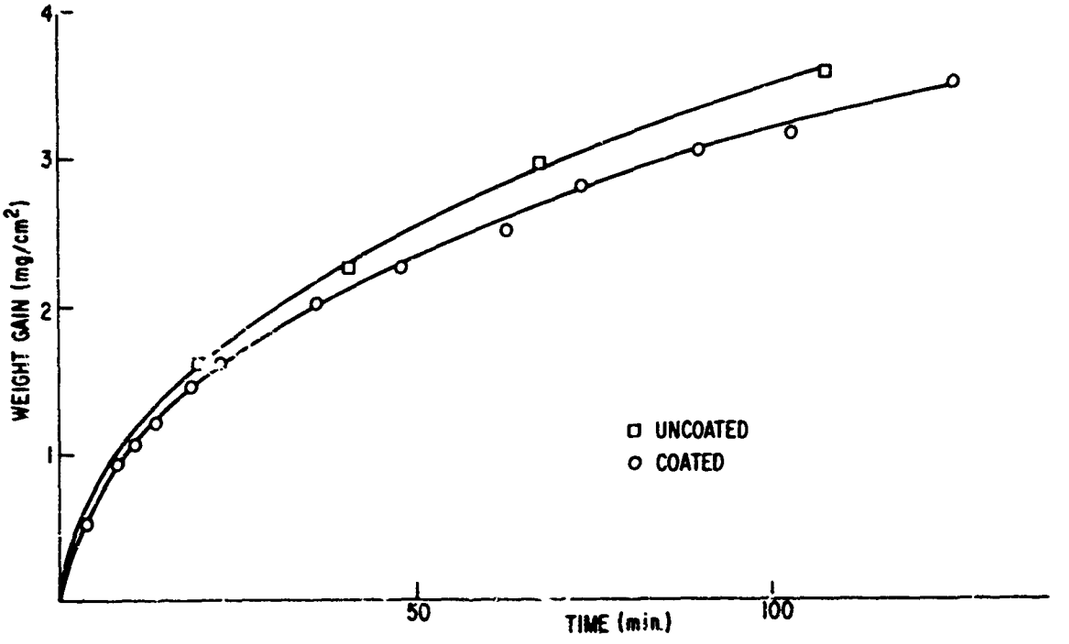

Fig. 18 Weight change of cobalt coated with sodium sulfate in dry oxygen at 855°C.

IV. MECHANISMS

A. General Considerations

The rate limiting step in sulfate-induced oxidation can be any of the following:

1. Reactions occurring at the gas-liquid or liquid-solid interface.
2. Transport of a species through a liquid or solid layer.
3. Electron transfer in the liquid or solid.

Several possibilities can be eliminated based on results on hand. It can be expected from general consideration that reactions at the gas-liquid interface, such as gas absorption, bond breaking, etc., would not be rate limiting at these high temperatures. Electron transfer in the liquid has been shown earlier not to be rate limiting in the liquid. Transport of any species through the molten salt layer cannot be rate limited at the lower temperatures since the initial oxidation rate did not change with a threefold increase in sulfate thickness whereas a decrease inversely proportional to the thickness would be expected. In addition, the observed temperature dependence of initial oxidation is not consistent with diffusion through liquids.

The quantitative temperature dependence can be obtained if wide latitude is used in ascribing linearity to the initial oxidation curves. The oxidation rate constants are plotted against reciprocal temperature in Fig. 19. The activation energy of the corrosion processes derived from the curves were comparable, almost 80 kcal/g-mole. In contrast, the oxidation data for commercial nickel at the two highest temperatures studied appears to indicate a low activation energy process in operating. The activation energy observed of about 80 kcal is not unreasonable for diffusion processes through solids such as nickel oxide, however. The only solids identified by x-ray analysis in this system were nickel oxide and nickel.

The initial rate of oxidation is approximately linear, i.e., oxygen absorption is proportional to exposure time. In oxidation and corrosion experience, linear behavior is associated with nonprotective oxide films. At least three types of phenomena can account for the linear kinetics observed in initial oxidation.

1. The oxide or products formed by the reaction of nickel and sodium sulfate could be dissolved by the sulfate thereby preventing the formation of a protective film.
2. The oxide film formed could become unstable because of physical or chemical reaction with the sodium sulfate or of the direct or indirect products of the nickel-sulfate reaction.
3. A metal-sulfide molten layer forms which could not be expected to provide a stable substrate for the development of a coherent-protective oxide film.

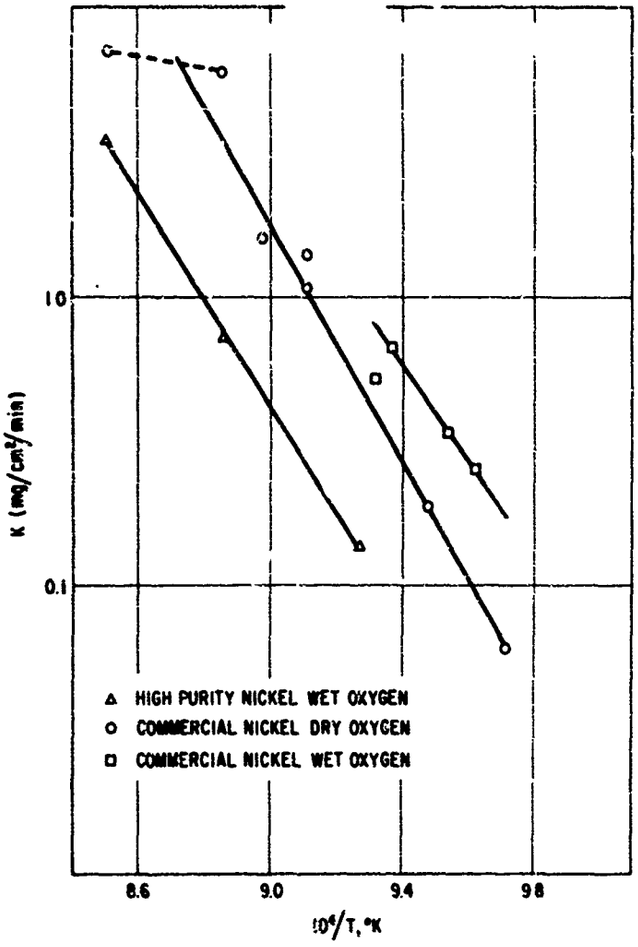

Fig. 19 Temperature dependence of nickel corrosion rates.

B. Mechanism Models

Enough information is available to make a preliminary attempt to formulate a mechanism model for nickel oxidation. The sodium sulfate reacts with nickel metal according to the following

$$Na_2SO_4 + 9/2\ Ni \rightarrow Na_2O + 3\ NiO + 1/2\ Ni_3S_2 \quad . \qquad (9)$$

A nickel sulfide-nickel eutectic forms at the metal surface. A minor amount, less than 1%, of sodium oxide is formed corresponding to the observed equilibrium concentration at about the melting point of sodium sulfate. When the equilibrium amount of sodium oxide forms, the reaction ceases. Concurrently, oxygen penetrates the molten salt layer and reacts with the sulfide as shown below:

$$Ni_3S_2 + 9/2\ O_2 \rightarrow 3\ NiO + 2\ SO_3 \quad . \qquad (10)$$

The SO_3 formed by reaction (10) can be expected to react with the sodium oxide formed by reaction (9).

$$Na_2O + SO_3 \rightarrow Na_2SO_4 \quad . \qquad (11)$$

This reduction of the sodium oxide concentration to low levels and removal of nickel sulfide from the surface allows reaction (9) to proceed again. The sulfate melt acts as a reservoir. The sulfur content is replenished by the oxidation reaction so that the melt is maintained in a "reactive" state.

This sequence of reactions (9), (10), and (11) constitutes a cyclic process shown that can persist until sulfur is lost from the system by diffusion into the interior, for instance. Such losses represent sulfur which cannot contribute to maintaining the sulfate concentration at the surface high or sodium oxide low and ultimately lead to the cycle's end.

If such a cycle were operating it would be expected that the transition from linear oxidation kinetics would coincide with initiation of a sodium oxide concentration plateau. The observation of such behavior during oxidation was reported earlier.

The foregoing does not account explicitly for the observed linear oxidation kinetics. It can be explained, however, if no coherent oxide or other barrier exists and sodium sulfate has free access to the metal surface. The ease with which sodium sulfate was observed to penetrate nickel oxide films suggests nickel oxide at least would not be an effective barrier.

As stated earlier, the high activation energy of the oxidation process at temperatures below 850°C suggests that diffusion in a solid is the rate limiting reaction. The value obtained for the activation energy, 80 kcal, is somewhat closer to that reported for sulfur diffusion in nickel, 90 kcal, than that for nickel (or oxygen) in nickel oxide, about 45 to 55 kcal. It is not apparent how sulfur diffusion through nickel can be rate limiting for the oxidation reaction as outlined.

At 850°C or above, the oxidation rate shows little temperature dependence and therefore the rate limiting transport process* must be different from that above. Transport through either of the two liquid films, i.e., sodium sulfate or nickel sulfide, would be a low activation energy process. (7)

The mechanisms presented above are reasonably consistent with the observed behavior of commercial nickel exposed to dry oxygen. However, nickel is oxidized more rapidly when exposed to wet oxygen rather than dry oxygen. The water vapor acts to remove sodium oxide from the sulfate layer to form a hydroxide and hence should allow thicker sulfide films as observed to form.

If the sodium sulfate acts to maintain a thin sulfide layer essential to accelerated oxidation, a discontinuity in oxidation rate should occur when no sulfide is formed. An experimental check on this possibility can be made by applying sodium sulfate along with sodium oxide, in amounts exceeding the equilibrium concentration. Because of the ease with which sodium oxide reacts with water, CO_2, etc., it must be introduced as a sodium salt, such as nitrite,

---

*Several possible reactions at the air-liquid or liquid-liquid interface could also have the observed temperature dependence.

which thermally decomposes readily into the oxide. A sodium sulfate-5% sodium nitrite mixture* was prepared and applied to high-purity nickel coupons. The oxidation rate of such a coupon exposed to dry oxygen at 900°C is markedly reduced as shown in Fig. 20. Complete elimination of accelerated oxidation was not obtained nor should be expected since sodium sulfate has a corrosion role akin to that observed for sodium chloride, a "nonreactive" salt, in addition to that outlined above. The observed behavior is a quantitative indication of the corrosion severity caused by this aspect of the sulfate role.

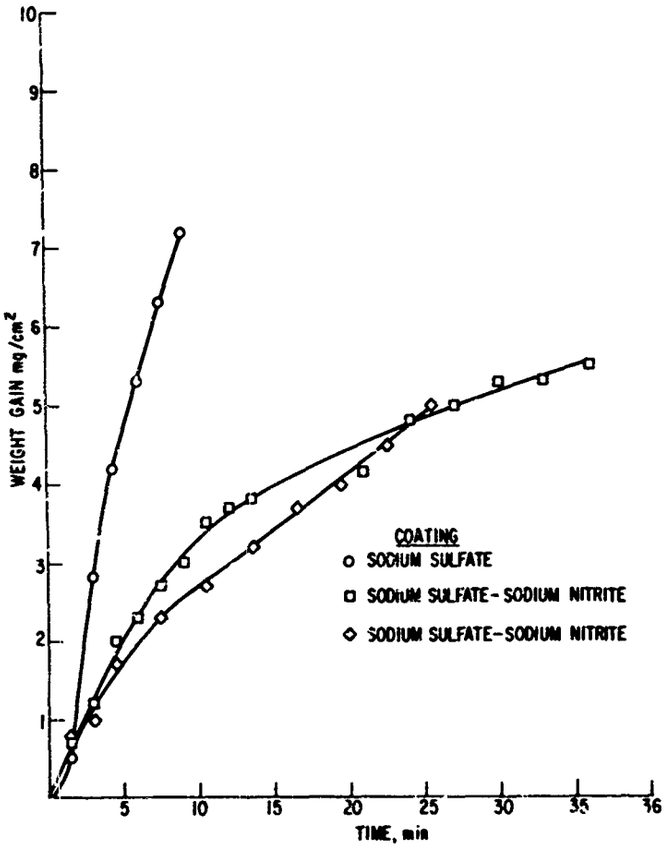

Fig. 20 Oxidation of high-purity nickel in dry oxygen at 900°C when coated with sodium sulfate-sodium nitrite mixtures.

When the sulfate-nitrate mixture is applied to commercial nickel, about a fivefold reduction in oxidation rate is noted as shown in Fig. 21 for exposure to dry oxygen at 900°C. The results can be expected since manganese impurity atoms are capable of reducing the sulfate even in the presence of this concentration of sodium oxide. As discussed earlier, the oxidation of manganese sulfide can release sulfide and then react with the nickel.

Caution in assigning a definite fraction of the corrosion to impurities must be used since impurities can be expected to have influences other than the one just indicated. One can distinguish by a simple experiment between the "internal" contribution as sulfide former and "external" one in which the sulfate-oxide film composition, structure, etc., is affected. If a nickel coupon is coated† with a sulfate-chromium oxide powder mixture, the oxidation at 900°C in dry oxygen is sharply reduced to almost normal oxidation (Fig. 22). The effect is nearly the same when the chromium oxide is replaced by either iron oxide or aluminum oxide. When nickel oxide, cobalt oxide, or magnesium oxide is used the reduction is minor or negligible. In general, amphoteric oxides seem most effective. The specific nature of the oxide activity in the sulfate film is under investigation.

*The composition was chosen to form sodium oxide in some excess since complete decomposition of the nitrite could not be assured.

†To form a coating about 3.0 mg/cm² of which one-half is oxide.

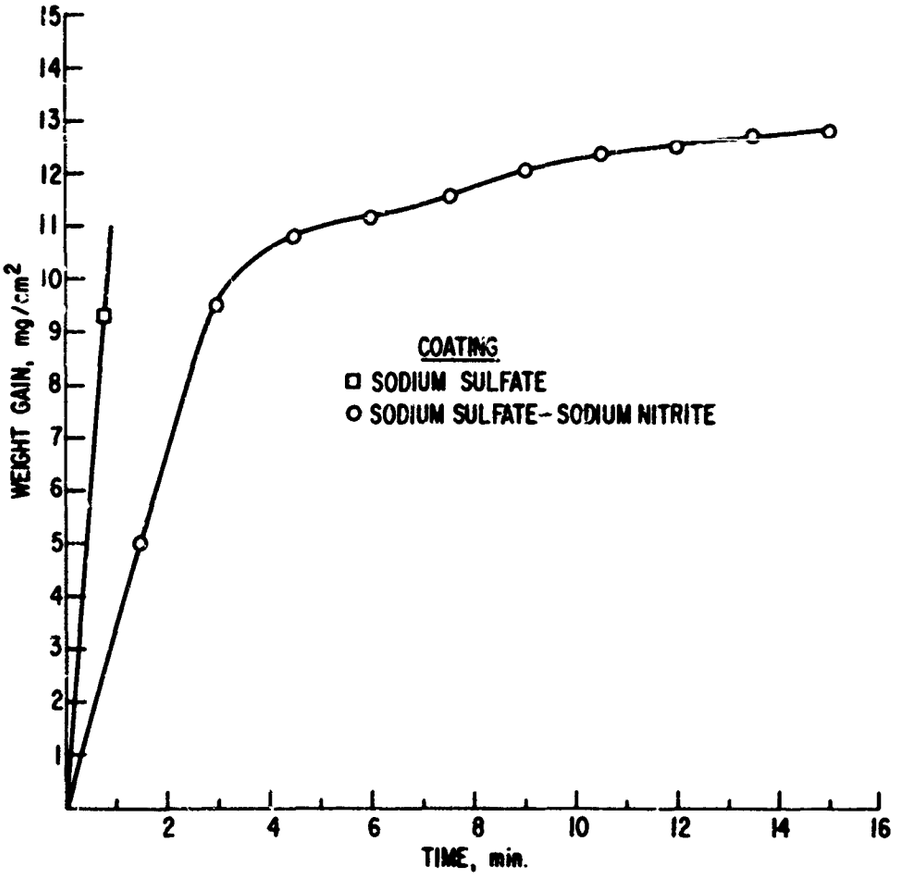

Fig. 21 Oxidation of nickel in dry oxygen at 900°C when coated with sodium sulfate-sodium nitrite mixtures.

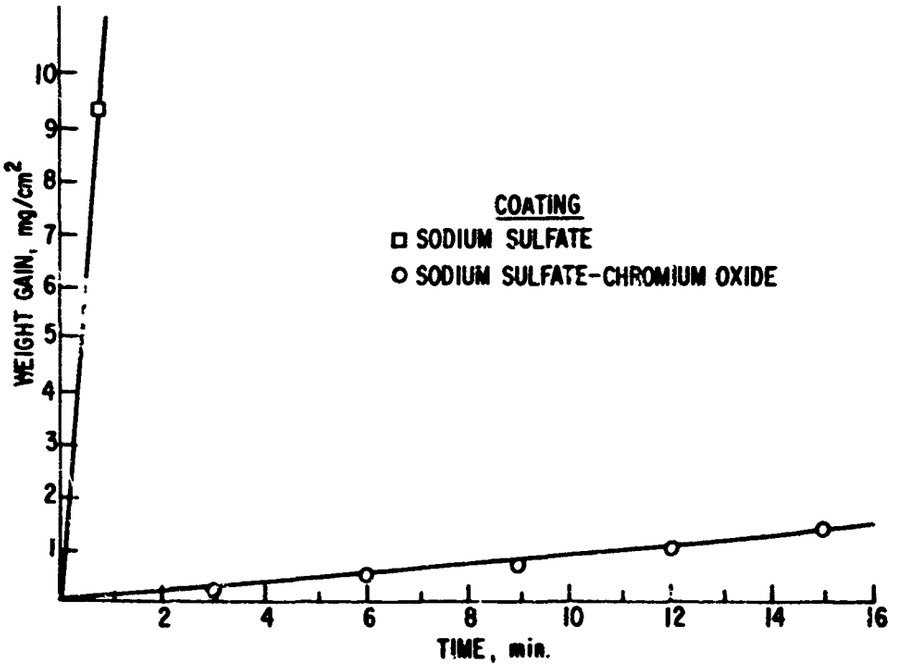

Fig. 22 Oxidation of nickel in dry oxygen at 900°C when coated with sodium sulfate-chromium oxide mixtures.

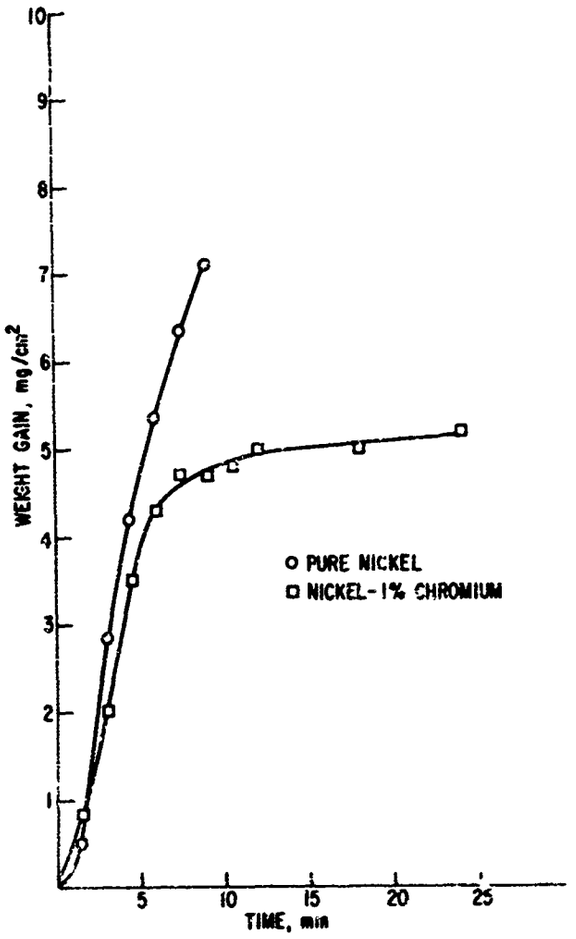

Fig. 23 Oxidation of a nickel-1% chromium alloy in dry oxygen at 900°C when coated with sodium sulfate.

The oxidation behavior of a nickel-1% chromium alloy in dry oxygen at 900°C is shown in Fig. 23. The rate should increase initially because of the "internal" sulfidation effect and when the chromium oxide concentration in the sulfate film increases sufficiently, the "external" effect causes the reaction to cease prematurely. Only the latter effect is noted.

V. STUDIES OF NICKEL AND COBALT ALLOYS

The initial oxidation kinetics of several simple and complex alloys were measured in the presence of thin molten salt films, also. The results of these studies are summarized in this section. Three categories of materials were studied:

1. Binary nickel-chromium and cobalt-chromium alloys.

2. Ternary alloys containing either nickel and chromium or cobalt and chromium.

3. Commercial alloys.

Experimental methods remained essentially the same as for nickel. The nickel-chromium and cobalt-chromium binary alloys studied were prepared by vacuum induction melting. The cast material was hot- and cold-rolled into sheets 20 mils thick from which specimens were cut. The commercial alloys studied were cut into plates from 20 to 40 mils. The ternary alloy specimens were cut from cast ingots into plates also.

A. Binary Alloys

1. Nickel-Chromium

Three compositions, 10, 20, 30 w/o chromium, were prepared and studied. Coupons made from the 10% chromium alloy composition were coated with sodium sulfate and exposed to dry oxygen at 900°, 850°, and 800°C. The weight gains indicate an increasing rate of attack with increasing exposure temperature, shown in Fig. 24. The weight change of an uncoated specimen is included for reference and is somewhat greater than that of the coated specimen under the same exposure conditions. The weight change behavior appears to be approximately parabolic under all conditions (Fig. 25). A photomicrograph of the sectioned and polished specimen exposed to 850°C is shown in Fig. 26. At least one distinct second phase is present, mainly along grain boundaries at the corroding front.

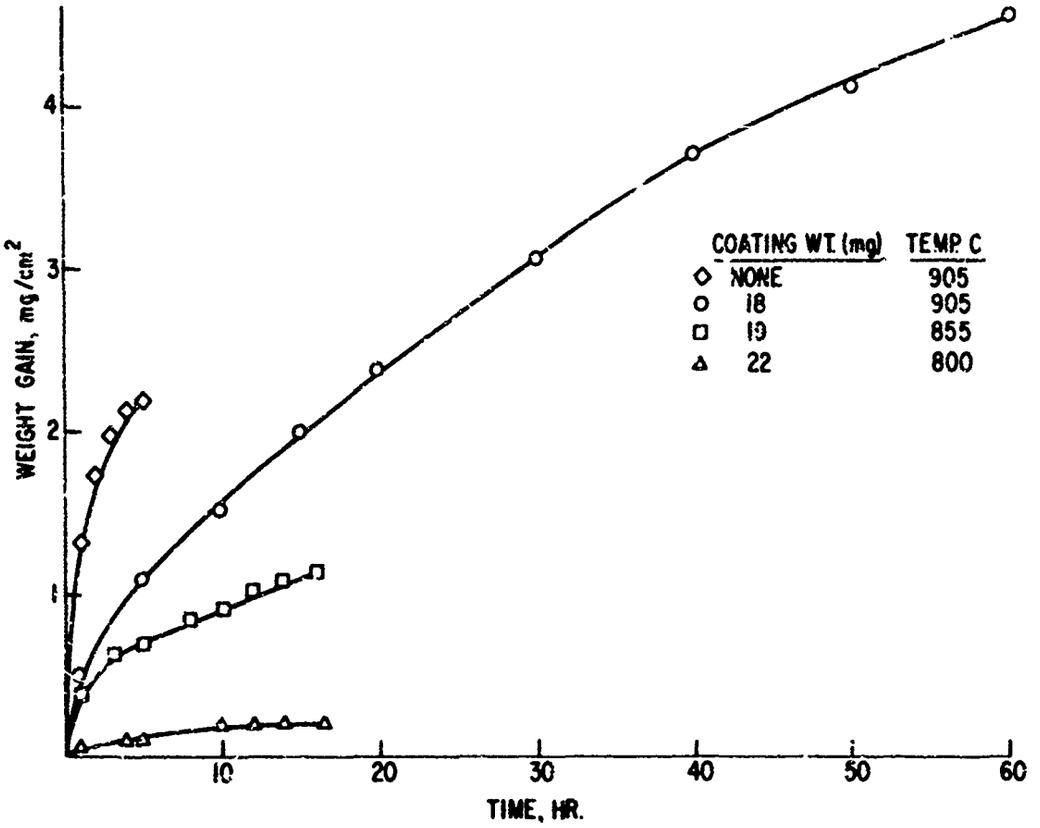

Fig. 24 Weight gain of nickel-10% chromium alloy coated with sodium sulfate during exposure to dry oxygen.

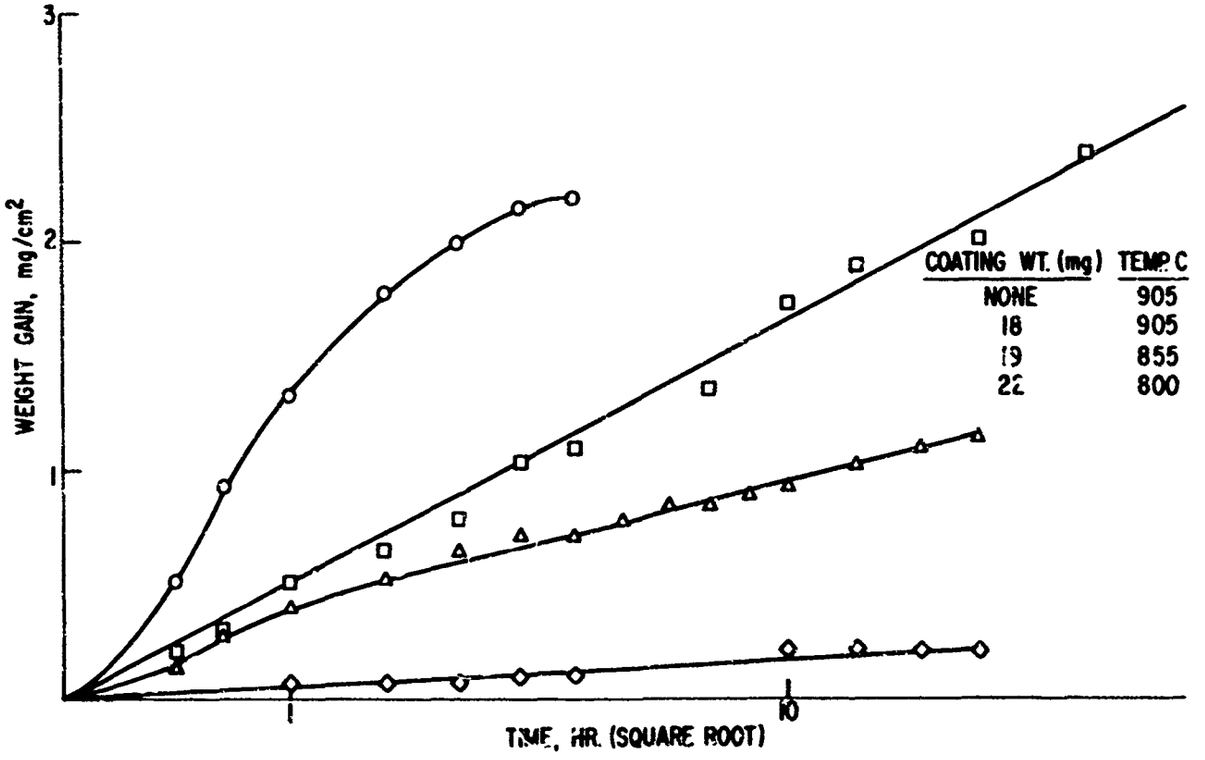

Fig. 25 Weight gain of nickel-10% chromium alloy coated with sodium sulfate during exposure to dry oxygen.

Fig. 26 Nickel-10% chromium alloy coated with sodium sulfate exposed to dry oxygen at 855°C for 16 hours (NC1-2a).

Specimens of 20% chromium alloys, coated with sodium sulfate and exposed to dry oxygen at 850° and 900°C, gained less weight than the 10% alloy. The weight change kinetics can be roughly described as parabolic and appear similar in magnitude to that of an uncoated specimen exposed at 900°C as indicated in Fig. 27. Nickel (without chromium additions) corrosion data are included for reference.

The weight change behavior of specimens made from the 10% and 20% chromium alloys and exposed to wet oxygen (saturated at room temperature) was not significantly different from that observed previously in dry oxygen.

Nickel (10% chromium alloy) specimens coated with a mixture of 50% sodium sulfate-50% sodium chloride were also exposed to wet oxygen at 850° and 900°C. The weight gain of these specimens was essentially the same as that observed for specimens coated with pure sodium sulfate and exposed under the same conditions.

Other 10% chromium alloy specimens were coated with sodium sulfate and were heated at 900°C under a wet or dry argon atmosphere for 15 minutes and subsequently under wet oxygen. No effect on the weight gain behavior was observed by the pretreatments in argon, despite the fact that specimens reacted with sodium sulfate under a wet or dry argon atmosphere for 1 hour at 900°C showed considerable evidence of interaction as illustrated in Fig. 28.

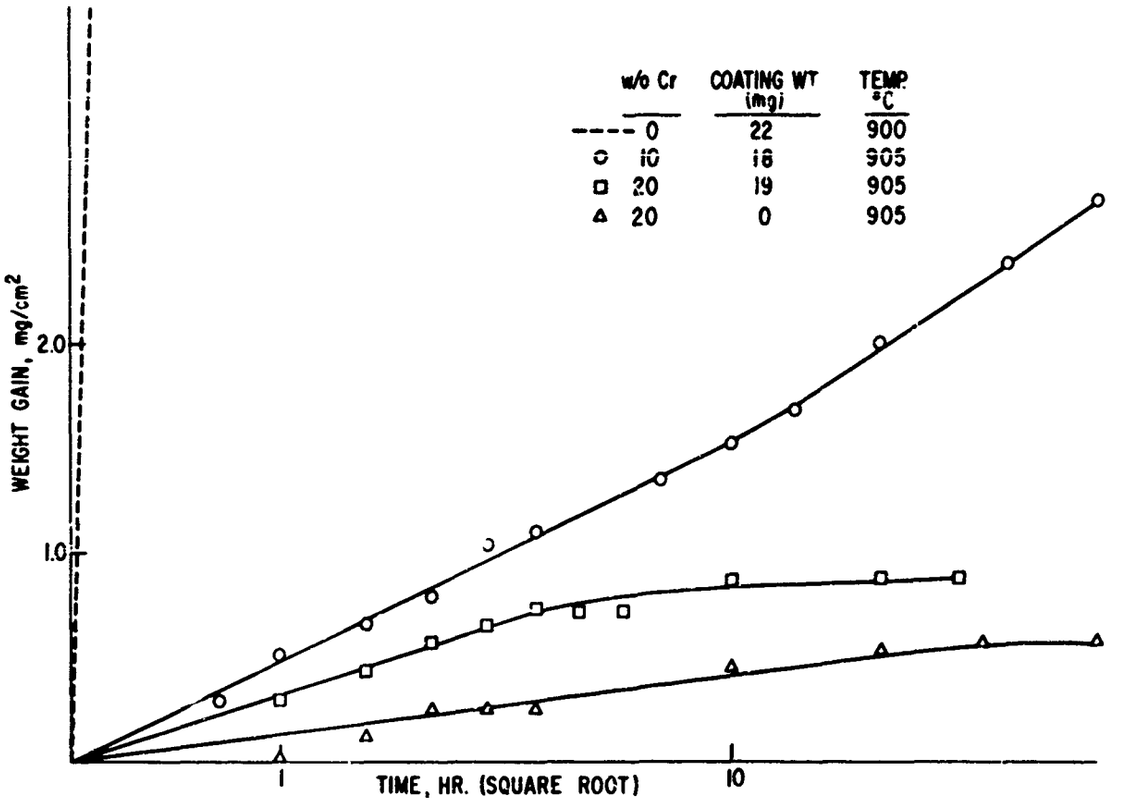

Fig. 27 Weight gain of nickel, -0%, -10%, -20% chromium alloys coated with sodium sulfate.

Fig. 28 Nickel-10% chromium alloy coated with sodium sulfate pretreated in wet argon and exposed to wet oxygen at 900°C for 4 hours (NC1-3). 500X

Heat treatments of this kind (under argon) were conducted with nickel-20% chromium alloy specimens coated with sodium sulfate containing 10 w/o carbon as carbon black particles. Subsequent corrosion in oxygen was enhanced as shown by the weight gain of specimens exposed at 850° and 900°C (Fig. 29). The reversal of the normal temperature dependence in this reaction is not understood, but may be due to spurious effects. The photomicrographs of these specimens (Fig. 30) indicate that attack was not uniform.

Considerable reaction enhancement resulted from presulfidation treatments also. Specimens reacted with hydrogen sulfide (about 5 mg per cm^2 absorption) were exposed to oxygen at 900°C either when uncoated or coated with sodium sulfate. The weight gain behavior of these specimens, along with a coated specimen without pretreatment, during oxygen exposure is shown in Fig. 31. The weight gain of the uncoated specimen was greater than that observed for the coated specimen. This apparent depression of the oxidation rate by the sulfate film was real. A corroding specimen was removed from the furnace during initial oxidation, washed free of sulfate and re-exposed; the rate increased to the higher level associated with the uncoated specimens.

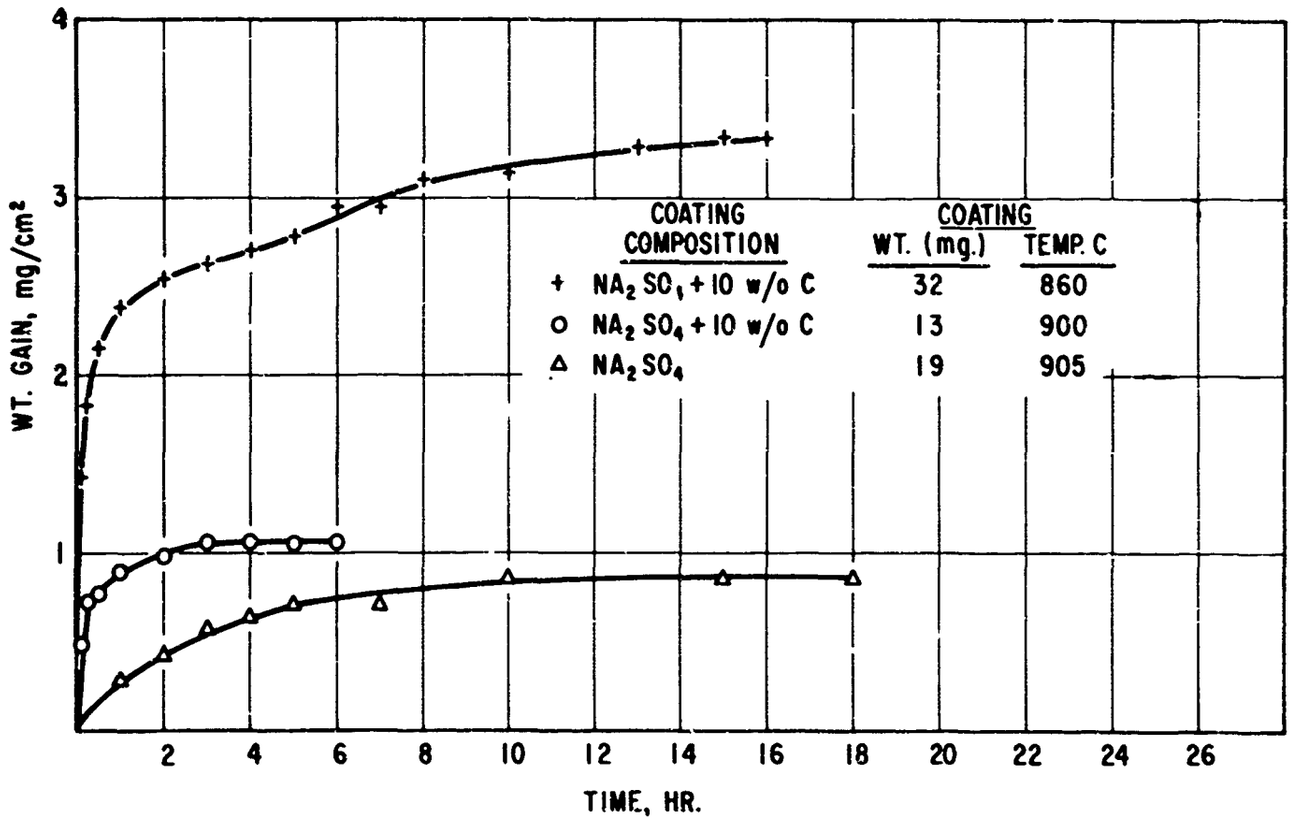

Fig. 29 Weight gain of nickel-20% chromium alloy prereacted with sodium sulfate-carbon mixtures and exposed to dry oxygen.

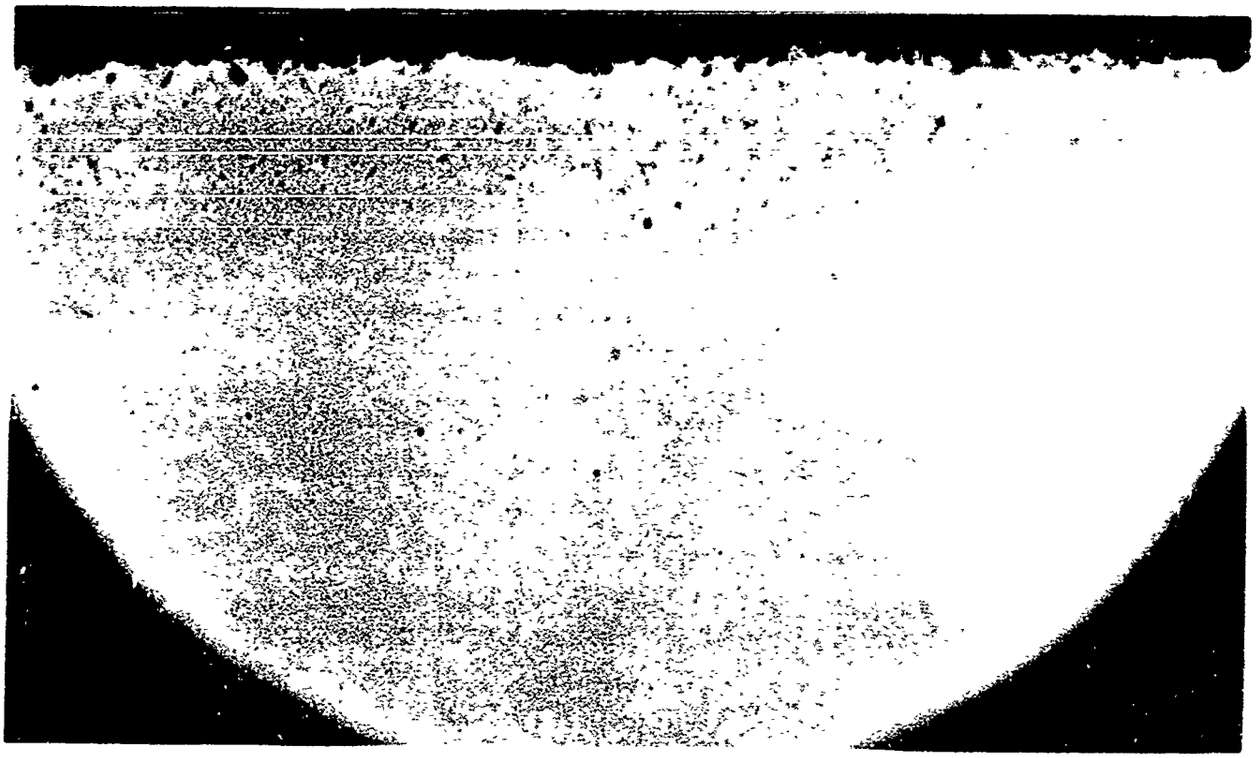

Fig. 30 Nickel-20% chromium alloy coated with sodium sulfate + 10% carbon pretreated in dry argon and exposed to dry oxygen at 900°C for 6 hours (NC2-12). 500X

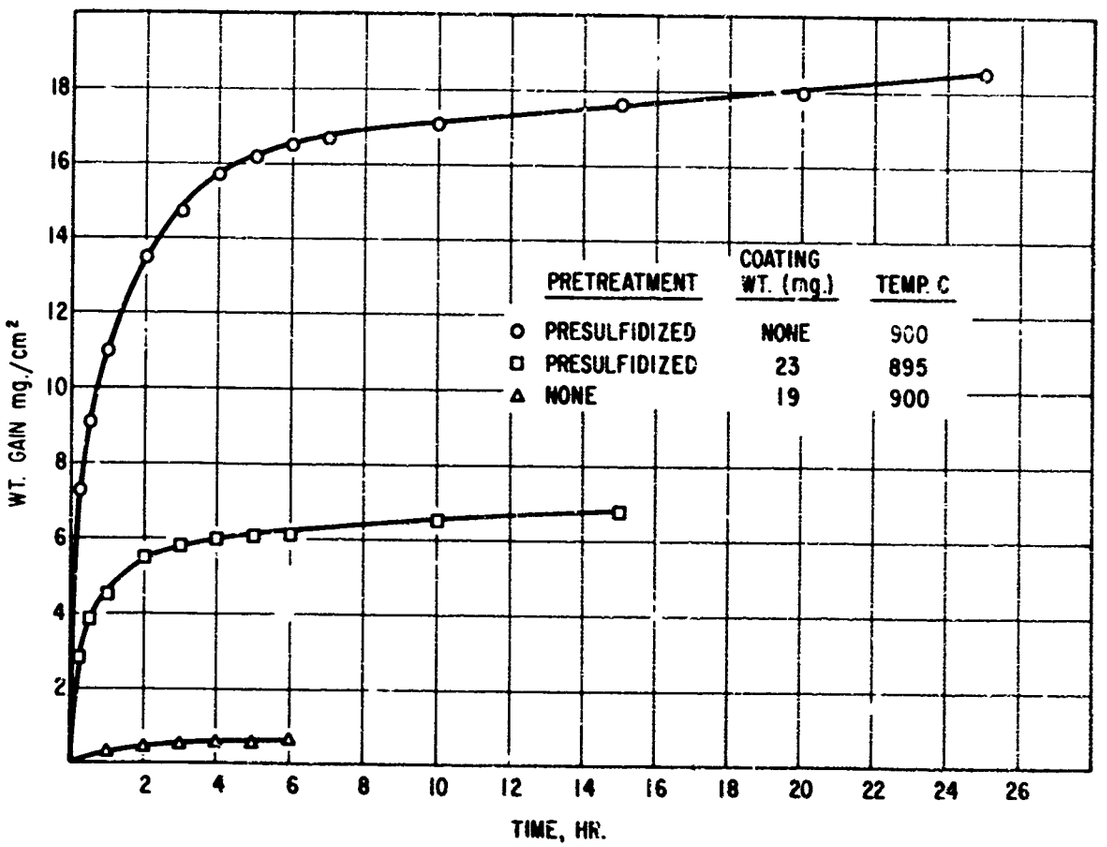

Fig. 31 The weight gain of presulfidized sodium sulfate coated and uncoated nickel-20% chromium alloy exposed to dry oxygen at 900°C.

2. Cobalt-Chromium

Three compositions of cobalt-chromium alloys (10%, 20%, and 30% chromium) were prepared. Coupons made from the 10% chromium alloy were coated with sodium sulfate and exposed to dry oxygen at 850° and 900°C. The weight change, shown in Fig. 32, appeared to be parabolic and to be about the same magnitude as that found for uncoated alloys exposed under the same condition. A nearly parabolic time law was also obeyed during corrosion of a coupon coated with sodium sulfate-50% sodium chloride mixture and exposed to dry oxygen at 850°C, shown in Fig. 33. The weight change of a specimen coated with pure sodium sulfate is somewhat less and is included for comparison. A photomicrograph of a specimen coated with 50% sodium chloride-50% sodium sulfate and exposed at 900°C is shown in Fig. 34. Sulfidation along grain boundaries can be noted.

The weight gain of the 20% chromium alloy also was larger when some of the sodium sulfate was replaced by sodium chloride. Curves are shown in Fig. 35 for the weight change of uncoated and coated coupons exposed to dry oxygen at 900°C.

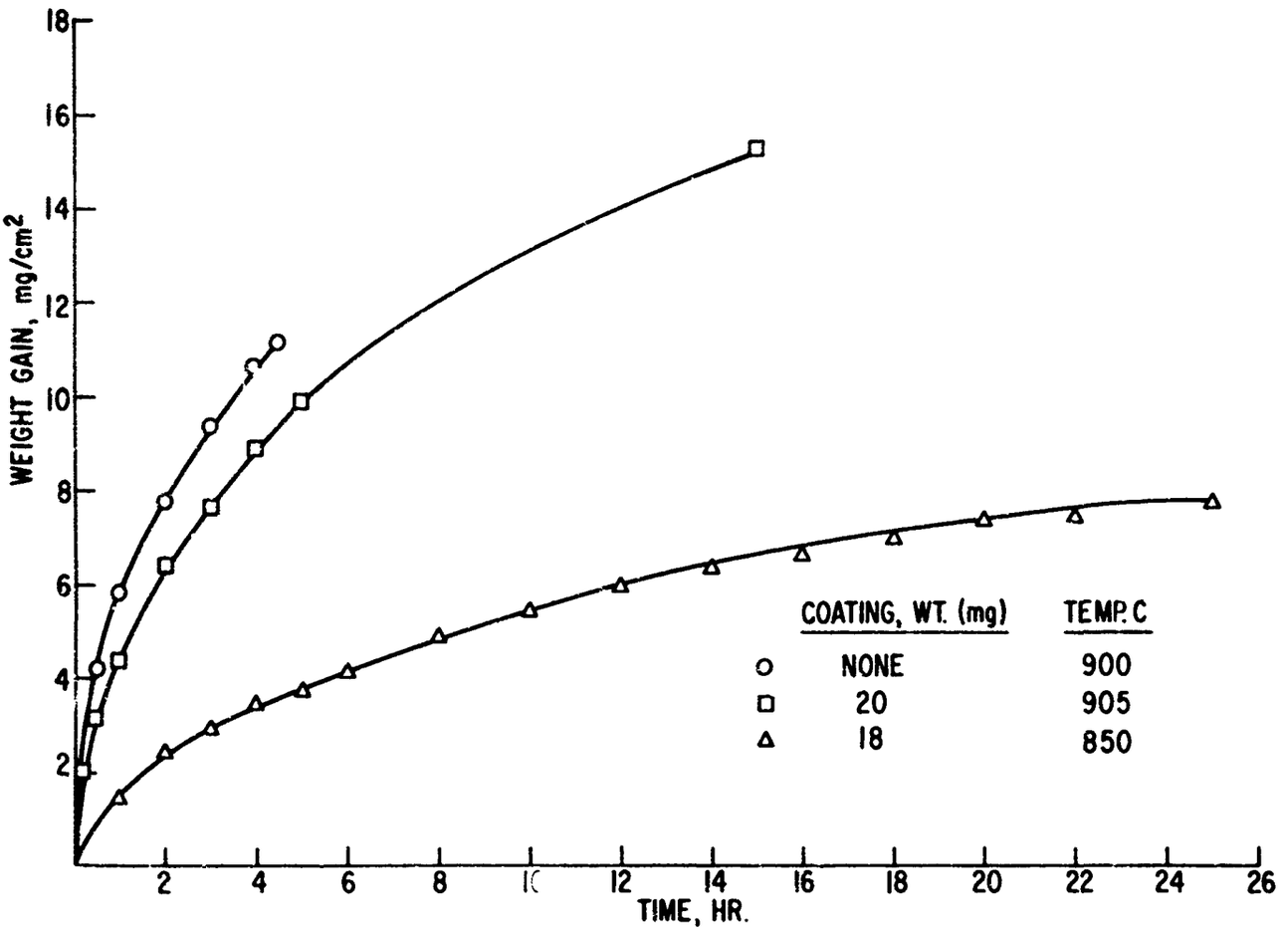

Fig. 32 Weight gain of cobalt-10% chromium alloy coated and uncoated with sodium sulfate during exposure to dry oxygen.

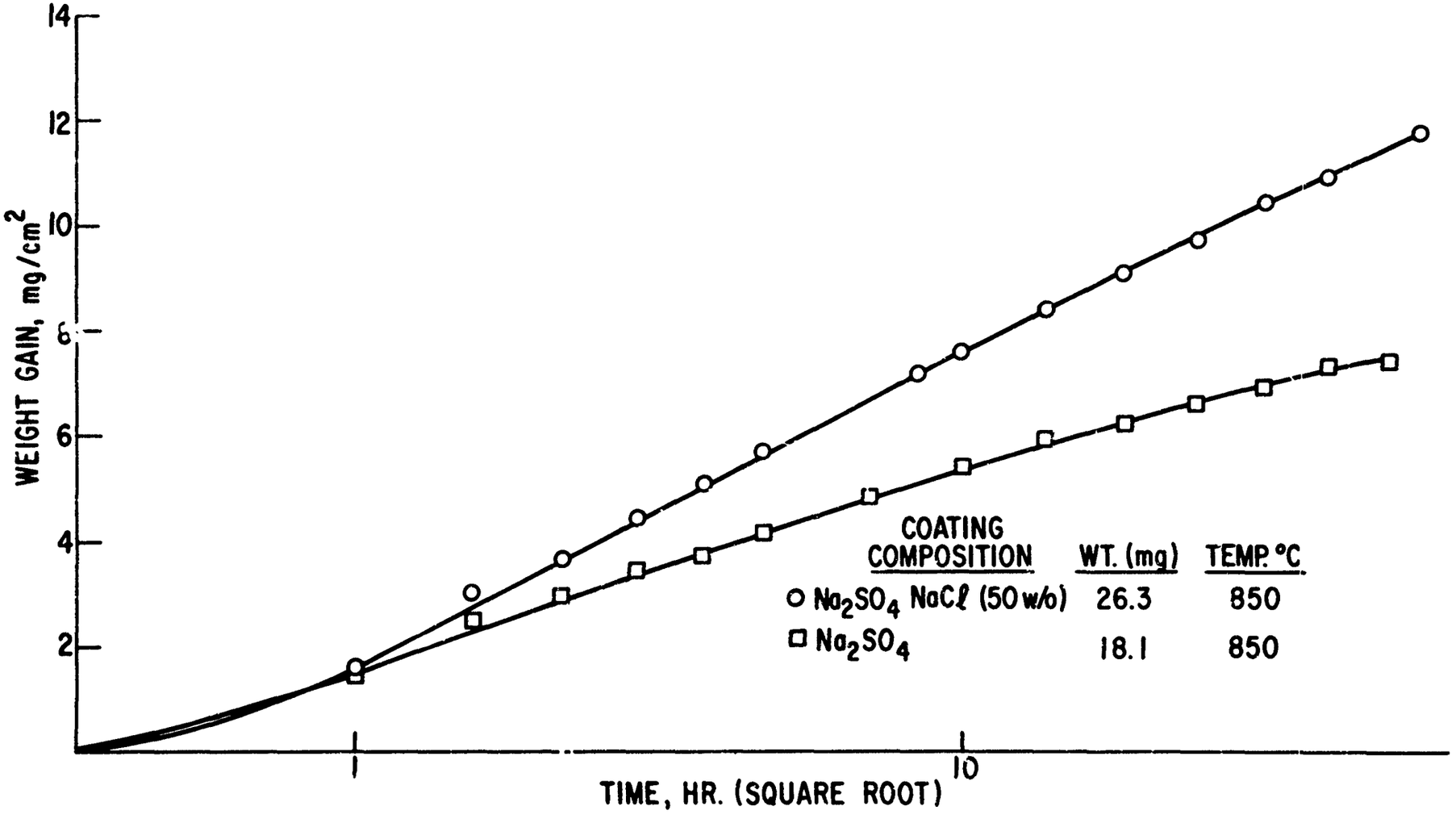

Fig. 33 Weight gain of cobalt-10% chromium alloy coated with sodium sulfate and sodium chloride mixtures.

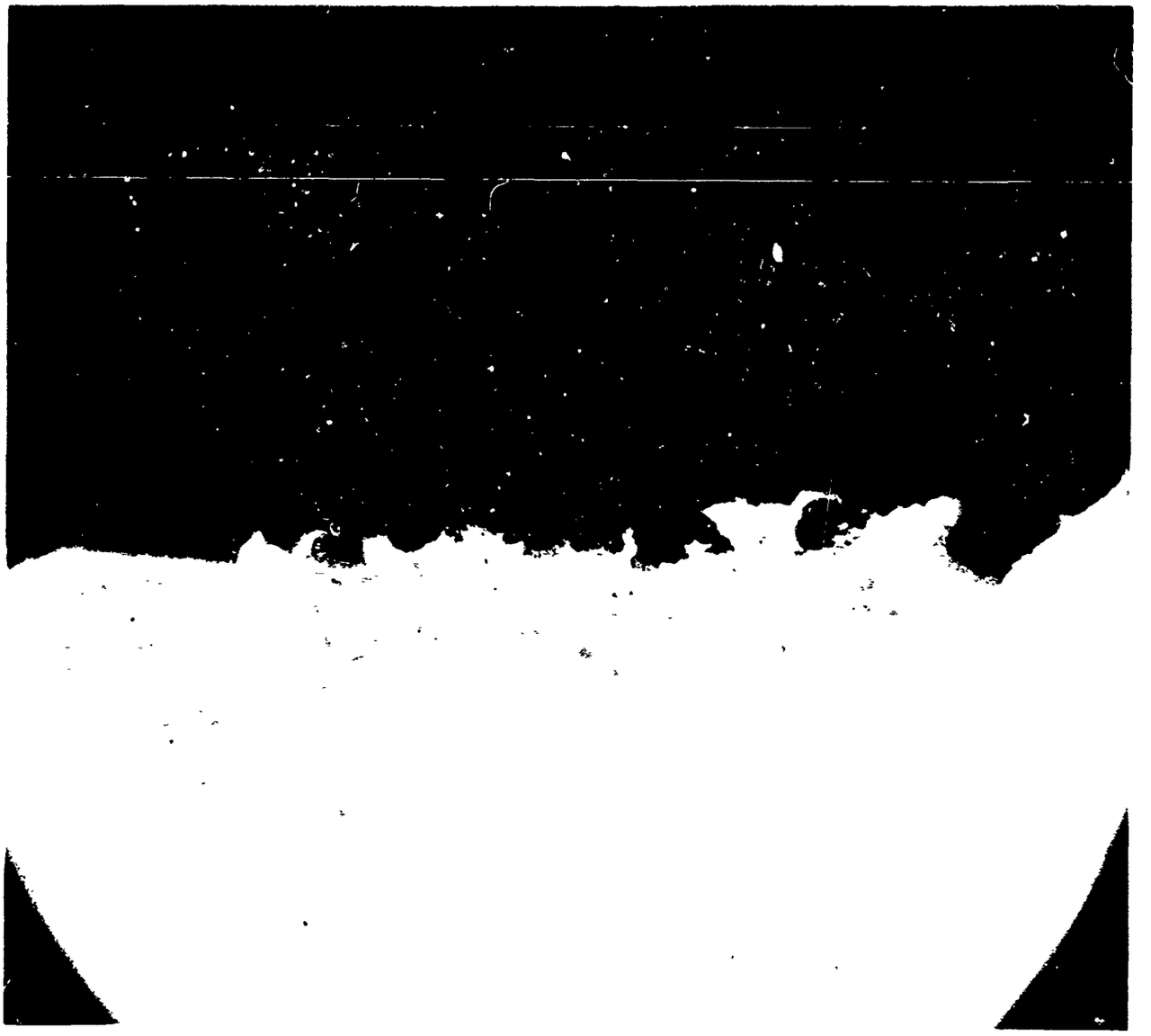

Fig. 34 Cobalt-10% chromium alloy coated with sodium sulfate and exposed to dry oxygen at 905°C for 25 hours (CC1-2). 500X

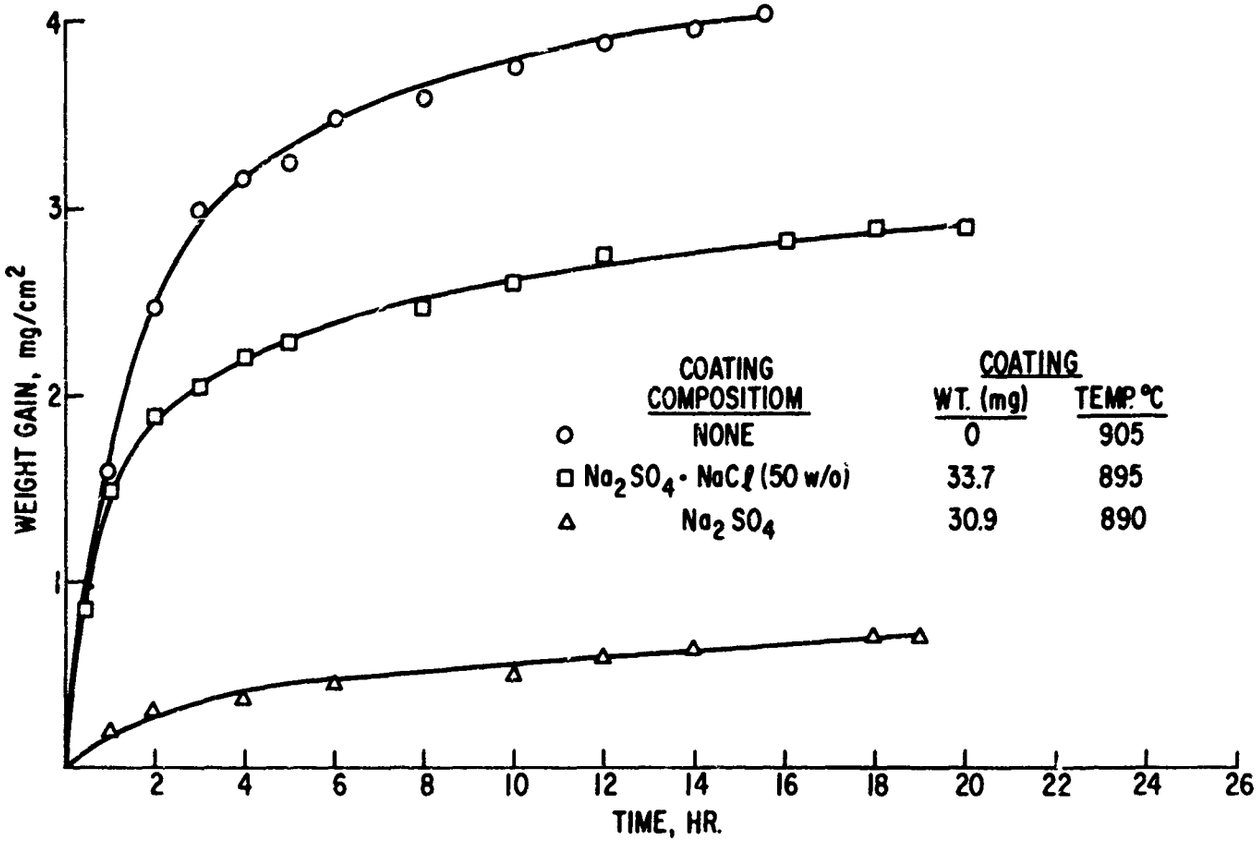

Fig. 35 Weight gain of cobalt-20% chromium alloy uncoated and coated with sodium sulfate during exposure to dry oxygen.

B. Commercial Alloys

A few commercial alloys were studied. Specimens were cut into plates 20 to 50 mils thick using a cutoff wheel. Other specimen preparation was identical to that used in the pure metal and binary studies.

1. 713C Alloy

Specimens made from a 713C alloy were coated and exposed to dry oxygen at 800°, 850°, and 900°C. The resulting corrosion behavior is illustrated in Fig. 36. The corrosion rate appears nearly linear initially, but apparently is more complex. The rate appears to be progressively but slowly increasing with time from initiation. A photomicrograph of the coated specimen exposed to dry oxygen at 900°C, shown in Fig. 37, demonstrates the sulfidation attack normally associated with hot corrosion.

Specimens corroded the same in wet oxygen as in dry oxygen. Specimens coated with sodium sulfate-sodium chloride mixtures (50%) gained weight initially somewhat more rapidly than those coated with pure sodium sulfate. A specimen pre-oxidized for 21 hours at 800°C in air underwent normal corrosion after an initial short incubation period when exposed to sodium sulfate in dry oxygen at 900°C.

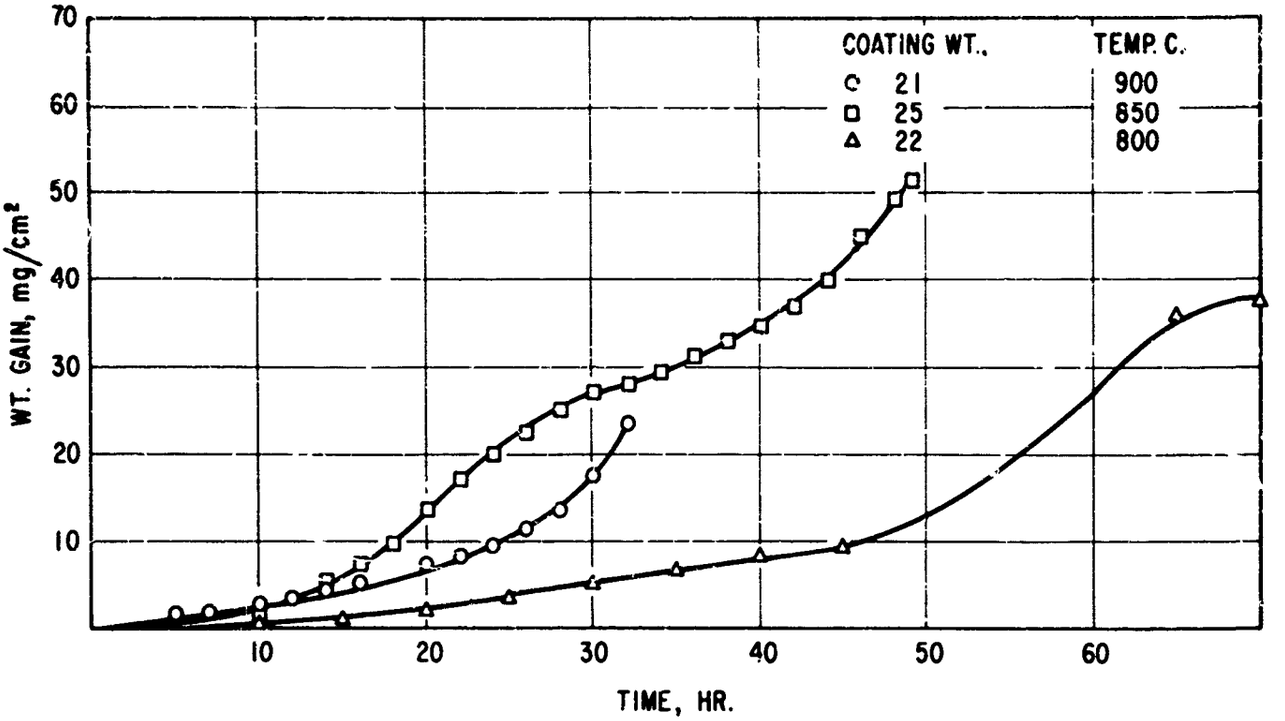

Fig. 36 Weight gain of sodium sulfate coated Inco 713C exposed to dry oxygen at various temperatures.

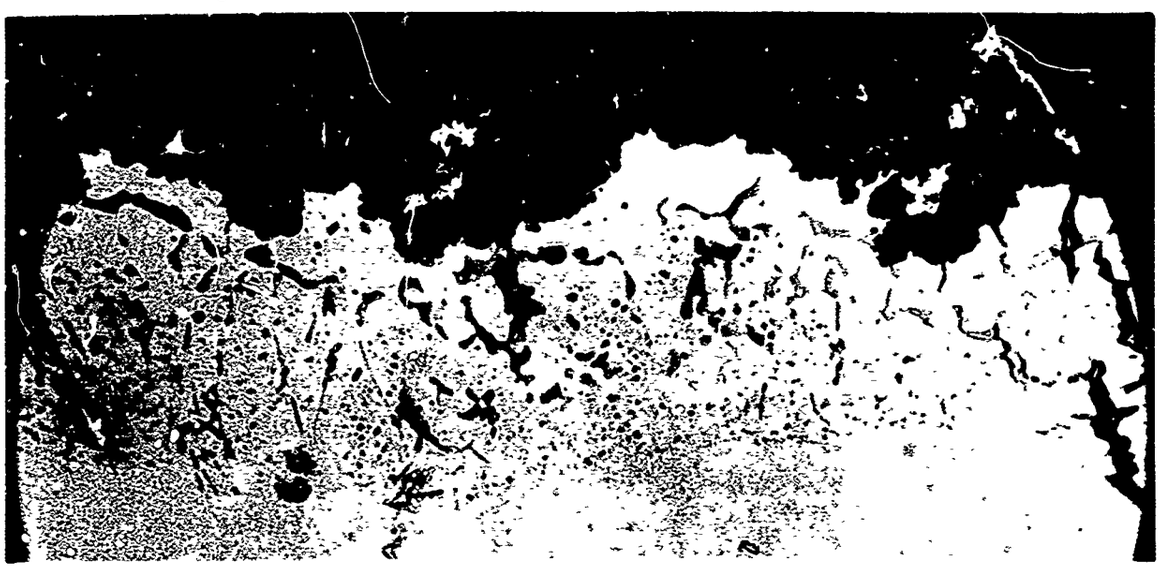

Fig. 37 Commercial alloy 713 coated with sodium sulfate and exposed to dry oxygen at 900°C for 33 hours (713-2). 500X

2. SEL Alloy

The other nickel-base alloy tested, SEL, was coated with pure sodium sulfate and a sulfate-chloride mixture. Although the weight change kinetics of the specimen appear to be complex and nonreproducible when exposed to oxygen at 900°C, the sulfate-chloride mixture apparently caused a more severe corrosion than the pure sulfate. The photomicrograph of the specimen exposed to sodium sulfate (Fig. 38) shows considerable sulfidation.

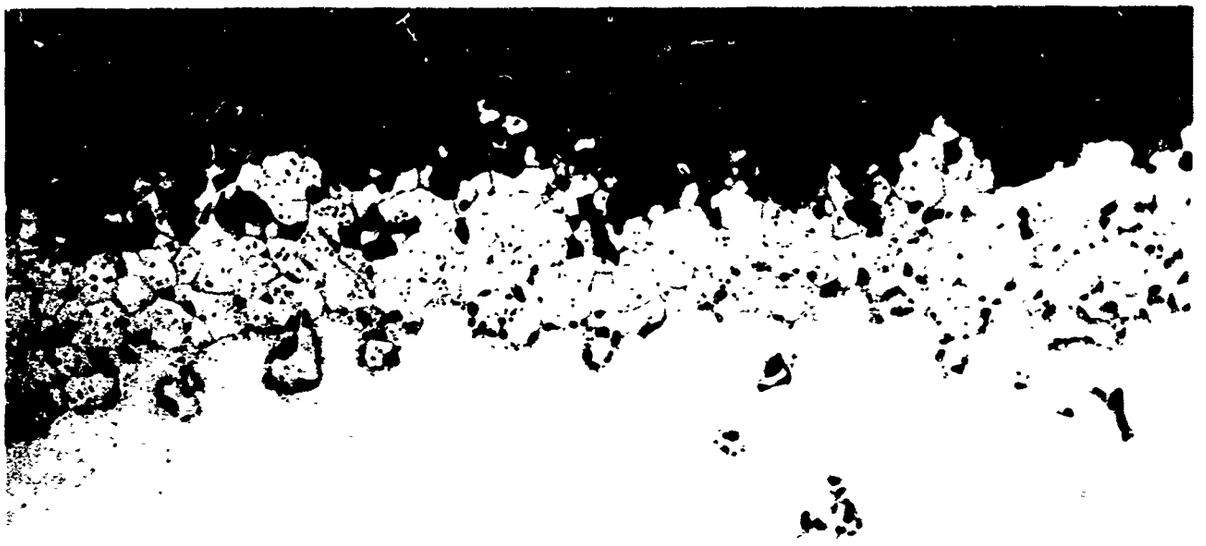

Fig. 38 Commercial alloy SEL coated with sodium sulfate and exposed to dry oxygen at 900°C for 70 hours (SEL-1). 500X

3. 509 Alloy

Only one commercial cobalt-based alloy has been tested. A specimen coated with sodium sulfate and with sodium sulfate-sodium chloride mixtures were exposed at 900°C. The weight change behavior is shown in Fig. 39.

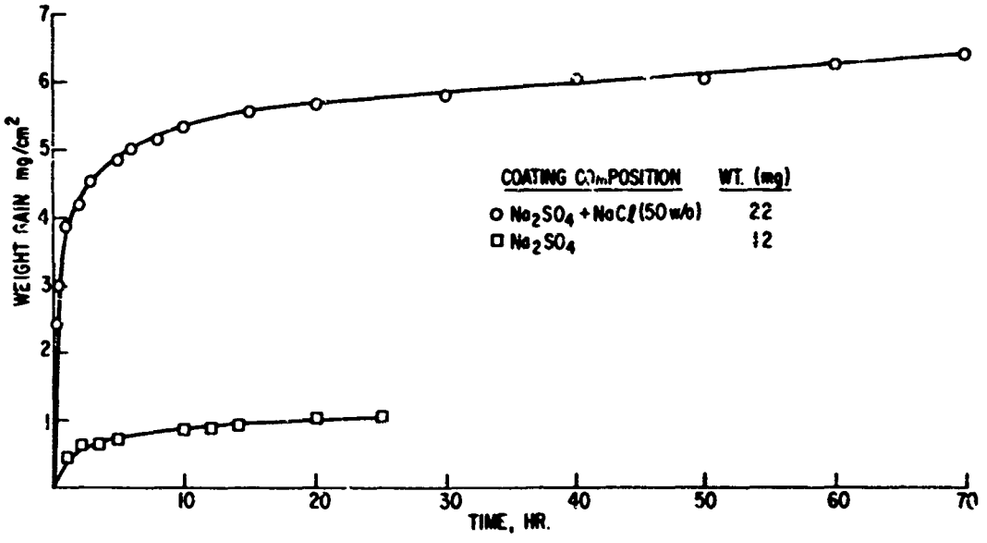

Fig. 39 Weight gain of coated 509 in dry oxygen at 900°C.

C. Ternary Alloys

1. Nickel-Chromium Base

The effects of several singly added additives on the corrosion rates of a nickel-15% chromium alloy were investigated. Coupons of four different compositions were coated with sodium sulfate and exposed to dry oxygen at 900°C. Weight gains are shown in Fig. 40. The composition containing 6% molybdenum was most severely attacked; the initial, linear oxidation rate appeared to increase after 10 hours' exposure. Rapid oxidation continued until the specimen was completely consumed. The oxidation of the alloy containing 8% aluminum appeared to be increasing in the initial period, but after about 20 hours the rate decreased. Alloys containing 8% tungsten or 5% titanium oxidized slowly.

In another experiment, the molybdenum composition was exposed to oxygen at 900°C without a sodium sulfate coating. Although the rates were lower, the behavior was similar to that observed with sulfate present. As shown in Fig. 41, the oxidation acceleration occurred later at about 20 hours, and then continued at the accelerated rate until all the alloy was consumed.

The alloys in this series were also presulfidized by treatment with H_2S. The sulfidation resistance based on total weight gains increased with additives

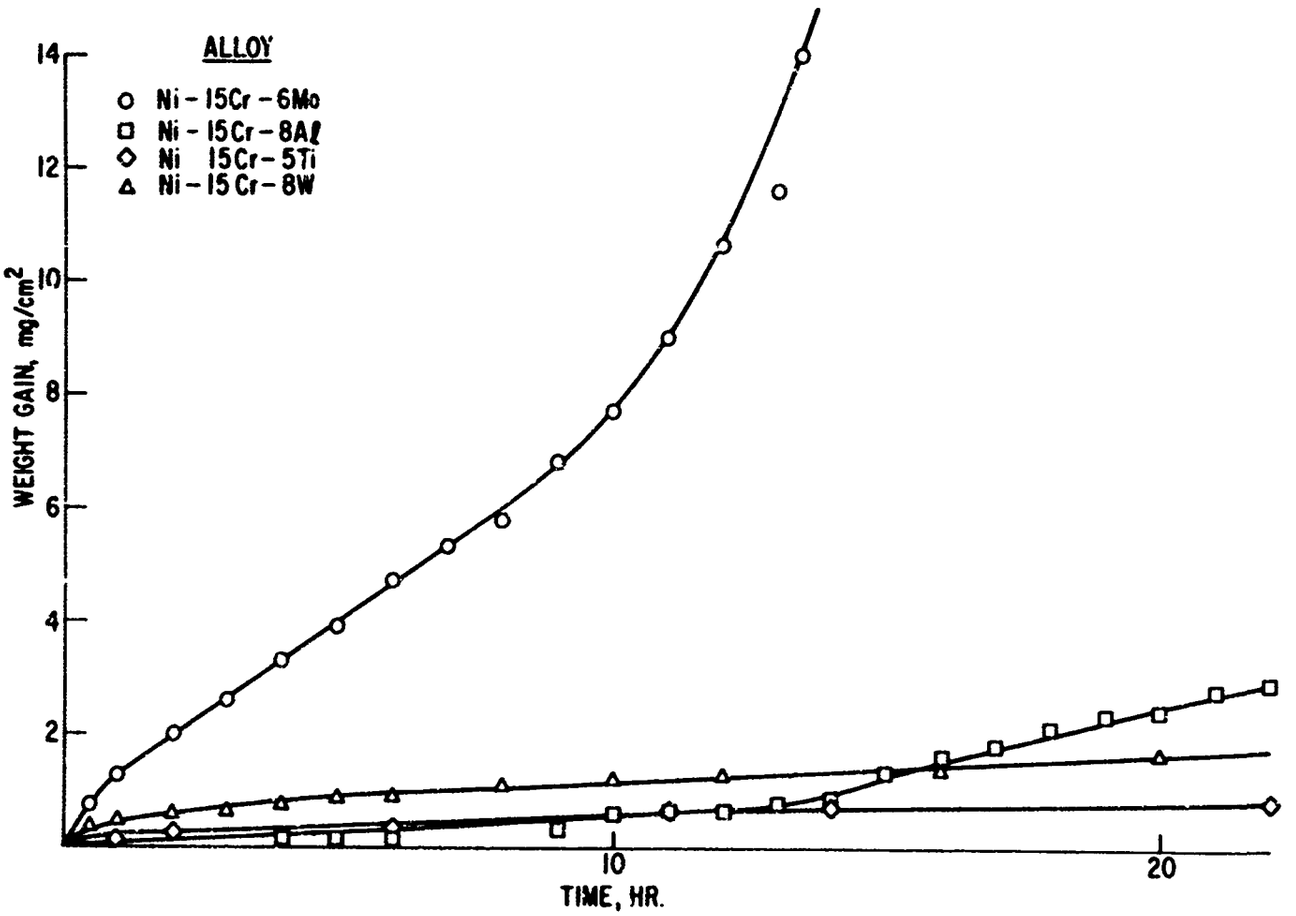

Fig. 40 The weight gain of several nickel-base alloys coated with sodium sulfate and exposed to dry oxygen at 900°C.

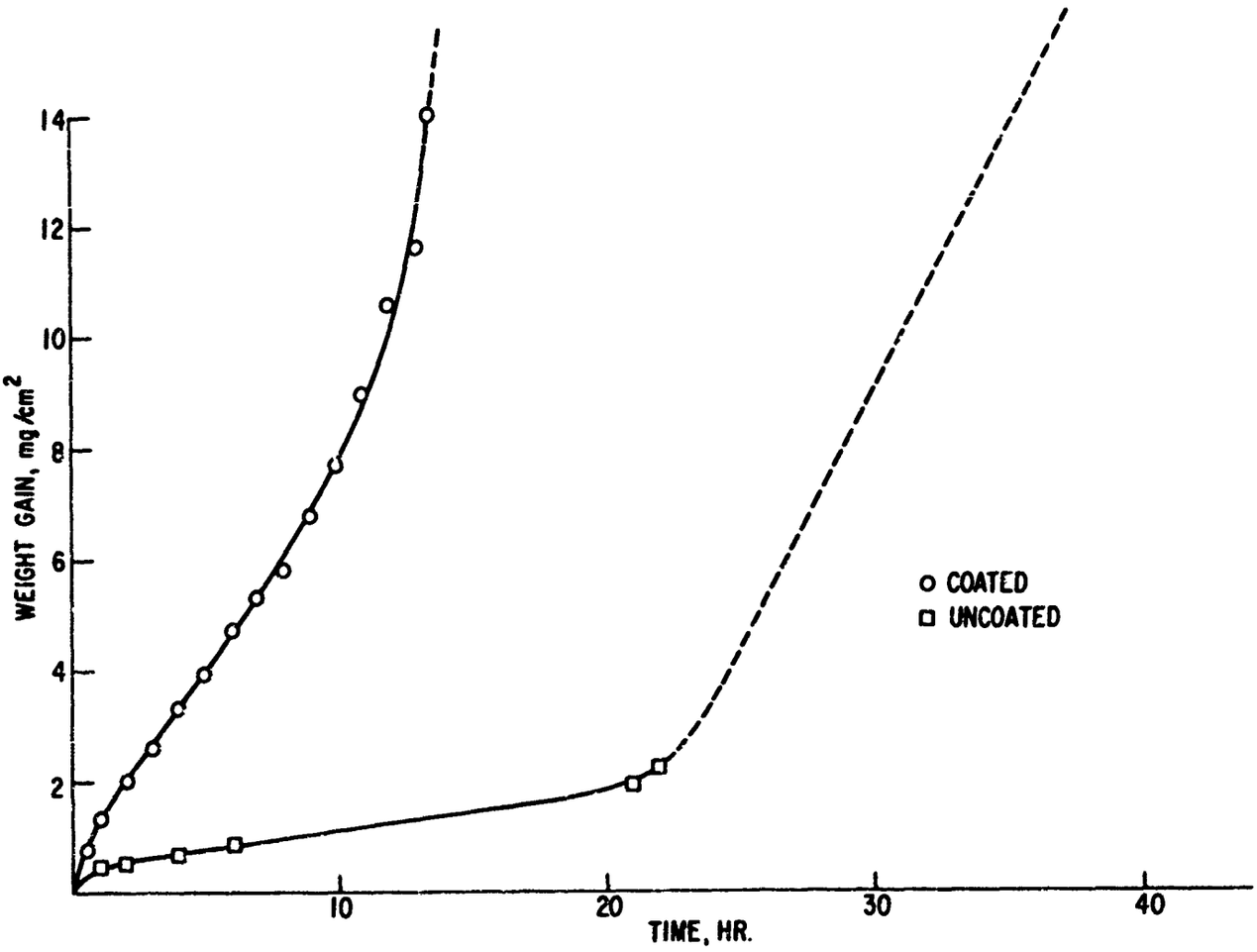

Fig. 41 The weight gain of a nickel-15% chromium-6% molybdenum alloy with and without a sodium sulfate coating during exposure to dry oxygen at 900°C.

in the order: molybdenum, tungsten, titanium, aluminum. This order does not correlate with sulfate-induced oxidation behavior because of the changing position of aluminum in the two ranked orders. In the oxidation studies, aluminum appeared to degrade the oxidation resistance of the nickel-chromium alloy. One alloy, with 8% titanium, was presulfidized to the extent of 3.5 mg/cm^2, before being exposed to oxygen at 900°C, and oxidized as shown in Fig. 42. The initial rapid weight gain rate changed in about 1 hour to what appears to be normal parabolic behavior.

2. Cobalt-Chromium Alloys

Several additive alloys based on the cobalt-25% chromium composition were studied. An alloy containing 6% molybdenum, whether coated with Na_2SO_4 or uncoated, oxidized mildly. The oxidation rates in both cases appeared to be parabolic, at 900°C in dry oxygen. The oxidation rates of a coupon coated with a sodium sulfate-sodium chloride mixture (50%) and exposed to the same conditions were significantly higher.* The weight change curve shown in Fig. 43 indicates

*Cobalt metal was also appreciably attacked when sodium sulfate-chloride mixtures were used. Sodium chloride alone, in contrast to sodium sulfate, enhanced oxidation.

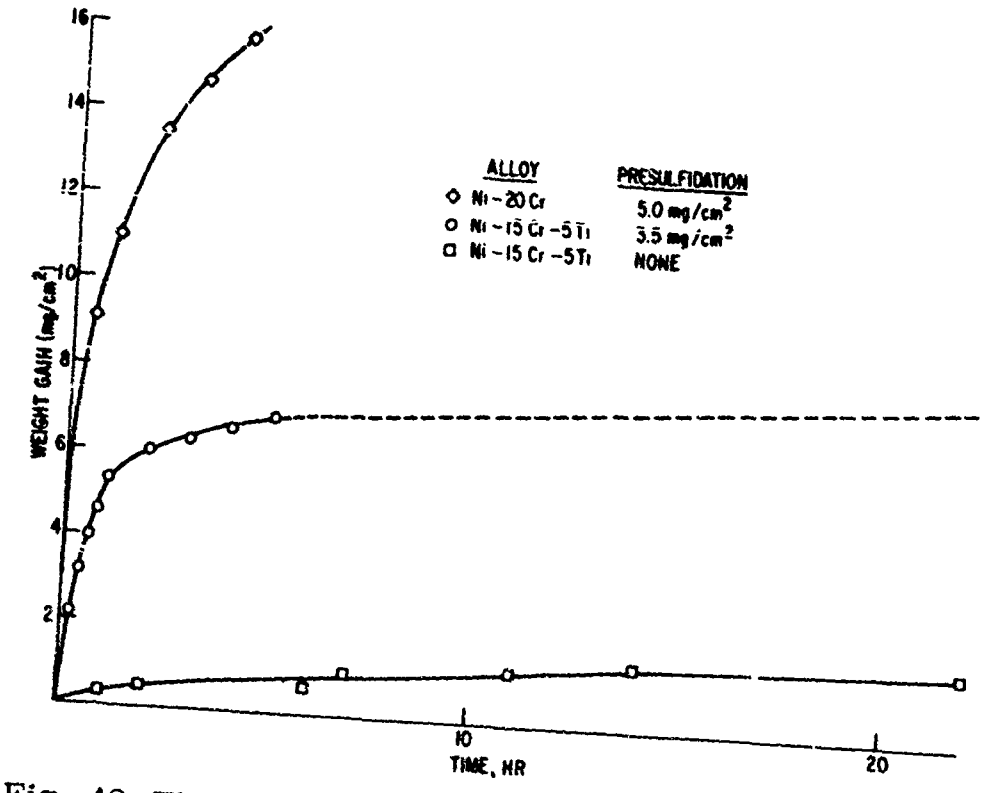

Fig. 42 The weight gain of a presulfidized nickel-15% chromium-8% titanium alloy exposed to dry oxygen at 900°C.

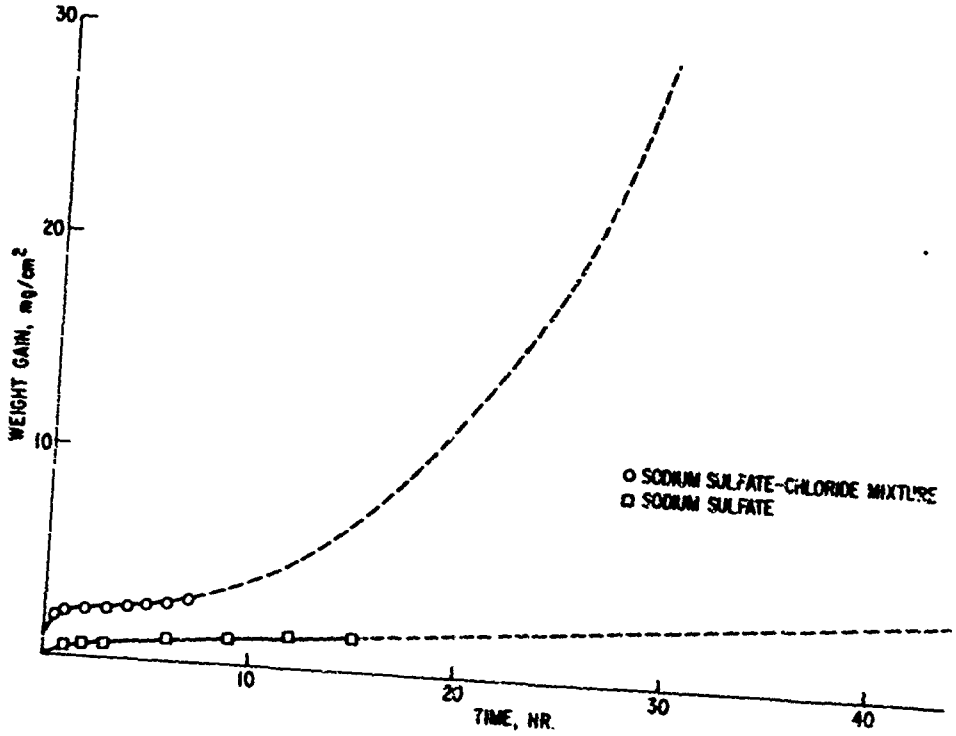

Fig. 43 The weight gain of a cobalt-25% chromium-6% molybdenum alloy exposed to dry oxygen at 900°C with either a sodium sulfate or a sodium sulfate-chloride coating.

that three stages of oxidation can be distinguished. A rapid, initial oxidation in the first hour is followed by a period of decreasing rate of oxidation. After several hours, the oxidation rate increases gradually until the metal is consumed.

The "first stage" rapid initial oxidation was also observed with coupons having tungsten or tantalum additives (8%) exposed to dry oxygen at 900°C. As illustrated in Fig. 44 (for the tungsten additive), no "third stage" rapid oxidation occurred comparable to that observed when molybdenum was the additive.

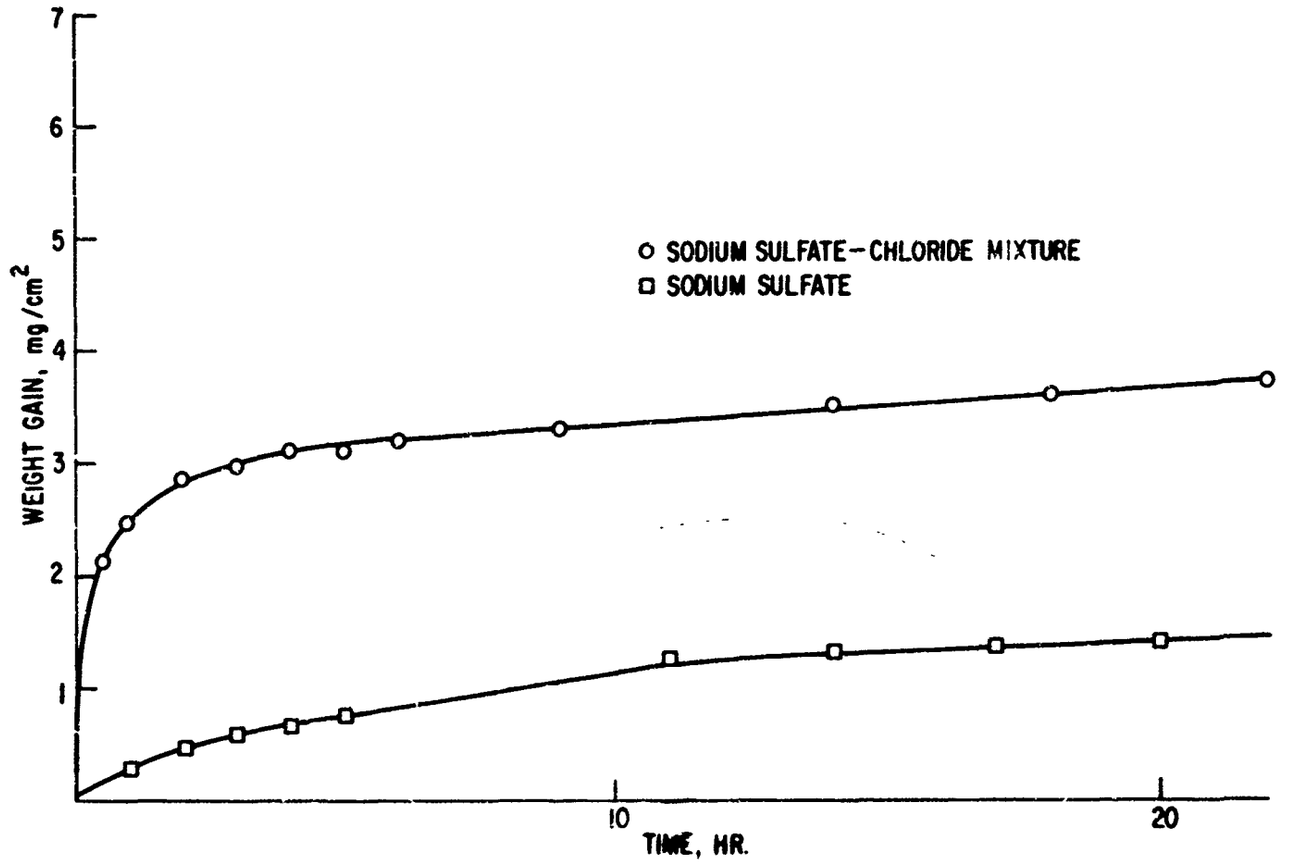

Fig. 44 The weight gain of a cobalt-25% chromium-8% tungsten alloy exposed to dry oxygen at 900°C with either a sodium sulfate or a sodium sulfate-chloride coating.

VI. SUMMARY AND CONCLUSIONS

Sodium sulfate was found to penetrate nickel oxide films on nickel at temperatures well below the melting point of sodium sulfate. When the sulfate contacted the metal accelerated oxidation of nickel was induced, but the rapid-initial oxidation ceased before either sulfate or nickel was consumed.

The initial oxidation kinetics of nickel coated with a thin film of sodium sulfate are determined using continuous weight change measurements. Based on the results of these studies and of experiments on related reactions, mechanisms for initial oxidation are proposed for several conditions. The primary role of sodium sulfate in the reaction appears to be a reservoir that maintained a sulfide-rich film at the metal surface through the cyclic reactions:

$$Na_2SO_4 + 9/2\ Ni \rightarrow Na_2O + \frac{1}{2} Ni_3S_2 + 3\ NiO \qquad (12)$$

$$Ni_3S_2 + 9/2\ O_2 \rightarrow 3\ NiO + 2SO_3 \quad (13)$$

$$Na_2O + SO_3 \rightarrow Na_2SO_4\ . \quad (14)$$

At 825°C and below, the oxidation rate and probably mechanism differ, probably depending on the sulfide film thickness. Both water vapor in the oxygen and impurities in the metal can cause appreciable increase in rates. A high activation energy process such as diffusion of sulfur into the metal or oxygen or metal ions in nickel oxide is probably rate limiting in these reactions. At 850°C and above, diffusion through the sulfate or sulfide film is probably rate controlling. The dual role of impurities in these reactions is demonstrated.

REFERENCES

1. E. Bradbury, P. Hancock, and H. Lewis, Metallurgia, 67, 3 (1963).
2. P. Bergman, "Saline Corrosion of Aircraft Gas Turbines Materials at Temperatures up to 2000F," General Electric Co. Rept. No. R 64-SE10 (April 1964).
3. P. Sulzer, ASME Paper No. 54-A-171.
4. E. Simon, G. Browning, and H. Liebhafsky, Corrosion, 11, 17 (1955).
5. C. Ilschner-Gensch, J. Electrochem. Soc., 105, 635 (1958).
6. C. Ilschner-Gensch and C. Wagner, ibid., p. 198.
7. I. Frenkel, Kinetic Theory of Liquids, Oxford (1946).

APPENDIX B

OBSERVATIONS ON THE HIGH-TEMPERATURE SULFUR-OXYGEN CORROSION OF NICKEL

by

A. U. Seybolt

General Electric Company
Schenectady, N. Y.

Submitted as a Topical Report
Related to the
Hot Corrosion Mechanism Study
Contract No. N-(600) (61533)-63219

Conducted for the
U. S. Naval Marine Engineering Laboratory
Annapolis, Md.

January 1966

OBSERVATIONS ON THE HIGH-TEMPERATURE SULFUR-OXYGEN CORROSION OF NICKEL

A. U. Seybolt

INTRODUCTION

The work reported here was carried out independently, but in collaboration with a program on the "Hot-Corrosion" of gas turbine alloys conducted for the Naval Marine Engineering Laboratory of Annapolis, Md. by the GE Advanced Technology Laboratories (now a part of the GE Research and Development Center), the Materials and Processes Laboratory in Schenectady, and the Thomson Engineering Laboratory in Lynn, Mass. "Hot-Corrosion" in the meaning used here refers to a rather specific phenomenon encountered when gas turbines are used in salt water environments and with fuel that contains around 0.25% sulfur. Under these conditions sodium sulfate is formed, and the presence of this salt leads to a severe corrosion at high temperatures on the nickel base, or to a somewhat lesser extent on cobalt-base alloys. What is generally observed is a combination of sulfide and oxide formation that can often penetrate rapidly into the structure, thus causing rapid engine deterioration. It appears that sulfides are formed first, and these become converted rapidly to oxides, because the sulfides cannot form a protective oxide layer. Presumably, some of the sulfur released by oxidation forms additional sulfides, but some of it probably escapes as SO_2.

One aspect of the investigation for the Navy was to attempt to learn about the details of the mechanism involved, and therefore to be in a better position to design materials that would resist the corrosive mechanism.

The observations recorded here were made as supplemental to those being carried out under the Navy contract.

PREVIOUS WORK

Several investigators[1-5] have examined facets of this problem, and one of the earliest and most informative is the contribution of Simons, Browning, and Liebhafsky.[1] Curiously enough, most of the subsequent investigators appeared to have ignored the very instructive findings of Simons et al.,[1] and have generally been satisfied to perform empirical corrosion tests without making any real attempt to understand the corrosive mechanism.

Simons et al.[1] show a generalized reaction to explain the formation of Na_2SO_4 as follows:

$$2\,NaCl + (\bar{S}) + 2\,(\bar{H}) + 2\,O_2 = Na_2SO_4 + 2\,HCl. \qquad (1)$$

There is no question about the formation of Na_2SO_4; it has been found in a wide variety of circumstances whenever a salt atmosphere and a sulfur-containing fuel combine in a combustion process. All investigators appear to be in agreement on this point, and evidently the formation of Na_2SO_4 is a necessary

precursor for most cases of hot corrosion. In a sense, reaction (1) serves to concentrate the sulfur sufficiently in the gas turbine for the subsequent corrosion to occur. What happens next is a subject about which there is no unanimity of opinion. There has been some doubt, for example, that Na_2SO_4 alone can react with metals like nickel or super alloys to cause a corrosive attack without some other (reducing) agent being present.

In an attempt to learn something about the mechanism of a simple case, a series of experiments has been carried out with pure nickel. Later, a few observations were made on two binary nickel alloys.

EXPERIMENTAL

The experiments were carried out using three grades of nickel: ordinary commercial "A" nickel which is about 99.5% Ni; a grade of reportedly 99.99% Ni from Driver-Harris; and finally a zone-melted Johnson and Matthey grade which was probably 99.99% to 99.999% Ni. Two alloys were used--Ni-2% Mn made from approximately 99.99% materials, and Ni-20% Cr which was in the vicinity of 99.9% pure. The Ni-2 Mn alloy was prepared to test the effect of a comparatively small concentration of a strong sulfide former, while the Ni-20% Cr alloy was intended to more nearly approximate a gas turbine alloy that generally contains 10% to 20% Cr. Chromium is also a strong sulfide former. For purposes of ready reference, some pertinent facts about the high metal end of a few binary metal-sulfide phase diagrams are listed in Table I.

TABLE I

Summary of Some Phase Diagram Data for Metal-Sulfide Systems

Ni-S:

Ni_3S_2-Ni eutectic, melts at 645°C.
Ni_3S_2 melts at about 810°C.

Co-S:

Co_4S_3-Co eutectic, melts at 877°C.
Co_4S_3 melts at ~930°C.
CoS melts at ~1182°C.

Cr-S:

CrS-Cr eutectic, melts at 1350°C.
CrS melts at ~1565°C.

Mn-S:

MnS-Mn monotectic, melts at 1580°C.
MnS melts at ~1610°C.

It has been observed that cobalt alloys are more resistant to sulfide attack than nickel, and that high chromium contents in nickel- or cobalt-base

materials improve resistance to sulfur attack. These observations are what one would expect from the approximate phase relationships summarized above. Displacement reactions of the type $2\ Cr + Ni_3S_2 \rightarrow 2\ CrS + 3\ Ni$ are known to occur, and an illustration will be provided later. Granted this possibility, it is obvious that if a limited amount of sulfur is present in a Ni-Cr alloy, only the more stable higher melting sulfide will be formed, thus offering the likelihood of removing a molten phase from the structure (if the temperature is above 645°C), and hence reducing the violence of oxidation attack. However, replacement of less stable sulfides by more stable ones is only a detail in the hot-corrosion problem.

Attention was first turned to examine the possibility of a reaction between Na_2SO_4 and nickel. To exclude the influence of external agents such as gaseous atmosphere, for example, the three grades of nickel were tested by completely immersing them in Na_2SO_4 in an evacuated capsule. The test was carried out as follows: a few grams of C.P. Na_2SO_4 was melted in a highly dense, high-purity (Morganite) Al_2O_3 crucible. To remove possible dissolved oxygen and moisture, the salt was heated to about 900°C (mp ~880°C) under vacuum for about an hour, at which time the original high pressure fell to about 10μ. The salt was allowed to freeze under vacuum. When the salt was cold, freshly abraded (600 SiC paper) and degreased samples were laid on top of the salt, and the crucible containing salt and sample was encapsulated in a fused silica envelope. The envelope was baked out at 300°C under a vacuum of 10^{-6} mm and sealed off. The crucible and contents were next heated to about 900°C to melt the salt and to allow the nickel samples to sink to the bottom. The temperature was now adjusted to that desired for the metal-salt reaction.

Two experiments were made. In one, a sample of "A" nickel was exposed at 950°C for 48 hours in liquid salt. At the end of this time, the salt was washed away in hot water, exposing a sample which appeared to show NiO on the surface; a section through this sample is seen in Fig. 1. X-ray diffraction confirmed the presence of NiO. Most of the metallographic samples were etched in a glycerine-nitric acid-acetic acid solution. The proportions varied somewhat, but a frequently used solution contained (in relative volumes) 40 glycerine, 40 nitric acid, and 20 acetic acid. The analogous test with the two purer nickel samples, 99.99% Ni strip and the zone-melted nickel, are shown in Figs. 2 and 3, respectively; in this instance, the exposure was to solid salt at 850°C for 68 hours. Some NiO was noted in these cases as well, but the extent of oxidation was not as great as in the case of the "A" nickel. However, sulfur penetration of the structure is completely through the 0.020-inch-thick strip for the 99.99% Ni strip, and the penetration on one side of the thicker zone-melted sample is about the same. The zone-melted sample was cold-worked prior to insertion into the capsule to ensure the presence of some grain boundaries.

These pictures prove at least two things: that pure nickel can react with Na_2SO_4, and that the reaction can proceed in the case of solid salt. There was a liquid eutectic present, however, in the 850°C experiment as can be seen from the shape of the sulfide-nickel interface, and as would be anticipated from

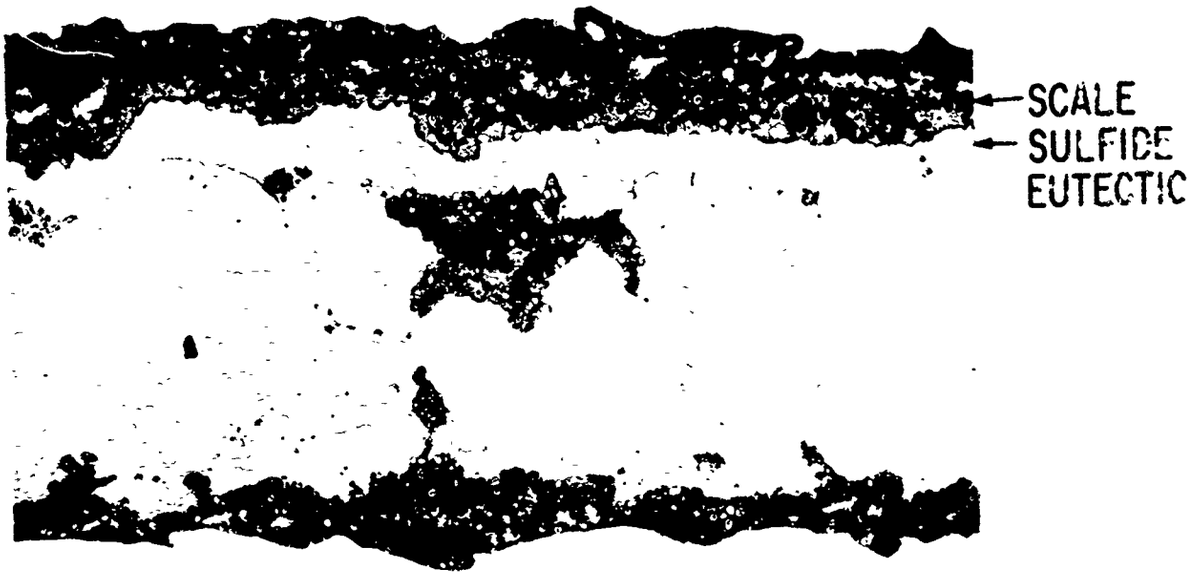

Fig. 1 "A" nickel heated 48 hours at 950°C in Na_2SO_4, evacuated capsule. 100X

Fig. 2 99.99% Nickel strip heated 68 hours at 850°C in Na_2SO_4, evacuated capsule. 150X

Fig. 3 Zone-melted nickel given same treatment as in Fig. 2. 150X

the known temperature of the Ni-Ni_3S_2 eutectic (645°C). Simons et al. (1) suggest the following reactions between Na_2SO_4 and some unspecified reducing agent:

$$Na_2SO_4 + 3\,R = Na_2O + 3\,RO + S \qquad (2)$$

and

$$M + S = MS \qquad (3)$$

where M in reaction (3) is some metallic component of a gas turbine alloy. The products of the reaction demonstrated in Figs. 1 through 3 were examined by x-ray diffraction with the result that NiO and Ni_3S_2 were identified, along with some Na_2SO_4 which had not been washed away. However, a pH paper test on the water solution of some of the salt at the end of the runs showed very clear evidence of a strong basic solution--presumably NaOH.

In view of the above, it seems possible to rewrite reactions (2) and (3) as follows:

$$Na_2SO_4 + \frac{9}{2}Ni = Na_2O + 3\,NiO + \frac{1}{2}\,Ni_3S_2 \qquad (4)$$

in which nickel is the reducing agent required.

Figure 4 shows a typical result of Na_2SO_4 attack on "A" nickel when heating in air; the nickel strip was half in and half out of solidified salt for 6 hours at 840°C. It shows very clearly the sequence: oxide, sulfide eutectic, metal, with sulfide penetration down grain boundaries.

In Fig. 5, sulfur diffusion is shown along grain boundaries and even twin boundaries all the way through a 10-mil-thick sheet after 1/2 hour at 950°C in liquid Na_2SO_4 in air. The particles observed are probably mainly MnS, and hence the sample shows internal sulfidation completely analogous to internal oxidation.

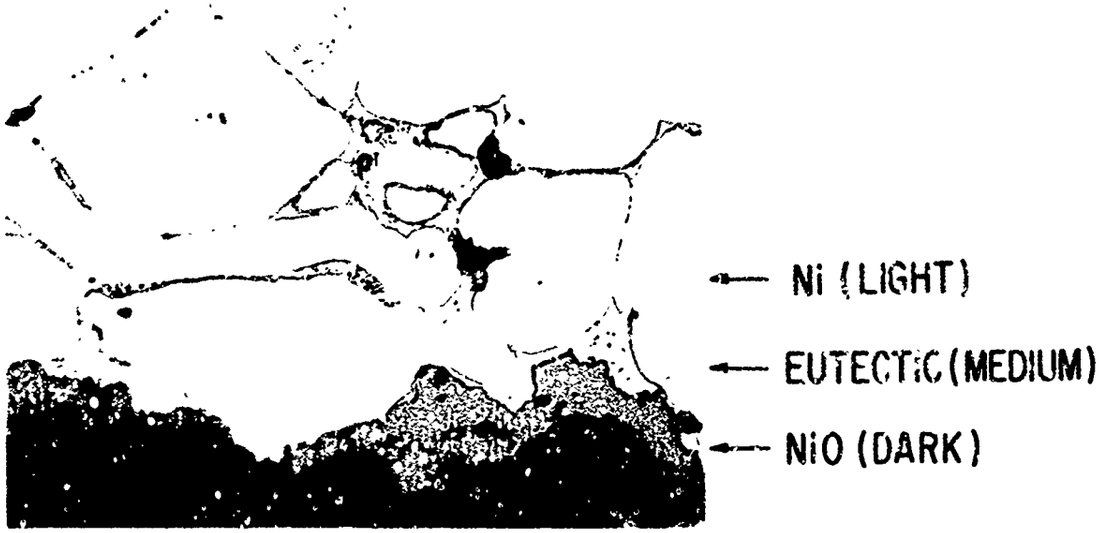

Fig. 4 "A" nickel heated 6 hours at 840°C partially immersed in Na_2SO_4, in air. 500X

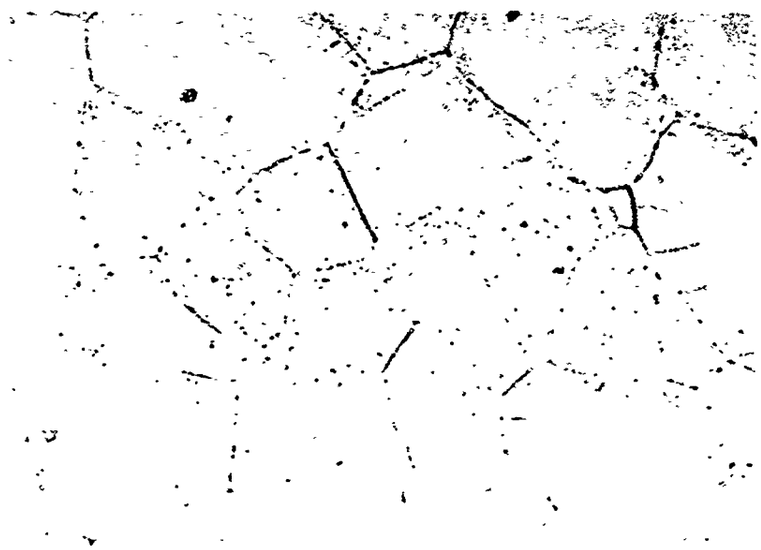

Fig. 5 "A" nickel heated 1/2 hour at 950°C, partially immersed in Na_2SO_4 in air. 500X

A few tests were made with H_2S/H_2 mixtures, using the gas ratio corresponding to the reaction

$$H_2S + \frac{3}{2}\ Ni = \frac{1}{2}\ Ni_3S_2 + H_2. \qquad (5)$$

Such experiments were conducted by preparing some Ni_3S_2, and by passing a slow stream of H_2 over the sulfide in the bottom of an Al_2O_3 crucible containing the sample to be sulfided. It was observed that the same grain boundary penetration of the sulfide eutectic occurred as was observed for the salt attack, except

of course that no NiO was formed. Figure 6 shows a typical example. Experiments of this type showed that there was nothing unique about the type of sulfur attack encountered with Na_2SO_4; the phenomenology is just the same as for H_2S attack.

Figure 7 shows a good example of the Ni_3S_2-Ni eutectic; this was an "A" nickel sample held for 4 hours at 950°C in Na_2SO_4, where H_2 was bubbled through the salt. H_2S was generated by some hydrogen reduction of the salt.

Fig. 6 "A" nickel heated 4 hours at 850°C in H_2S/H_2 mixture. 100X

Fig. 7 "A" nickel heated 4 hours at 950°C in Na_2SO_4, H_2 bubbled through melt. 500X

EFFECT OF NICKEL PURITY ON SALT ATTACK

It was mentioned earlier that the purer grades of nickel did not react as much with the evacuated salt as did the less pure "A" nickel. This trend was noted also in Na_2SO_4 partial immersion tests conducted in air. For example, see Fig. 8. This shows the 99.99% Ni heated partially submerged in Na_2SO_4 for two hours at 850°C. Some surface scaling occurred, and some grain boundary sulfiding is evident. Contrast this with Fig. 9 (at only 100X) where severe attack and opening up of the grain structure have occurred to about one-third the thickness of the strip. This sample had only half the exposure of the high-purity sample of Fig. 8.

Fig 8 99.99% Nickel heated 2 hours at 850°C in Na_2SO_4, in air. 500X

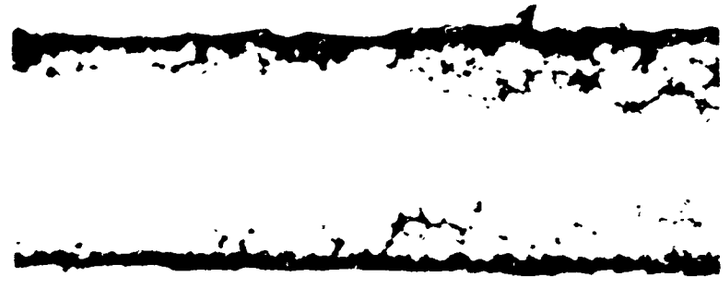

Fig. 9 "A" nickel heated one hour at 850°C in Na_2SO_4, in air. 100X

EFFECT OF TEMPERATURE

A series of "A" nickel samples was heated for 1 hour each partly submerged in Na_2SO_4 in air at temperatures of 800°, 850°, 900°, and 950°C. Figure 9 noted just above gave the structure at 850°C just below the melting point of Na_2SO_4, and Fig. 10 shows the results at 900°C, somewhat above the melting point of the salt. It is clear that the attack was considerably accelerated at 900° compared to 850°C, and at 950°C it is somewhat more advanced, particularly as regards oxidation of the broken-up structure. There was not a large difference between the attack at 800° and 850°C.

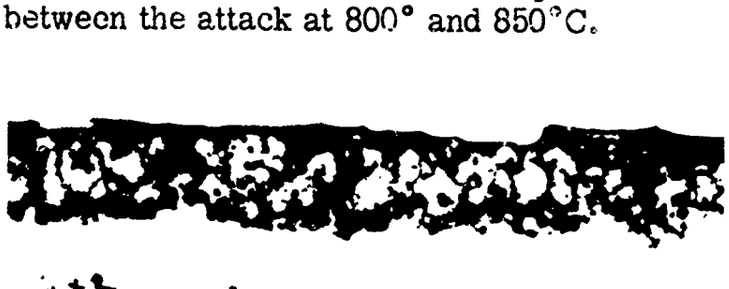

Fig. 10 "A" nickel heated 1 hour at 900°C in Na_2SO_4, in air. 100X

EFFECT OF PRE-SULFIDATION ON OXIDATION RATE

To test the idea that oxidation occurs preferentially in sulfided areas, the following experiment was conducted. A sample of "A" nickel was sulfidized using the Ni_3S_2-H_2 procedure as outlined above; the sample was heated close to Ni_3S_2 in a hydrogen atmosphere for 4 hours at 850°C. That this treatment preferentially sulfidizes the grain boundaries has already been shown (Fig. 6). The sulfided sample was then heated in air at 850°C for 4 hours, and a section is shown in Fig. 11. The dark NiO scale is seen to form cusps at the grain boundaries where the Ni_3S_2 eutectic had been located. Figure 12 shows an unetched section of the same sample which shows the entrance of oxide into the grain boundaries particularly clearly.

Fig. 11 "A" nickel sulfidized 4 hours at 850°C, then oxidized 4 hours at 850°C in air. 500X

Note oxidation follows sulfide in grain boundary.

Fig. 12 Same as Fig. 11, but unetched. 500X

BEHAVIOR OF Ni-2 Mn, Ni-20 Cr

These two alloys were exposed to Na_2SO_4 and H_2S/H_2 in the same manner as the pure nickel samples. Figure 13 shows the Ni-2 Mn alloy after exposure to H_2S/H_2 whose ratio corresponds to Ni_3S_2/Ni equilibrium. At the surface is the Ni_3S_2-Ni eutectic that has penetrated grain boundaries, forming MnS during the sulfur penetration. Evidence of interaction between MnS particles and liquid may be seen at the surface frozen liquid layer, where the boundary between MnS and nickel sulfide-nickel eutectic is not very sharp. Internal sulfidation is shown by the presence of MnS at some distance from the liquid-solid boundaries. Also, as is characteristic of internal oxidation, the MnS particles are smaller when farther from the surface where the sulfur diffusion distance is at a maximum.

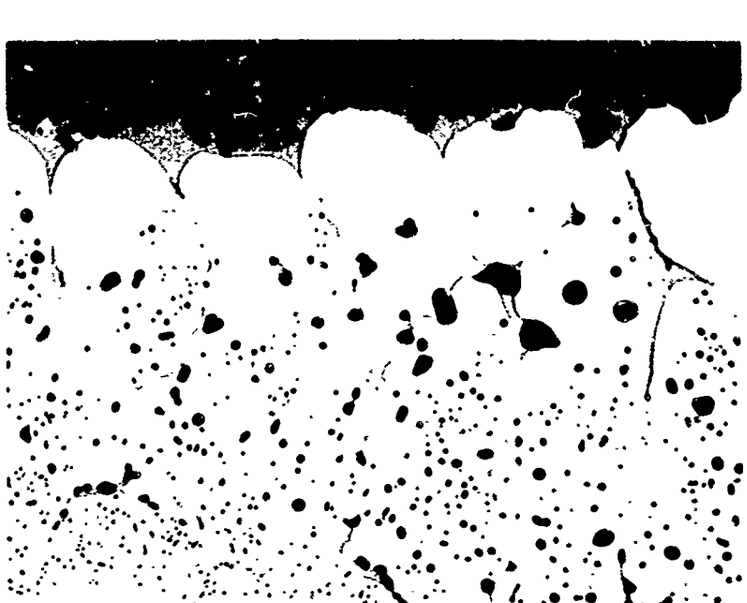

Fig. 13 Ni + 2% Mn alloy heated 4 hours at 950°C in H_2S/H_2. 250X

The same alloy was subjected to the same time and temperature partially immersed in liquid Na_2SO_4, and shows an appearance (Fig. 14) more like unalloyed nickel since there is less evidence of MnS. A few particles of MnS may be seen, but apparently most of the manganese must have been preferentially oxidized, and hence has been incorporated into the scale. Manganese would be expected to oxidize preferentially to nickel since $\Delta F^\circ_{MnO} = \sim -70$ cal at 950°C, while $\Delta F^\circ_{NiO} = \sim -32$ kcal.

The Ni-20 Cr 20-mil strip was heated for 2 hours at 850°C in a crucible containing molten Ni_3S_2 using a slow stream of hydrogen gas. The molten sulfide wet the sample and flowed up to about two-thirds of the length of the Ni-20 Cr strip. A metallographic section revealed the structure shown in Fig. 15. The coarser structure at the left was the area that was originally Ni_3S_2, but now contains a large volume fraction of CrS. Some Ni_3S_2-Ni eutectic, however, may be seen at many places, and appears to be a light gray color. Farther to the right is the location of the original Ni-20 Cr strip, now largely converted to Ni + CrS. In this region there is no sign of the Ni_3S_2-Ni eutectic, since the chromium has robbed the eutectic of all sulfur. However, with longer exposure, the region of eutectic would become extended, since when all the chromium is converted to CrS, the liquid Ni_3S_2-Ni eutectic becomes stable again. Figure 16 shows the junction between the liquid eutectic contact and the gas phase contact with the alloy. When the gas phase was solely present, the extent of the attack was very limited, since here sulfur penetration occurs by solid state diffusion, which is much slower than diffusion in the liquid. It will be noted that in this case there is no evidence of preferential attack at grain boundaries. On the contrary, the sulfide "subscale"

Liquid eutectic penetrated grain boundary.

Fig. 14 Ni + 2% Mn alloy heated 4 hours at 950°C in Na_2SO_4, in air. 150X

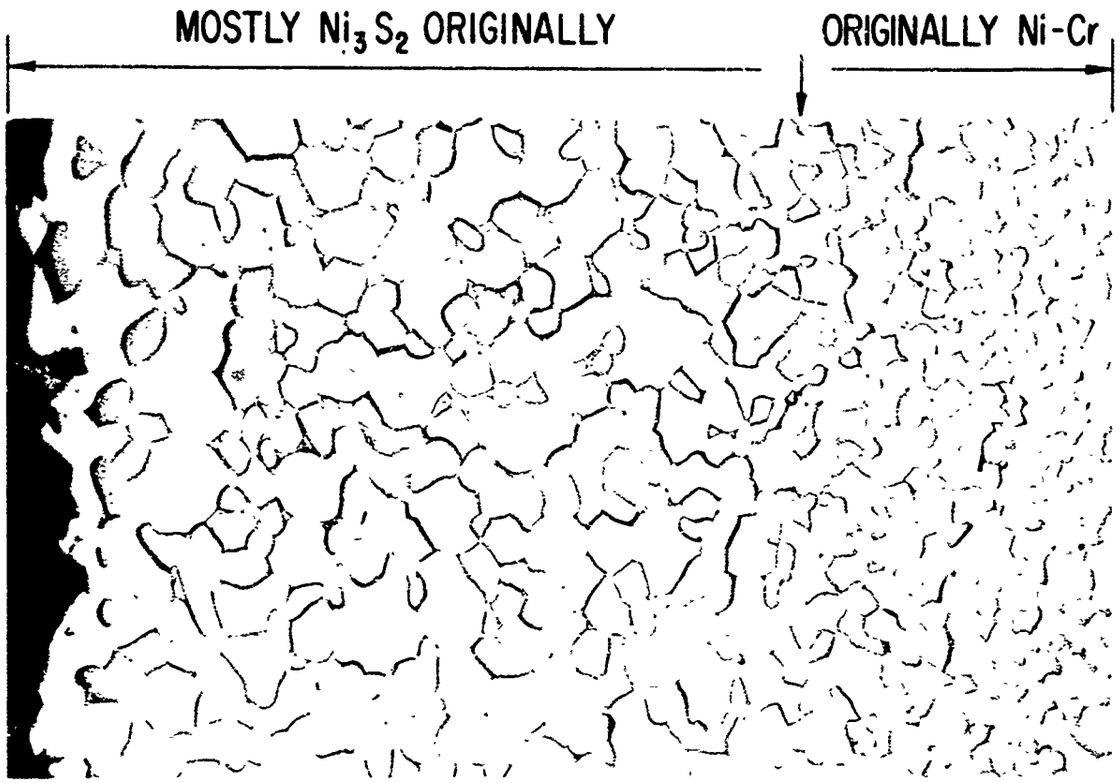

Fig. 15 Ni + 20% Cr alloy heated 2 hours at 850°C in contact with $Ni_3S_2 + H_2$. 250X

is quite uniform in depth and CrS appears to have nucleated in a more or less random pattern, possibly at the sites of nonmetallic inclusion or at other discontinuities in the solid solution structure.

Experiments with partial submersion of the freshly abraded Ni-20 Cr samples in Na_2SO_4 in an air atmosphere at temperatures from 850° to ~1000°C have in general shown no clear-cut evidence of attack, except for superficial oxidation. This behavior is probably due to the protective nature of the Cr_2O_3 oxide film which forms immediately upon placing the sample into the molten salt.

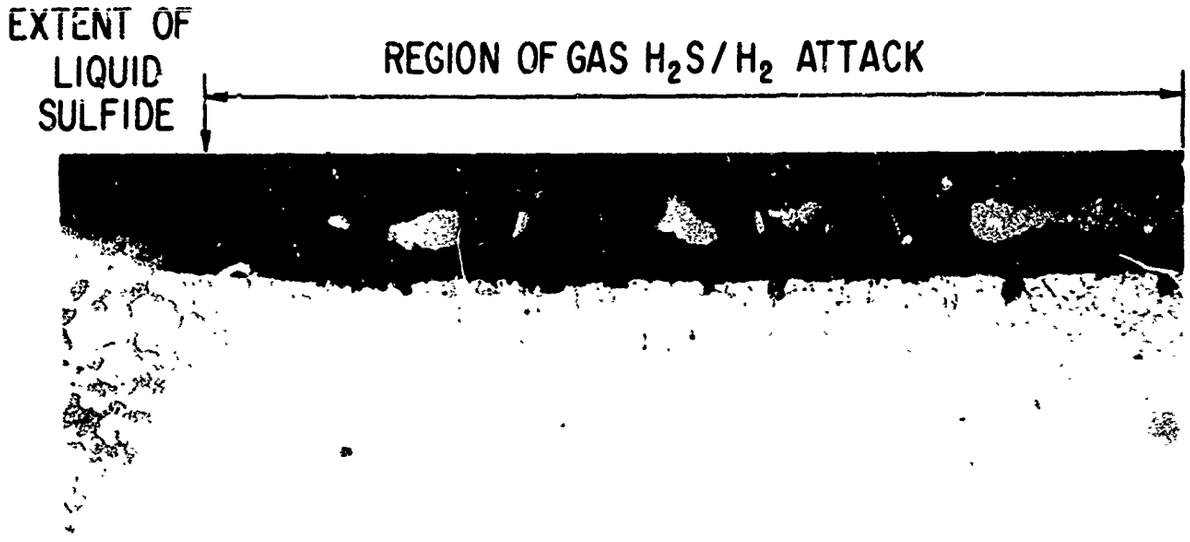

Fig. 16 Same as Fig. 15 but shows limit reached by liquid Ni_3S_2-Ni eutectic. 500X

To test this point, an arrangement was prepared to allow the strip sample to be flexed repeatedly while under the salt or when brought up into the air above the salt. Deformation by bending breaks up the protective film, and attack in certain spots where the film continuity was broken was noticed; see Fig. 17. The attack here is practically identical in nature with that observed for the sample alloy subjected to H_2S/H_2 gas (Fig. 16).

Fig. 17 Ni-20 Cr alloy, heated 1 hour at 950°C in Na_2SO_4 in air; sample flexed at temperature to break oxide film. 1000X

RESULTS OF HEATING SAMPLES IN SO_2 GAS

All of the samples used in the various experiments cited above were given a 2-hour treatment at 850°C in flowing SO_2 gas. This proved to be the most drastic treatment of all as regards pure nickel, since both the "A" nickel and the 99.99% nickel were completely converted to the Ni_3S_2-Ni eutectic except for the heavy oxide scale at the surface; see Fig. 18. The Ni-20 Cr (Fig. 19) alloy suffered about the same degree of attack as in the H_2S/H_2 case (Fig. 16), and the nature of the attack was the same.

Fig. 18 99.99% Nickel, heated 2 hours at 850°C in SO_2 gas; complete conversion to sulfide eutectic. 150X

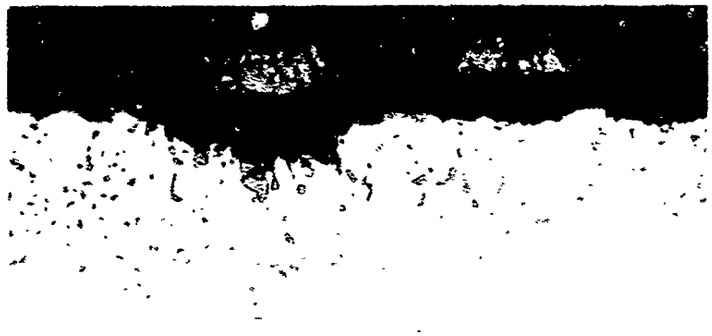

Fig. 19 Ni-20 Cr alloy heated 2 hours at 850°C in SO_2 gas. 1000X

SUMMARY AND DISCUSSION

The results of this investigation have shown that nickel and nickel alloys can react directly with either solid or liquid Na_2SO_4 without the need for any extraneous reducing agent. The attack in the case of nearly pure nickel is particularly drastic, probably because of the presence of the liquid Ni_3S_2-Ni eutectic which has a rather low freezing point,~645°C. The liquid readily penetrates down nickel grain boundaries; and because of rapid diffusion in the liquid, sulfur is quickly transported large distances into the structure. It has been shown that the nickel sulfide-rich areas oxidize more rapidly than the metallic structure. The details of the oxidation reaction are not as yet understood, but it is possible that for a eutectic it proceeds as suggested by Simons et al.:[1]

$$M \cdot MS \text{ (eutectic)} + 1/2\ O_2 = MO + MS. \qquad (6)$$

This reaction indicates that the sulfur is always combined as a sulfide, and that only the excess metal part of the eutectic becomes oxidized. Another possibility would be to generate SO_2 during oxidation, which in turn forms oxide and sulfide as already demonstrated. In the case of Ni-20 Cr and apparently also in nickel-base jet engine alloys, a eutectic liquid is not created, and only isolated but closely packed sulfide particles such as CrS are formed. In this case, one must suppose that the CrS oxidizes directly to Cr_2O_3 since one sees clear evidence for oxide taking the place of sulfides by observing the precise similarity in size and shape of the sulfide and oxide particles. See Fig. 20. In this case (more applicable to what is experienced in practice), the reactions may be

$$2\ CrS + \frac{3}{2}\ O_2 = Cr_2O_3 + 2S \qquad (7)$$

$$2\ S + 2\ Cr = 2\ CrS\ . \qquad (8)$$

The structure shown in Fig. 20 is a Udimet 500* engine blade which had suffered considerable hot corrosion owing to simultaneous presence of NaCl and sulfur in the combusting gases. It is quite clear from this that the oxide particles just above the sulfur particles had been sulfide particles originally. It is not clear why there exists a comparatively clean metallic layer between the external scale and the internal oxidized zone. A few unaffected sulfides may be seen in this area, apparently bypassed by the oxygen that had perhaps penetrated this region by passing along cracks or easy paths of some kind. Several oxidized paths may be seen cutting from left to right.

The details of the corrosion behavior is apparently greatly affected by the effectiveness of the oxide blocking layer on the surface. This layer is quite

*Nominally: 19 Cr; 19 Co; 4 Mo; 3 Ti; 2.9 Al; small amounts of Fe, B, C; bal. Ni.

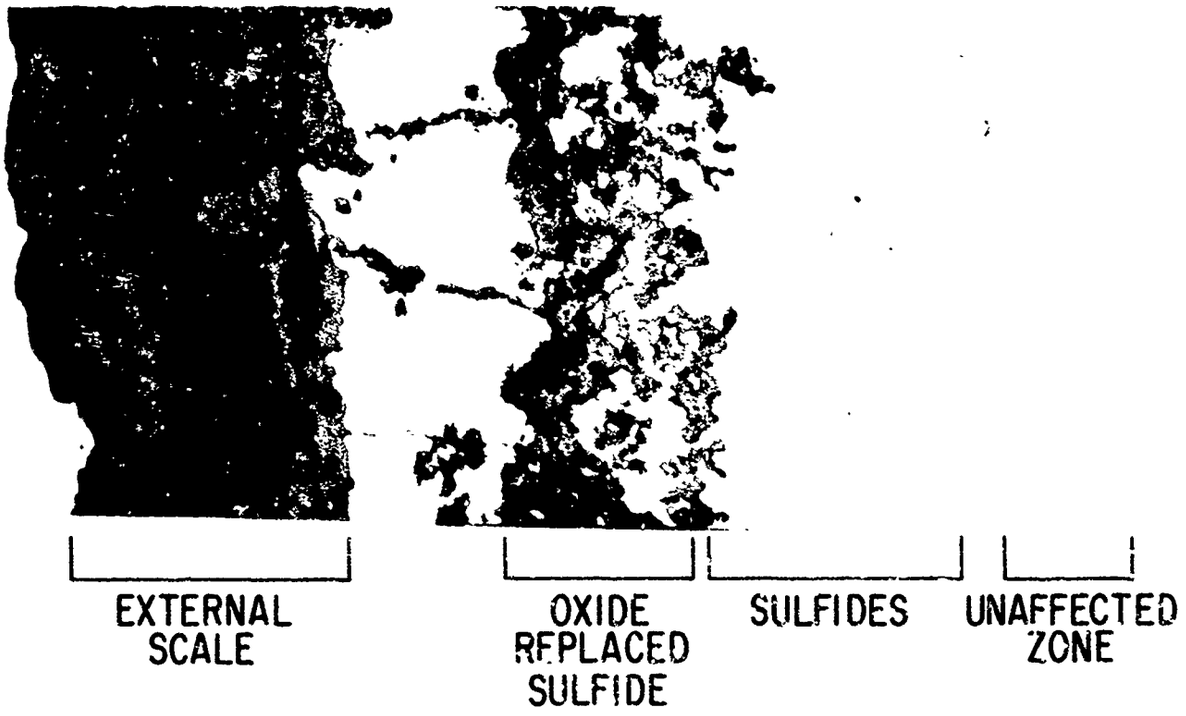

Fig. 20 Udimet 500 gas turbine blade in test 340 hours at 1600°C in atmosphere causing hot corrosion. 500X
Note: This photograph was obtained through courtesy of the "Marinization Program" Contract No. B. S. 88423, Project SS 501-C00, Task 3900.

protective in the case of Ni-20 Cr as shown above. This may also account for the slower kinetics of Na_2SO_4 attack on the higher purity nickel, which may have a more perfect protective layer of NiO than the less pure "A" nickel. Certainly the Na_2SO_4 attack in the evacuated capsules was essentially as severe as regards sulfide penetration for both grades of nickel, although again the oxidation resistance of the purer nickel grades was better.

CONCLUSIONS

There is no doubt that nickel and nickel alloys can react directly with Na_2SO_4 to form sulfides without the need of any extraneous reducing agent. In conformance with well-established chemical principles, the most stable sulfides form at the expense of less stable sulfides. Therefore, in gas-turbine alloys containing substantial amounts of chromium, CrS is a principal sulfide formed. Also, no appreciable quantity of low melting (645°C) Ni_3S_2-Ni eutectic or Co_4S_3-Co eutectic (mp 877°C) will be formed as long as there is unreacted chromium present. This in turn means that the alloy is more subject to oxidation if in some surface areas much of the chromium is present as CrS. This acts in a double manner: (1) by impoverishing the base metal in chromium and (2) by the fact that CrS is more susceptible to oxidation than the base metal.

If all the sulfur formed from Na_2SO_4 remained in the structure, one would expect an autocatalytic reaction between sulfur and oxygen, thus greatly speeding up the destructive process. This does not, in general, appear to happen.

The reason for the reaction remaining moderately rapid, but not catastrophic, may be that an appreciable fraction of the sulfur leaves the gas turbine part as SO_2, which is swept out of the system.

Some remaining questions are those of rate control in the sulfidation-oxidation process, the details of the oxidation process of the sulfides, and what factors determine the shape and distribution of the sulfide particles. It is not at present clearly demonstrated that sulfur penetration into alloy structures occurs primarily by volume diffusion, although often metallographic evidence seems to suggest this. On the other hand, in some cases there is evidence of a fine-grained matrix structure around the sulfides, which may indicate short-circuiting sulfur diffusion paths since the grain boundaries seem to link up the sulfide particles. Finally, the degree of protection from hot corrosion offered by various oxide films needs investigation, as well as the question of the mechanism of film breakdown in the presence of Na_2SO_4.

ACKNOWLEDGMENTS

The author wishes to express appreciation to colleagues in the Navy Hot-Corrosion program who were of great assistance in discussing various phases of the work, and in providing some of the samples. These include Richard Hardt and John Gambino of the Research and Development Center, and Paul Bergman of the Thomson Engineering Laboratory in Lynn, Mass.

REFERENCES

1. F. L. Simons, G. V. Browning, and H. A. Liebhafsky, Corrosion, 11, 505t (1955).
2. H. Shirley, J. Iron Steel Inst., 182, 144 (1956).
3. P. Hancock, First Inst. Congr. Metallic Corrosion, London (1961).
4. H. Lewis and R. Smith, ibid.
5. E. Bradbury, P. Hancock, and H. Lewis, Metallurgia, 4 (1963).

APPENDIX C

THE BEHAVIOR OF COBALT IN HIGH-TEMPERATURE SULFUR-OXYGEN ENVIRONMENTS

by

A. Beltran and A. U. Seybolt

General Electric Company
Schenectady, N. Y.

Submitted as a Topical Report
Related to the
Hot Corrosion Mechanism Study
Contract No. N-(600) (61533)-63219

Conducted for the
U. S. Naval Marine Engineering Laboratory
Annapolis, Md.

January 1966

APPENDIX C

THE BEHAVIOR OF COBALT IN HIGH-TEMPERATURE SULFUR-OXYGEN ENVIRONMENTS

A. Beltran* and A. U. Seybolt†

INTRODUCTION

In an earlier report, [1] one of us described the results of combined sulfidation-oxidation attack on nickel and some nickel alloys. These experiments were mainly concerned with "crucible tests" where metal samples were heated in Na_2SO_4, but in some experiments H_2S and SO_2 were used as corrosive media. In this earlier work, one of the main results was the finding that nickel and nickel alloys react directly with Na_2SO_4 to form nickel sulfides that then preferentially oxidize to NiO. In the presence of chromium, CrS is formed and then oxidizes to Cr_2O_3. The rate of oxidation of alloys containing CrS is considerably less than that of Ni_3S_2, partly because CrS is a solid while Ni-Ni_3S_2 forms a low-melting eutectic, and partly because of the morphology of the formation of CrS which occurs as isolated small particles.

The objective of the present work was to find out if the behavior of Co or Co-Cr was the same as that of Ni or Ni-Cr.

Current complex carbide-strengthened cobalt-base superalloys in gas turbine service contain a minimum of 20 w/o chromium for oxidation/corrosion resistance, and in fact, recent work at the GE Materials and Processes Laboratory has determined the optimum chromium level to be 30 w/o in X-45 type alloys. [2]

Therefore, experiments were performed using pure cobalt and cobalt binary alloys containing 20 or 30 w/o chromium with the impurity levels listed in Table I for pure cobalt and the 30 w/o chromium alloy.

TABLE I

Elements	Co	Co/30 Cr
Ni	0.08 %	0.1 %
Cu	.03	.04
Fe	.002	.006
Si	.006	.001
Al	.002	.002
Mg	.001	.001

*General Electric Materials and Processes Laboratory, Schenectady.
†General Electric Research and Development Center, Schenectady.

Some melting temperatures pertinent to this investigation are listed in Table II.

TABLE II

Compound	Melting Point (°C)
Ni_3S_2	810
Ni_3S_2-Ni eutectic	645
Co_4S_3	930
Co_4S_3-Co eutectic	877
CrS	1565
CrS-Cr eutectic	1350
Na_2SO_4	883
72% Na_2SO_4/28% NaCl	750

EXPERIMENTAL

In general, the tests were conducted by partially immersing the strip specimens in the salt contained in a high-purity, high-density Al_2O_3 crucible. The specimens were first prepared by metallographically polishing through 600-grit SiC paper and then rising in toluene and acetone. After testing, the specimens were rinsed in hot water to remove the salt, and then nickel plated to retain the reaction products. In some cases, a conductive silver paint (DuPont #4817) was first sprayed on to prepare the oxide for plating. Standard metallographic procedures were used, followed by etching with alcohol/HCl/3% H_2O_2 in 50:50:10 proportions.

BEHAVIOR OF PURE COBALT IN Na_2SO_4

The effect of Na_2SO_4 on pure cobalt in an air environment was studied at temperatures that ranged from 850° to 1050°C. The lowest temperature (850°C) is below the melting point both of the salt and the Co-Co_4S_3 eutectic. In this case, the salt was first heated to 900°C to produce the liquid, the sample was inserted, and the salt cooled rapidly to 850°C and held for 2 hours. All of these tests showed much the same type of attack; hence only some results from the 950° and 1000°C tests are shown in the following photomicrographs.

Figure 1 shows the corroded surface layer of pure cobalt after immersion for 2 hours at 950°C in molten Na_2SO_4. This picture shows two sulfide-rich layers between the dark cobalt oxide and the cobalt matrix. The darker sulfide layer next to the oxide is the cobalt-cobalt sulfide eutectic, but the smooth-appearing sulfide next to the metal is probably a homogeneous sulfide phase. The latter has formed cusps protruding into the base metal, which in Fig. 2 appear as oxide cusps, indicating the replacement of sulfide by oxide. Figure 2 shows the air-exposed half of the sample, which was similarly but less

Fig. 1 Cobalt immersed 2 hours at 950°C in Na_2SO_4. 500X

Fig. 2 Cobalt heated 2 hours at 950°C in Na_2SO_4, exposed to air. 500X

severely attacked, evidently caused by wetting of the surface by the salt. In addition, the higher partial pressure of oxygen has nearly completely oxidized the sulfide leaving a barely visible sulfide layer at the interface. Figure 2 also shows sulfide stringers in the grain boundaries.

The sample tested for 2 hours at 1000°C was severely attacked. Figures 3 and 4 clearly reveal the penetration of the sulfide eutectic along the grain boundaries with subsequent formation of massive oxides. These figures provide confirmation that preferential oxidation of the eutectic sulfide is an integral feature of the hot corrosion attack of cobalt. The more broken-up or granular appearance of the oxide in Fig. 4 may have been caused by more

Fig. 3 Cobalt heated 2 hours at 1000°C in Na_2SO_4, in air. 500X

Fig. 4 Cobalt heated 2 hours at 1000°C in Na_2SO_4, in air. 500X

direct contact between salt and oxide in this sample. The Na_2SO_4 appears to cause a disintegration of the oxide structure, thus preventing the formation of a protective oxide scale.

These tests have shown that cobalt, the same as nickel, displays the ability to reduce Na_2SO_4 that results in the formation of Co_4S_3. Indeed, a liquid Co-Co_4S_3 eutectic was found over the entire range of test temperatures,

including the case of solid salt at 850°C, which indicates the eutectic melts somewhat below the accepted value of 877°C when oxygen is present. Severe attack of the base metal occurs by penetration of the liquid eutectic along grain boundaries. The eutectic in turn is preferentially oxidized, resulting in rapid degradation of base metal integrity.

BEHAVIOR OF Co-20% AND 30% Cr IN Na_2SO_4

Two exposures of Co-20 w/o Cr in Na_2SO_4/air for 2 hours at 850°C produced only oxidation of the base metal. As in the case of pure cobalt, raising the temperature to 950°C and above caused a large increase in rate of attack, but as in the case of Ni-Cr alloys, the rate of attack was considerably less compared to the base metal. Two hours at 950°C was sufficient to develop tiny particles of sulfide (CrS) just below the metal/oxide interface, but due to the significant reduction of attack in the presence of chromium, the Co-30 w/o Cr specimen was tested for 48 hours at 950°C in order to obtain well-defined corrosive attack. The immersed half of the 5/32-inch-thick specimen was competely traversed by networks of CrS (light gray, Fig. 5). The preferential oxidation of CrS is again obvious from the overlay of dark oxide. From a thermodynamic standpoint, the formation of the more stable CrS would be expected to proceed until the chromium is used up. Once this occurs, the less stable Co_4S_3 can appear. This forms the liquid Co-Co_4S_3 eutectic, at temperatures above ~877°C, and this has been observed to happen in portions of this same sample.

Fig. 5 Co-30 w/o Cr heated 48 hours at 950°C in Na_2SO_4, in air. 750X

This sequence of experiments has shown that chromium concentrations approaching the levels found in commerical cobalt-base superalloys significantly reduce the severity of hot corrosion attack. Penetration of the alloy proceeds by formation of CrS networks with subsequent preferential oxidation of the sulfide.

BEHAVIOR OF Co AND Co-20% Cr IN A Na_2SO_4/NaCl MIXTURE

The thermogravimetric analysis phase of the mechanism study indicated a greater susceptibility of cobalt to attack in mixtures of NaCl and Na_2SO_4.[3] Tests were therefore conducted in a mixture of 72 w/o Na_2SO_4 plus 28 w/o NaCl, which has an approximate melting point of 750°C. However, careful examination of a series of cobalt and Co-Cr samples in the salt mixture between 800° and 900°C showed the same microstructural behavior as in Na_2SO_4. Figure 6 shows the CrS formation near the surface of the Co-20% Cr alloy after 4 hours at 900°C. No obvious difference in rate of attack or type of attack was noted, although tests of this kind are essentially qualitative or at least only semiquantitative.

Fig. 6 Co-20 w/o Cr heated 4 hours at 900°C in 72 w/o Na_2SO_4 + 28 w/o NaCl, in air. 500X

EFFECT OF PRE-OXIDATION ON Co-20% Cr

A sample of Co-20% Cr was first oxidized for 4 hours at 980°C in static air, then tested for 4 hours at 800°C in the mixed salts. Although this corrosion exposure was not very severe, pre-oxidizing did prevent the formation of sulfides for 4 hours.

EFFECT OF SO_2 ON Co

As in the case of nickel, the attack produced by a SO_2 atmosphere was the most severe of the conditions investigated. Figure 7 shows the broad front of sulfide and oxide occurring after one-half hour at 950°C. Figures 8 and 9 show in detail the cusp-like nature of the interface. Also evident are the spheroidal oxide particles resembling in appearance a subscale. The precise mechanism for the formation of this structure is not known. Qualitatively, the results produced by SO_2 and the salts are the same. Although Co-20% Cr was not tested in SO_2 it would be expected to behave identically to the case of Ni-20% Cr.

Fig. 7 Cobalt heated 0.5 hour at 950°C in SO_2. 100X

Fig. 8 Cobalt heated 0.5 hour at 950°C in SO_2. 500X

Fig. 9 Cobalt heated 0.5 hour at 950°C in SO_2. 500X

DISCUSSION

While no kinetic studies were made during this part of the investigation, it would appear from metallographic evidence that there is comparatively little difference in susceptibility to hot corrosion attack between the nickel-base and cobalt-base materials. Certainly the same corrosion mechanism[1] is operating in both cases. While there are no x-ray diffraction results available on

the cobalt materials to confirm the metallographic identification as yet, the very close similarity in morphology between the two classes of alloys leaves no real doubt about the nature of the attack.

It is interesting that the addition of NaCl to Na_2SO_4 appeared to make no difference in the type of attack, statements in the literature to the contrary.

While it was mentioned above that, in general, there was little difference in behavior between the cobalt- and nickel-base materials, there was a noticeable difference in susceptibility to Na_2SO_4 attack between pure cobalt and pure nickel. Perhaps because the $Co\text{-}Co_4S_3$ eutectic melts at a higher temperature than the $Ni\text{-}Ni_3S_2$ eutectic, the attack on cobalt was somewhat less severe than on nickel at identical test temperatures, but at 200°C above the respective eutectic melting points the attack on cobalt was more severe. This may possibly be due to the higher diffusion rate of sulfur at the higher temperature used for testing cobalt, but it may also point to a less protective oxide film. It is well established that at comparable temperatures, nickel oxidizes less rapidly than cobalt.

Chromium plays the same important role in the corrosion of cobalt binary alloys as it does in nickel binary alloys. That is, CrS forms in preference to the solvent metal sulfide. This eliminates the possibility of liquid sulfide formation initially, and subsequent rapid transfer of sulfur over great distances. Regardless of the actual sulfide present, metallographic evidence has been given for the preferential oxidation of the sulfide. Although the exact mechanisms of oxide film penetration and breakdown are currently unresolved, the formation of Cr_2O_3 on the cobalt binary alloys may be more effective in blocking sulfide formation that the corresponding CoO film on pure cobalt. However, the more favorable morphology of the CrS as compared to that of the cobalt sulfide eutectic may be a more important factor in reducing the severity of hot corrosion.

CONCLUSIONS

It has been shown that the behavior of cobalt and cobalt/chromium alloys in Na_2SO_4 under an oxidizing atmosphere is essentially identical to that of nickel and nickel alloys. Reduction of the salt is followed by sulfide formation--liquid $Co\text{-}Co_4S_3$ eutectic (above 877°C) in the case of pure cobalt--and CrS when chromium is present. Rapid attack of the structure then occurs by preferential oxidation of the sulfide. Thus, optimum levels of chromium are required in commerical gas turbine cobalt-base superalloys for two reasons:

1. To promote the formation of an adherent Cr_2O_3 surface oxide, which assists in blocking sulfur penetration.

2. To prevent the formation of liquid sulfide eutectic.

ACKNOWLEDGMENTS

The authors wish to express appreciation to Richard Hardt (GE R&DC) and Chester Sims (GE M&P Lab) for their helpful discussions concerning this work, to John Godfrey (R&DC) and Frank Duci (M&P Lab) for processing the samples, and to John Tomlinson (M&P Lab) for the excellent metallographic work.

REFERENCES

1. A. U. Seybolt, "Observations on the High-Temperature Sulfur-Oxygen Corrosion of Nickel," General Electric Research and Development Center Rept. No. 65-C-060 (October 1965).

2. D. E. McGarrigan, C. T. Sims, and A. D. Foster, private communication.

3. "Hot-Corrosion Mechanism Study," First Quarterly Report, Contract No. N600 (61533) 63219 (May 17, 1965).

APPENDIX D

HOT CORROSION BEHAVIOR OF NICKEL AND COBALT BINARY AND TERNARY ALLOYS

by

P. A. Bergman

General Electric Company
West Lynn, Mass.

Submitted as a Topical Report
Related to the
Hot Corrosion Mechanism Study
Contract No. N-(600) (61533)-63219

Conducted for the
U. S. Naval Marine Engineering Laboratory
Annapolis, Md.

January 1966

APPENDIX D

HOT CORROSION BEHAVIOR OF NICKEL AND COBALT BINARY AND TERNARY ALLOYS

P. A. Bergman

I. INTRODUCTION

In January 1965, the U. S. Navy awarded two contracts to General Electric Company relative to the hot corrosion problem of gas turbine engines operating in marine environments. One program is the Hot Corrosion Mechanism Study, and the other program is Development of Alloys Resistant to Hot Corrosion. The ultimate purpose of both programs is the development of high-temperature alloys for gas turbine engine application in naval vessels--specifically a nickel-base alloy for turbine bucket application at 1600°F with the strength capacity of Inco 713, and a cobalt-base alloy for 1900°F with a strength equivalent to WI 52.

This investigation was part of the mechanism program, entailing a study of the effects of alloying elements on hot corrosion behavior. Binary and ternary alloys were chosen to avoid the synergistic effects of alloying elements in the complex compositions. It is expected that this type of approach would provide information for the development of complex alloys and would eventually dovetail into the alloy development program.

Nickel and cobalt and their binary and ternary alloys were evaluated. All of them were vacuum cast of high-purity metals and nominal compositions are shown below:

Pure nickel;

Three binary nickel alloys (10%, 15%, and 25% Cr);

Five ternary nickel alloys (15% Cr plus one of the following elements: 8% W, 25% Co, 5% Ti, and 8% Al);

Pure cobalt;

One binary cobalt alloy (25% Cr);

Four ternary cobalt alloys (25% Cr plus one of the following elements: 8% W, 6% Mo, 8% Ta, and 10% Ni).

The ternary nickel-base alloys contained 15% chromium since it is considered a borderline amount for corrosion resistance. The cobalt-base alloys were designed with 25% chromium since most of the applicable commercial cobalt-base alloys contain 20% to 25% chromium. For comparative purposes, PDRL-163, SEL, and X40 were tested. * The chemical compositions of all alloys are shown in Table I.

*PDRL-163--an International Nickel Company development alloy, nickel base.
SEL--a nickel-base alloy developed at the Thomson Engineering Laboratory, General Electric Company, West Lynn, Mass.
X40--a cobalt-base alloy

Tests were conducted in the MEL Hot Corrosion Test Rig, which promotes the type of hot corrosion encountered in gas turbine engines. Specimens were exposed to the products of combustion of sulfur-enriched (1%) diesel fuel and a high concentration of sea salt (200 ppm) for 100 hours at 1675°, 1750°, and 1900°F. Afterwards, the specimens were metallographically evaluated for the type and the amount of attack, and comparisons were drawn. The results demonstrate that some alloying elements have a pronounced effect on hot corrosion behavior.

In addition, for specimens tested at 1675° and 1900°F, the surface oxides were identified by x-ray diffraction analyses. The corrosion behavior of a metal is, of course, directly related to its oxides. The identification of the oxides and their behavior can lead to a greater understanding of the hot corrosion mechanism. The enclosed data are a beginning in this field of endeavor. Although the information is not extensive, there are some interesting and noteworthy observations made.

II. PROCEDURES

A. Testing

A hot corrosion test stand was designed and built for burning diesel and distillate fuels at relatively low pressures and velocities. A cross-sectional view and photograph of the MEL Hot Corrosion Test Rig are shown in Figs. 1 and 2.

Fuel is metered through a hypodermic needle and is atomized by a stream of air passing over the needle and burned in the forward zone of a 2 3/4-inch-diameter ceramic tube. Sea water is atomized and introduced into the combustion zone. Secondary air enters tangential slots in the ceramic tube into the combustion zone for cooling of the tube, for mixing purposes, and for adding the desired quantity of bulk air. The products of combustion and sea water pass through the remainder of the tube into the test chamber and out the exhaust tube. The ceramic tube and test chamber are surrounded by electrical resistance windings that are used to aid in maintaining constant and uniform temperatures.

The furnace above the test specimens can be opened while the test rig is in operation. This feature allows the fixture with specimens to be put into or taken out of test without disrupting the operation of the rig. Thus, fuel-rich conditions during firing of the rig are avoided.

Monitoring of temperatures is accomplished with an optical pyrometer after calibration and spot checking with a thermocouple. The temperature variation is between ± 10° and ± 15°F.

Standard test conditions include an excess of air at a 30:1 air-to-fuel ratio. The diesel fuel (MIL-F-16884) that is used has a 625°F end point, 0.840 g/cc density, and 0.69% sulfur. Ditertiary butyl disulfide is added to increase the sulfur to 1.0%. Artificial sea water* is used in concentration of 200 parts sea salt per million parts of air (ppm). All tests were scheduled for 100 hours ± 5 hours.

*ASTM designation D665-60, ASTM standards 1961, part 7, page 312.

For each test temperature in this program, all specimens (20) were tested at the same time in a rotating fixture at about 25 rpm. The specimens were in the cast condition with no prior heat treatment; they were centerless ground to 0.130-inch diameters and cut to 0.750-inch lengths. The test fixtures were made of Hastelloy X, which has a relatively good resistance to hot corrosion.

Specimens were measured with micrometers and cleaned in acetone and trichloroethylene prior to testing.

B. Specimen Evaluation

It is felt that metallographic measurements are the most pertinent and representative rating system for registering the degree of attack. For this method, two cross-sectional areas of each specimen are mounted for metallographic examination. One represents a zone of maximum visual attack, and the other one represents a zone of average visual attack. For a specimen corroded over half or less of its length, the sections are taken in a corroded zone and a noncorroded zone. Each of the cross-sectional areas is measured for hot corrosion effects across two diameters approximately 90° apart; thus, each specimen is measured in four places. Two types of hot corrosion effects are determined, namely, gross (massive) attack and maximum attack, which are illustrated in Fig. 3. All values are reported as losses in diameter (mils).

Gross attack is a measurement of complete material loss plus massive oxidation and sulfidation and does not factor in other types of subsurface attack; e.g., intergranular attack. For each specimen, four measurements are reported to show the consistency of attack. The measurements were averaged together and this new value is reported and plotted as the gross attack. Basically, this is a modification of the weight-change type method except the depth of massive oxides and sulfides is factored in, and more emphasis is placed on localized attack.

Maximum attack is a measurement which includes gross attack plus the depth of penetration of all sulfides and oxides which may be scattered or in local concentrations; e.g., grain boundaries. A measurement for each cross-sectional area is reported to indicate the consistency of attack, but only the greatest value is considered the maximum attack for the alloy.

The main disadvantages of the metallographic technique are the lack of a quantitative method to locate representative areas for examination and the judgment required in measuring the degree of attack.

A photomicrograph was taken in a representative area for each alloy. Descriptions of the type of attack and typical photomicrographs are included. The gray globular phases and the golden phases (characteristic color during metallographic examinations but not in photomicrographs) were presumed to be chromium-rich sulfides (M_2S_3) and the nickel-nickel sulfide eutectic ($M:M_2S_3$), respectively, based on metallographic similarities to specimens subjected to electron microprobe analyses in a Company-sponsored program.

C. X-ray Diffraction Analyses

After test, the specimens were rinsed in hot water to remove the salt since most of them were stuck in the test fixture, especially after testing at

the low temperature. The surface oxides were scraped off and submitted to powder pattern x-ray diffraction analyses.

III. RESULTS

A. Amount and Type of Attack

The amounts of gross attack and maximum attack are shown in Tables II, III, and IV and plotted in Figs. 4 through 9. Effects of elements in the ternary alloys are established by comparison to binary alloys with equivalent chromium contents.

1. Nickel Alloys Tested at 1675°F (Fig. 4)

Nickel. The entire specimen (RL-1) was affected and it was converted to an oxide and the nickel-nickel sulfide eutectic (Fig. 10).

Binaries. Additions of 10% chromium (RL-2), 15% chromium (RL-3), and 25% chromium (RL-4) resulted in a marked improvement in the corrosion resistance. There was a small amount of gross attack and some maximum attack as evidenced by the small chromium-rich sulfides in the grain boundaries (Fig. 11). The sulfides were not quite as deep in the 25% chromium alloy.

Ternaries. The alloy with 8% tungsten (RL-4) showed the same amount of attack as the binary. Microstructural examination revealed a similar type of attack except for small localized oxidation sites (Fig. 12). Some of these were narrower at the surface and wider at the bottom, but they were not deep enough to register as a significant measurement.

The 25% cobalt addition (RL-6) did not influence the degree or type of attack except that the small chromium-rich sulfides were not quite as deep. Alloys with 6% molybdenum (RL-7) and 5% titanium (RL-8) had the same degree and type of attack as the binary except that the two alloys appeared to have slightly more surface oxidation. This was not deep enough to influence the measured amounts of attack.

The addition of 8% aluminum (RL-9) caused an increase in the gross attack and a slight increase in the maximum attack. About half of the specimen was corroded in random areas. There was a band of small chromium-rich sulfides below the surface and parallel to it. In some areas near the surface, the nickel-nickel sulfide was seen and Ni_3S_2 was identified by x-ray diffraction analyses (Table V). These phases are characteristic of alloys susceptible to severe hot corrosion effects. There were no subsurface oxides or sulfides detected in the other half of the specimen which was virtually unaffected.

Commercial Alloys. PDRL-163 and SEL contained large but localized zones of subsurface oxides and a band of small chromium-rich sulfides plus larger ones in the SEL specimen (Fig. 13). There were extensive areas of the PDRL-163 specimen that appeared to be unaffected by the hot corrosion environment.

2. Nickel Alloys Tested at 1750°F (Fig. 5)

Nickel (RL-1) was subject to a severe attack resulting in the formation of large quantities of an oxide and the nickel-nickel sulfide eutectic. A small

core of the nickel was intact but the grain boundaries were completely penetrated by the eutectic.

Binaries. Addition of 10% chromium (RL-2) improved the corrosion resistance of nickel but the alloy was subject to some gross attack and considerable maximum attack. The microstructure contained large chromium-rich sulfides (Fig. 14). Higher levels of chromium, 15% (RL-3) and 25% (RL-4), made a marked improvement in the corrosion resistance. There was a small gross attack and some maximum attack as shown by the small subsurface chromium-rich sulfides (Fig. 15).

Ternaries. The 8% tungsten alloy (RL-5), had an amount and type of attack equivalent to the binary, except in one area where there was a large oxide blister (Fig. 16). It was similar in shape but much larger than the ones in the 1675°F test (Fig. 12). The oxide blister did not register as a significant gross attack since this is an average value.

An addition of 25% cobalt (RL-6) resulted in the same degree and type of attack as the binary except that it was not quite as deep. A 6% molybdenum addition (RL-7) promoted an increase in the attack which was in the form of massive oxidation and a deep subsurface penetration of small chromium-rich sulfides (Fig. 17).

There was a slight increase in attack in the alloy containing 5% titanium (RL-8). The microstructure showed small subsurface oxides and chromium-rich sulfides (Fig. 18). The alloy with 8% aluminum (RL-9) had an appreciable increase in corrosion. The type of attack varied; in some areas, there were large chromium-rich sulfides (Fig. 19), other areas had complete oxidation with no visible subsurface effects (Fig. 20), and other zones showed an intergranular attack.

Commercial Alloys. SEL was subject to about the same amount of attack as RL-9. The microstructure was similar to the 1675°F SEL microstructure (Fig. 13) except the chromium-rich sulfides were larger in the 1750°F specimen.

3. Nickel Alloys Tested at 1900°F (Fig. 6)

Nickel (RL-1) was attacked throughout the specimen comparable to the one tested at 1675°F. The products of corrosion were an oxide and the nickel-nickel sulfide eutectic (Fig. 21). Nickel sulfide (Ni_3S_2) was identified by x-ray diffraction analyses (Table V).

Binaries. Alloys with 10% chromium (RL-2), 15% chromium (RL-3), and 25% chromium (RL-4) were all subject to some gross attack and considerable maximum attack. The higher chromium alloy was better than the other two that were comparable to each other. The 10% chromium alloy showed large chromium-rich sulfides and some nickel-nickel sulfide eutectic (Fig. 22). In the 15% chromium alloy there were numerous small chromium-rich sulfides that penetrated deeply into grain boundary areas (Fig. 23); the attack in the 25% chromium alloy was similar but not as deep.

Ternaries. The addition of 8% tungsten (RL-5) resulted in an increase in corrosion, especially the gross attack. The type of subsurface attack was similar to that of the binary alloy. The 25% cobalt alloy (RL-6) had a similar type of attack (Fig. 24), but somewhat less extensive.

The addition of 6% molybdenum (RL-7) had a catastrophic effect. The specimen was removed from the test after only 12 hours since there was only a small portion of it left. The microstructure showed a massive oxidation with no visible subsurface effects (Fig. 25). The 5% titanium alloy (RL-8) showed an improved corrosion behavior in terms of depth of attack; in fact, it was equivalent to the 25% chromium binary. However, there was a different type of attack that was a denser concentration of medium-size chromium-rich sulfides (Fig. 26) and an unidentified gray angular-shaped phase (Fig. 27).

The alloy with 8% aluminum (RL-9) had an appreciable increase in attack. There was a band of small chromium-rich sulfides below the surface and parallel to it. Near the surface were large chromium-rich sulfides and large quantities of the nickel-nickel sulfide eutectic (Fig. 28).

Commercial Alloys. SEL had less corrosion that the 8% aluminum ternary alloy. The type of attack was similar to that in the SEL specimen tested at 1750°F. The PDRL-163 specimen showed less attack than any other nickel alloy. There was a subsurface attack of a fine network of oxides and chromium-rich sulfides.

4. Cobalt Alloys Tested at 1675°F (Fig. 7)

Cobalt (RL-11) was subject to a catastrophic attack that consumed all of the specimen.

Binary. The addition of 25% chromium (RL-10) achieved a marked improvement in corrosion behavior. There was practically no gross attack and a very small amount of maximum attack consisting of a few small subsurface chromium-rich sulfides (Fig. 29) and occasionally a few small oxides.

Ternaries. The alloys with 8% tungsten (RL-12), 6% molybdenum (RL-13), 8% tantalum (RL-14), and 10% nickel (RL-15) had an amount and type of attack equivalent to the binary.

Commercial Alloy. X40 showed a corrosion behavior similar to the binary and ternary alloys.

5. Cobalt Alloys Tested at 1750°F (Fig. 8)

Cobalt (RL-11) was attacked through the entire specimen. The products of corrosion were an oxide and a phase that was probably the cobalt-cobalt sulfide eutectic (Fig. 30).

Binary. An addition of 25% chromium to the cobalt conferred good resistance to corrosion. The degree and type of attack were similar to the specimen tested at 1675°F.

Ternaries. The alloys with 8% tungsten (RL-12) and 8% tantalum (RL-14) had a corrosion behavior similar to the binary, but the alloy with 6% molybdenum (RL-13) showed a severe attack. There was a shallow subsurface attack shown by a fine network of chromium-rich sulfides and oxides (Fig. 31).

The 10% nickel (RL-15) did not cause much of an effect except that the subsurface attack was slightly deeper (Fig. 32).

Commercial Alloy. X40 had a corrosion behavior equivalent to the binary.

6. Cobalt Alloys Tested at 1900°F (Fig. 9)

Cobalt (RL-11) was subject to considerable corrosion. There were no visible subsurface effects, but at the surface there was a phase similar in appearance to the one in Fig. 30 which was probably the cobalt-cobalt sulfide eutectic.

Binary. The alloy with 25% chromium (RL-10) was considerably better and had a small amount of gross attack and some maximum attack. There were small subsurface chromium-rich sulfides (Fig. 33) and a few small oxides in some areas.

The addition of 8% tungsten (RL-12) caused an increase in corrosion and the subsurface phases were similar but deeper than the binary. The alloy with 6% molybdenum (RL-13) was destroyed.

The 8% tungsten alloy (RL-14) and 10% nickel alloy (RL-15) showed about the same corrosion behavior as the binary except that there was slightly less gross attack. The microstructures contained small subsurface chromium-rich sulfides and oxides.

B. X-ray Diffraction Analysis of Surface Products

The results of x-ray diffraction analyses of the surface products on all alloys tested at 1675° and 1900°F are shown in Tables V and VI.

1. Nickel Alloys

Spinels in relatively small amounts were found on 13 out of 16 specimens of the binary and ternary alloys and one of the commercial alloys. Most of their lattice parameters were between 8.31 Å and 8.33 Å. The aluminum-containing alloys showed larger amounts of the spinels, and three out of four had the lowest lattice parameters, 8.16 Å, 8.22 Å, and 8.28 Å. However, one of the high-aluminum containing alloys (PDRL 163) had no spinel.

Although the spinels were not analyzed, their chemical compositions are suggested by the chemical composition of the alloys and by comparison to known spinels. Those with parameters of 8.28 Å to 8.33 Å are almost certainly $NiCr_2O_4$ and for the high-cobalt-containing alloys, $(Ni, Co)Cr_2O_4$ or $CoCr_2O_4$. The high-aluminum alloys generate spinels with lower lattice parameters due to aluminum in solid solution.

NiO was detected on 20 out of 28 specimens in relatively large amounts. This was the only oxide on the nickel specimens.

Co·(Cr, Ni)O formed on the cobalt-containing alloys tested at 1900°F instead of on NiO.

Cr_2O_3 was found on eight out of 21 specimens, including three alloys tested at 1675° and 1900°F (this accounted for six of the eight specimens). There were relatively small amounts of the Cr_2O_3 except on PDRL 163 (tested at 1900°F) which had a medium amount.

$(Cr, Ti)_2O_3$ was present on the highest titanium-containing alloy, RL-8 (5% titanium).

Others. Nickel sulfide (Ni_3S_2) was detected on two alloys, both of which showed the nickel-nickel sulfide eutectic (metallographic examination).

Na_2SO_4 was found on several of the specimens and appeared related to the high amounts of NiO.

2. Cobalt Alloys

Spinels were found on eight out of 11 specimens of the alloys, in small to medium amounts with lattice parameters of 8.275 Å to 8.33 Å. These are almost certainly $CoCr_2O_4$. The three specimens without spinels were the ternary alloys containing tungsten or molybdenum.

Cr_2O_3 was detected on eight out of 11 specimens in relatively small amounts except for RL-13 (1675°F) which had a medium amount.

CoO·(Cr, Ni)O formed on several of the specimens, including the cobalt specimens, in relatively large amounts.

Others. $NaTaO_3$ was detected on the tantalum-containing alloy, and Na_2SO_4 was found on only one specimen.

IV. DISCUSSION AND SUMMARY

A. Effect of Alloying Elements

Nickel and cobalt were subject to catastrophic attack at 1675°, 1750°, and 1900°F.

1. Nickel Alloys (Figs. 4, 5, and 6)

Chromium

This element conferred a marked improvement in corrosion resistance that was dependent on the amount of chromium and the test temperature.

	Relative Corrosion Resistance		
Temp (°F)	10% Cr	15% Cr	25% Cr
1675	Good	Good	Good
1750	Poor	Good	Good
1900	Poor	Poor	Fair

Chromium becomes less effective as a function of temperature.

Tungsten (8%)

No effect at 1675° and 1750°F although there was a suspicious oxidation.
Detrimental at 1900°F.

Cobalt (25%)

No effect or slightly beneficial at 1675°, 1750°, and 1900°F.

Molybdenum (6%)

No effect at 1675°F.
Detrimental at 1750°F.
Catastrophic at 1900°F.

Titanium (5%)

No effect at 1675°F.
Slightly detrimental at 1750°F.
Beneficial at 1900°F.

Aluminum (8%)

Slightly detrimental at 1675°F.
Detrimental at 1750°F.
Severely detrimental at 1900°F.

Complex Alloys

At 1675°F, SEL (4.4% Al) and PDRL-163 (6.3% Al) showed some hot corrosion effects. The only ternary showing much of an effect was the aluminum-containing alloy (8% Al in RL-9).

At 1750°F, SEL was attacked similar to RL-9.

At 1900°F, SEL showed more resistance to attack than RL-9 and PDRL-163 was considerably better; in fact, it was the best nickel alloy tested.

Comparisons of the binary and ternary alloys to complex alloys (tested in this program and others) show many equivalent effects of alloying elements and one noteworthy variation. At low temperatures, aluminum is detrimental in the ternary and complex alloys; but at 1900°F it is detrimental in the ternary, and may even be beneficial in a complex alloy. Another interesting result shows that although aluminum is detrimental at 1675°F, half of the specimens have a superior corrosion resistance. Since aluminum and titanium are essential for strength considerations, a heavier emphasis is recommended for establishing the corrosion behavior of alloys containing these elements.

2. Cobalt Alloys (Figs. 7, 8, and 9)

Chromium (25%)

Beneficial at 1675°, 1750°, and 1900°F.

Tungsten (8%)

No effect at 1675° and 1750°F.
Detrimental at 1900°F.

Molybdenum (6%)

No effect at 1675°F.
Severe effect at 1750°F.
Catastrophic effect at 1900°F.

Tantalum (8%)

No effect at 1675°, 1750°, and 1900°F.

Nickel (10%)

No effect at 1675°, 1750°, and 1900°F.

At 1900°F, tungsten promoted a severe attack in nickel and cobalt alloys. It is suggested that a tungstate compound was responsible for the attack, although none was found in x-ray diffraction analysis of surface products. Molybdenum caused a catastrophic attack in both types of alloys. This was probably due to the formation of the highly volatile molybdenum trioxide.

B. Cobalt vs Nickel Alloys (Figs. 4 through 9)

A comparison of the most corrosion resistant cobalt and nickel alloys is as follows:

1675°F--cobalt alloys were slightly better.
1750°F--cobalt alloys were slightly better.
1900°F--cobalt alloys were considerably better.

Part of these effects may be due to the high chromium contents of the cobalt alloys. However, the high chromium-containing nickel alloy (25% Cr) was subject to deeper subsurface attack than the cobalt alloys containing an equivalent amount of chromium.

C. Effect of Temperature (Figs. 4 through 9)

The effect of temperature on the most corrosion resistant alloys is as follows:

Nickel--same degree of attack at 1675° and 1750°F and a large increase at attack at 1900°F.

Cobalt--same degree of attack at 1675° and 1750°F and a slight increase at 1900°F.

D. Oxides

1. Nickel Alloys

The oxides appeared characteristic of particular compositions and independent of test temperature since most of the alloys formed the same oxides at 1675° and 1900°F.

Most of the alloys had relatively small amounts of spinels and large amounts of NiO. The spinels were $NiCr_2O_4$ and for the cobalt-containing alloys, most likely (Ni, Co) Cr_2C_4 or $CoCr_2O_4$. Two of the alloys with aluminum had spinels with lower lattice parameters due to aluminum in solid solution in the structure.

The NiO did not provide any degree of corrosion resistance judging from the severe attack of nickel. The addition of small amounts of spinels conferred a marked improvement in corrosion behavior at 1675°F and less of an improvement at 1900°F. The spinels with aluminum were present in greater amounts but were not as effective.

At 1900°F the cobalt-containing alloys formed CoO·(Cr, Ni)O in preference to NiO, but this did not influence corrosion behavior.

The Cr_2O_3 was detected on a few alloys in small amounts. There was a tendency for either Cr_2O_3 or a spinel to form. Higher chromium contents (15%) suppressed the formation of Cr_2O_3, but the high cobalt alloys tended to form both oxides.

Over-all, the Cr_2O_3 and nickel, cobalt, and chromium spinels showed the same degree of corrosion protection. In fact, at times there were more variations in corrosion behavior for alloys containing similar oxides as shown below:

	1900°F		
	Oxide		
Alloy	Cr_2O_3	Spinel	Attack Maximum (mils)
10% Cr	W	--	46.0
15% Cr	--	VW (Å=8.33)	41.5
25% Cr	--	W (Å=8.33)	17.6

As a barrier to corrosion, the Cr_2O_3 on the 10% chromium alloy was equivalent to the spinel on the 15% chromium alloy, but they were not as effective as a similar spinel on a 25% chromium alloy. The difference in behavior was probably due to subsurface diffusion in the alloy and/or mechanical characteristics of the oxides (adherence, coherency, vacancies, etc.).

PDRL-163 showed a very unusual behavior. Although it contained high aluminum (6.3%) and high chromium (17%), there were no spinels. At 1900°F, it had the greatest amount of Cr_2O_3 and was the only alloy without NiO or CoO·(Cr, Ni)O, and it had a better corrosion behavior than any other nickel alloy.

The $(Cr, Ti)_2O_3$ was detected on the high titanium (5%) ternary besides a spinel and NiO. This alloy showed less depth of attack at 1900°F than other 15% chromium alloys.

2. Cobalt Alloys

Most of the alloys developed small amounts of Cr_2O_3, small to medium amounts of $CoCr_2O_4$, and in several, CoO·(Cr, Ni)O. The latter oxide did not provide any degree of protection judging from the severe attack of cobalt specimens, but Cr_2O_3 and $CoCr_2O_4$ conferred a marked improvement in corrosion resistance.

It appeared that molybdenum and tungsten suppressed the formation of a spinel at 1675°F, but there were no changes in corrosion behavior of the alloys. At 1900°F the molybdenum-containing alloy did not have Cr_2O_3 or a spinel. Apparently, the corrosion reaction was so rapid, these oxides did not form. This was probably a molybdenum trioxide problem.

Three of the alloys (25% chromium binary, and 8% tantalum and 10% nickel ternaries) had a similar combination of oxides and showed an equivalent corrosion behavior at each temperature.

In comparing the oxides on cobalt and nickel alloys, it is noted that the cobalt alloys have more of a tendency to form Cr_2O_3 besides a spinel. Even the nickel alloys with high cobalt content developed both oxides.

None of the oxides provided complete protection since at least small, scattered, subsurface chromium-rich sulfides were found in all alloys.

V. CONCLUSIONS

1. Chromium additions to nickel and cobalt were beneficial.

2. Cobalt and titanium in nickel alloys, and nickel and tantalum in cobalt alloys, had small or no effects.

3. Tungsten, molybdenum, and aluminum in nickel alloys and tungsten and molybdenum in cobalt alloys were detrimental; the effects became more pronounced at high temperatures.

4. The best cobalt alloys were more resistant to attack than the best nickel alloys.

5. It appeared that nickel, cobalt, chromium-rich spinels conferred as much protection as Cr_2O_3. None of the oxides provided complete resistance to attack.

TABLE I
Chemical Compositions

Alloy	Type	Composition (w/o) C	Cr	Ni	Co	W	Mo	Ta	Al	Ti	Cb
RL-1	Nominal	>0.05		100							
	Actual	.01									
RL-2	Nominal	.05	10.0	Bal.							
	Actual	.02	10.2	Bal.							
RL-3	Nominal	.05	15.0	Bal.							
	Actual	.01	15.0	Bal.							
RL-4	Nominal	.05	25.0	Bal.							
	Actual	.02	25.5	Bal.							
RL-5	Nominal	.05	15.0	Bal.		8.0					
	Actual	.01	15.1	Bal.		8.05					
RL-6	Nominal	.05	15.0	Bal.	25.0						
	Actual	.02	15.4	Bal.	24.0						
RL-7	Nominal	.05	15.0	Bal.			6.0				
	Actual	.01	15.0	Bal.			6.05				
RL-8	Nominal	.05	15.0	Bal.						5.0	
	Actual	.01	15.4	Bal.						4.96	
RL-9	Nominal	.05	15.0	Bal.					8.0		
	Actual	.04	15.4	Bal.					8.03		
SEL	Nominal	.08	15.0	Bal.	26.0		4.5		4.4	2.3	
PDRL-163	Nominal	.05	17.0	Bal.		2.0	1.6	1.9	6.3	0.1	1
RL-11	Nominal	.05			100						
	Actual	.02									
RL-10	Nominal	.05	25.0		Bal.						
	Actual	.01	25.6		Bal.						
RL-12	Nominal	.05	25.0		Bal.	8.0					
	Actual	.03	25.7		Bal.	7.88					
RL-13	Nominal	.05	25.0		Bal.		6.0				
	Actual	.01	26.2		Bal.		6.04				
RL-14	Nominal	.05	25.0		Bal.			8.0			
	Actual	.02	25.0		Bal.			7.08			
RL-15	Nominal	.05	25.0	10	Bal.						
	Actual	.02	26.4	10.2	Bal.						
X-40	Nominal	.45	25.0	10.5	Bal.	7.5					

TABLE II
1675°F Hot Corrosion Data*

Alloy	Composition (w/o) Ni	Co	Cr	Others	Loss in Diam. (mils) Gross Attack Sect. 1	Sect. 2	Avg	Maximum Attack Sect. 1	Sect. 2
RL-1	100	--	--	--	130.0	130.0	130.0	130.0	130.0
RL-2	Bal.	--	10	--	0.1, 0.9	0.3, 1.1	0.6	9.7	10.5
RL-3	Bal.	--	15	--	.4, .6	.4, 1.6	.8	9.6	10.6
RL-4	Bal.	--	25	--	.3, .7	.5, 0.7	.6	6.3	5.5
RL-5	Bal.	--	15	8 W	.4, 1.0	.6, 1.2	.8	9.2	10.0
RL-6	Bal.	25	15	--	+.1, +0.3	+.3, 0.5	.0	4.1	4.9
RL-7	Bal.	--	15	6 Mo	.4, 0.6	1.2, 1.2	.9	8.0	7.6
RL-8	Bal.	--	15	5 Ti	.9, 1.1	0.9, 1.1	1.0	7.1	8.5
RL-9	Bal.	--	15	8 Al	.1, 0.3	8.5, 9.3	4.6	0.3	13.7
SEL	Bal.	26	15	4.5 Mo 4.4 Al 2.3 Ti	.4, .4	2.4, 4.4	1.9	3.2	15.2
PDRL-163	Bal.	--	17	1.6 Mo 2.0 W 6.3 Al 1.0 Cb	+.1, .5	21.1, 23.1	11.2	1.1	26.7
RL-11	--	100	--	--	130.0	130.0	130.0	130.0	130.0
RL-10	--	Bal.	25	--	0.2, 0.2	0.2, 0.6	0.3	3.2	3.6
RL-12	--	Bal.	25	8 W	.6, .6	1.2, 1.4	1.0	1.8	3.8
RL-13	--	Bal.	25	6 Mo	.6, .8	1.0, 1.2	0.9	3.0	5.4
RL-14	--	Bal.	25	8 Ta	.7, .9	0.7, 1.3	.9	4.1	4.7
RL-15	10	Bal.	25	--	.4, 1.0	.6, 1.0	.8	5.6	6.4
X-40	10.5	Bal.	25	7.5 W 0.45 C	.1, 0.5	.1, 0.3	.3	2.7	3.5

*Time: 100 hours
Fuel: diesel (1% sulfur)
Air/fuel: 30/1
Sea salt: 200 ppm
Specimen size: 0.130-in. diam.

TABLE III
1750°F Hot Corrosion Data*

Alloy	Composition (w/o) Ni	Co	Cr	Others	Loss in Diam. (mils) Gross Attack Sect. 1	Gross Attack Sect. 2	Gross Attack Avg	Maximum Attack Sect. 1	Maximum Attack Sect. 2
RL-1	100	--	--	--	47.8, 81.0	59.8, 89.8	69.6	130.0	130.0
RL-2	Bal.	--	10	--	2.0, 3.8	20.2, 25.8	13.0	25.0	51.4
RL-3	Bal.	--	15	--	+0.4, 0.2	+0.4, 0.2	0.0	6.0	9.2
RL-4	Bal.	--	25	--	1.0, 1.4	1.2, 1.4	1.3	9.0	10.6
RL-5	Bal.	--	15	8 W	0.2, 0.8	1.2, 3.4	1.4	8.8	10.4
RL-6	Bal.	25	15	--	0.3, .3	1.1, 1.3	0.8	5.9	5.7
RL-7	Bal.	--	15	6 Mo	4.2, 5.6	6.2, 7.0	5.8	25.0	14.0
RL-8	Bal.	--	15	5 Ti	1.8, 2.0	1.6, 2.4	2.0	13.8	11.2
RL-9	Bal.	--	15	8 Al	11.2, 19.6	17.2, 19.2	16.8	21.2	21.6
SEL	Bal.	26	15	4.5 Mo 4.4 Al 2.3 Ti	1.4, 2.0	23.6, 23.6	12.7	8.0	29.4
SEL					12.2, 14.0	22.4, 24.8	18.4	20.4	27.6
RL-11	--	100	--	--	130.0	130.0	130.0	130.0	130.0
RL-10	--	Bal.	25	--	0.0, 0.8	0.4, 0.4	0.4	3.2	3.6
RL-12	--	Bal.	25	8 W	+ .4, + .4	.0, 0.0	0.0	4.6	3.8
RL-13	--	Bal.	25	6 Mo	.8, 1.0	61.2, 62.0	31.3	4.4	66.0
RL-14	--	Bal.	25	8 Ta	.8, 0.8	1.0, 1.2	1.0	5.2	5.4
RL-15	10	Bal.	25	--	.6, 1.0	1.0, 1.0	0.9	9.0	9.0
X-40	10.5	Bal.	25	7.5 W 0.45 C	+ .4, 0.6	0.4, 0.6	0.3	3.0	3.2

*Time: 100 hours
Fuel: diesel (1% sulfur)
Air/fuel: 30/1
Sea salt: 200 ppm
Specimen size: 0.130-in. diam.

TABLE IV
1900°F Hot Corrosion Data*

Alloy	Composition (w/o) Ni	Co	Cr	Others	Loss in Diam. (mils) Gross Attack Sect. 1	Sect. 2	Avg	Maximum Attac Sect. 1	Sect. 2
RL-1	100	--	--	--	130.0	130.0	130.0	130.0	130.0
RL-2	Bal.	--	10	--	1.0, 3.0	6.2, 11.8	5.5	41.4	45.8
RL-3	Bal.	--	15	--	1.6, 6.8	2.2, 6.6	4.3	30.6	41.4
RL-4	Bal.	--	25	--	0.9, 1.5	0.9, 2.5	1.5	17.3	17.7
RL-5	Bal.	--	15	8 W	14.1,20.1	16.3, 16.9	16.9	52.1	54.5
RL-6	Bal.	25	15	--	1.1, 1.9	1.3, 2.9	1.8	24.7	34.3
RL-7†	Bal.	--	15	6 Mo	40.8,66.2	130.0	91.8	66.2	130.0
RL-8	Bal.	--	15	5 Ti	1.2, 1.8	1.8, 4.2	2.3	18.8	20.2
RL-9	Bal.	--	15	8 Al	26.6,35.4	≈90.0	60.5	47.8	≈90.0
SEL	Bal.	26	15	4.5 Mo 4.4 Al 2.3 Ti	12.6,17.4	16.2, 25.4	17.9	27.0	33.2
SEL	Bal.				12.9,13.7	14.5, 15.1	14.1	26.5	25.3
PDRL-163	Bal.	--	17	1.6 Mo 2.0 W 6.3 Al 1.0 Cb	0.9, 0.9	1.7, 2.1	1.4	7.7	11.7
RL-11	--	100	--	--	59.8,65.0	62.6, 68.6	64.0	67.0	68.6
RL-10	--	Bal.	25	--	2.5, 2.9	2.9, 3.3	2.9	9.5	10.5
RL-12	--	Bal.	25	8 W	2.0, 3.8	29.8, 34.0	17.4	16.6	42.0
RL-13	--	Bal.	25	6 Mo	130.0	130.0	130.0	130.0	130.0
RL-14	--	Bal.	25	8 Ta	0.6, 1.0	1.0, 1.6	1.1	9.8	9.8
RL-15	10	Bal.	25	--	1.3, 1.8	2.1, 2.3	1.9	12.9	12.9

*Time: 100 hours
Fuel: diesel (1% sulfur)
Air/fuel: 30/1
Sea salt: 200 ppm
Specimen size: 0.130-in. diam.

†Specimen removed from test after 12 hours.

TABLE V

X-ray Diffraction Analyses of Oxides (Ni-base Alloys)

Alloy	Composition (w/o) Ni	Cr	Others	Temp (°F)	X-ray Diffraction Results Cr_2O_3	$(CrTi)_2O_3$	Spinel	NiO	CoO·(Cr, Ni)O*	Ni_3S_2	Na_2SO_4
RL-1	100	--	--	1675	--	--	--	s	--	--	w
				1900	--	--	--	s	--	w	w
RL-2	Bal.	10	--	1675	w	--	--	s	--	--	w
				1900	w	--	--	s	--	--	w
RL-3	Bal.	15	--	1675	?	--	w (Å=8.31)	ms	--	--	?
				1900	--	--	vw (Å=8.33)	s	--	--	vw
RL-4	Bal.	25	--	1675	--	--	w (Å=8.33)	s	--	--	m
				1900	vw?	--	w (Å=8.33)	ms	--	--	--
RL-5	Bal.	15	8 W	1675	--	--	w (Å=8.33)	ms	--	--	?
				1900	--	--	? (Å=8.33)	ms	--	--	vw
RL-6	Bal.	15	25 Co	1675	vw	--	w (Å=8.32)	w	--	--	--
				1900	w	--	wm (Å=8.28)	--	m (25%)	--	--
RL-7	Bal.	15	6 Mo	1675	--	--	vw (Å=8.31)	s	--	--	--
				1900	--	--	w (Å=8.32)	m	--	--	?
RL-8	Bal.	15	5 Ti	1675	--	m	w (Å=8.32)	vw	--	--	--
				1900	--	w	vw (Å=8.32)	m	--	--	--
RL-9	Bal.	15	8 Al	1675	--	--	--	m	--	w	--
				1900	--	--	m (Å=8.16)	ms	--	--	w
SEL	Bal.	15	26 Co 4.5 Mo 4.4 Al 2.3 Ti	1675	vw	--	m (Å=8.28)	w	--	--	--
				1900	--	--	m (Å=8.22)	m	--	--	--
				1900	--	--	m (Å=8.33)	--	m (55%)	--	--
PDRL-163	Bal.	17	1.6 Mo 2.0 W 6.3 Al 1.0 Cb	1675	vw	--	--	m	--	--	vw
				1900	m	--	--	--	--	--	--

*% Cobalt based on lattice parameter measurements only.

TABLE VI
X-ray Diffraction Analyses of Oxides (Co-base Alloys)

Alloy	Composition (w/o) Co	Cr	Others	Temp (°F)	X-ray Diffraction Results Cr_2O_3	Spinel	NiO	CoO·(Cr, Ni)O*	$NaTaO_3$	Na_2SO_4
RL-11	100	--	--	1675	--	--	--	s (100% Co)	--	w
				1900	--	--	--	s (100% Co)	--	--
RL-10	Bal.	25	--	1675	w	w (Å=8.30)	--	--	--	--
				1900	vw	w (Å=8.29)	--	m (75% Co)	--	?
RL-12	Bal.	25	8 W	1675	w	--	--	w (100% Co)	--	--
				1900	--	m (Å=8.275)	--	--	--	--
RL-13	Bal.	25	6 Mo	1675	m	--	--	--	--	--
				1900	--	--	--	s (100% Co)	--	--
RL-14	Bal.	25	8 Ta	1675	vw	w (Å=8.28)	--	--	--	--
				1900	vw	m (Å=8.33)	--	m (65% Co)	w	--
RL-15	Bal.	25	10 Ni	1675	?	w (Å=8.32)	--	--	--	--
				1900	vw	m (Å=8.33)	--	m (70% Co)	--	--
X-40	Bal.	25	10.5 Ni 7.5 W 0.45 C	1675	vw	m (Å=8.28)	vw	--	--	--

*% Cobalt based on lattice parameter measurements only.

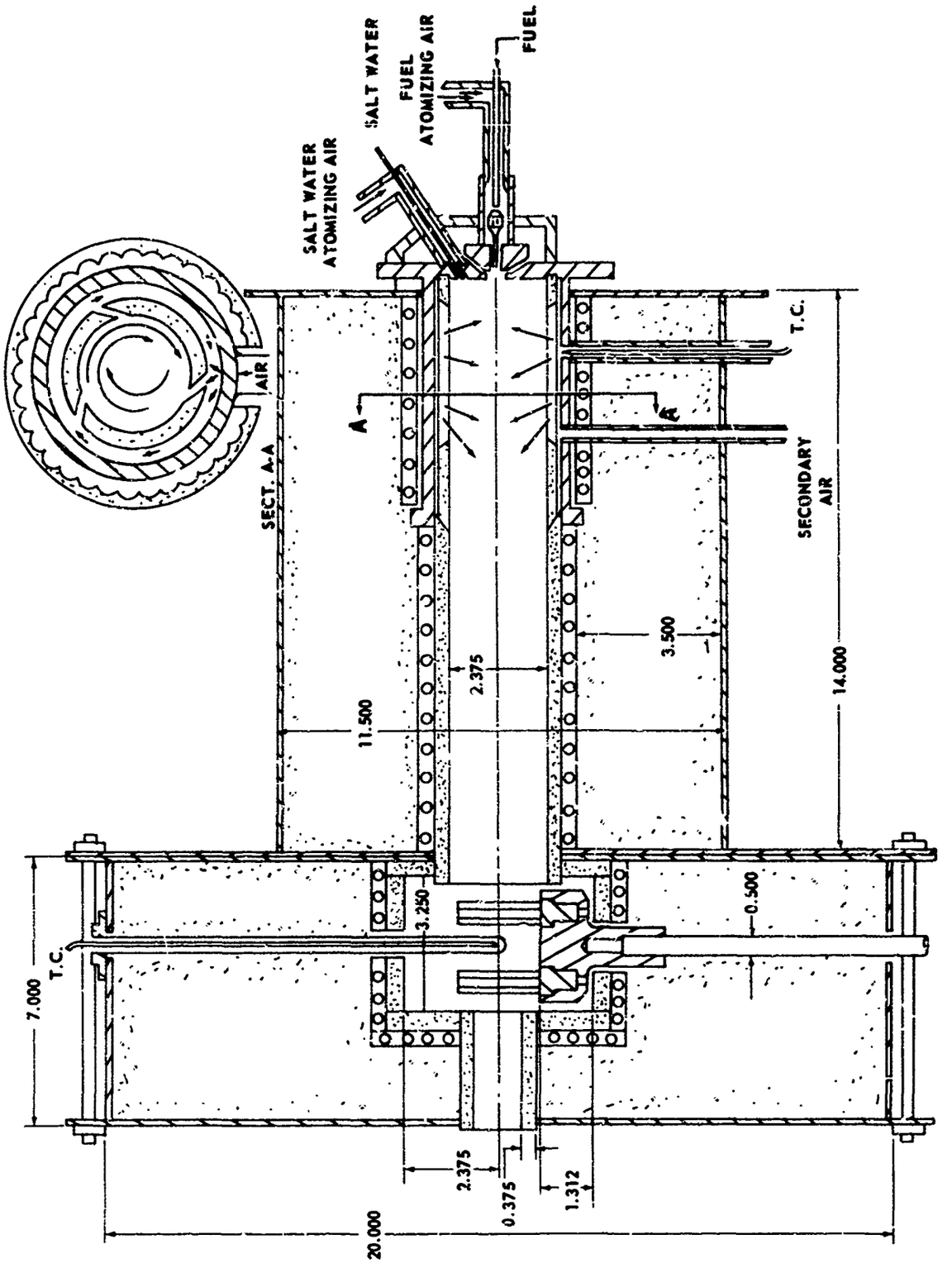

Fig. 1 A cross-sectional view of the MEL Hot Corrosion Test Rig.

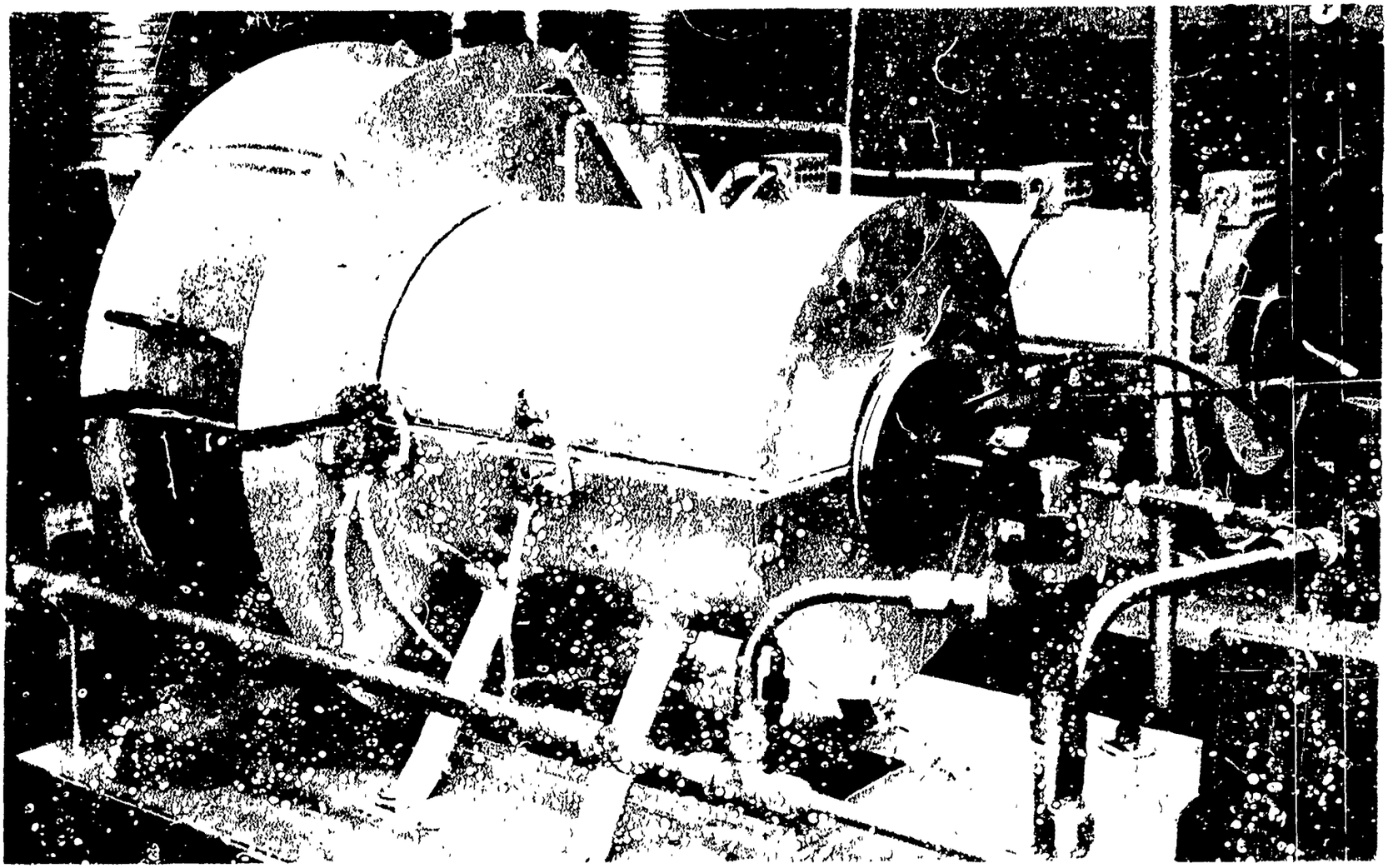

Fig. 2 The MEL Hot Corrosion Test Rig.

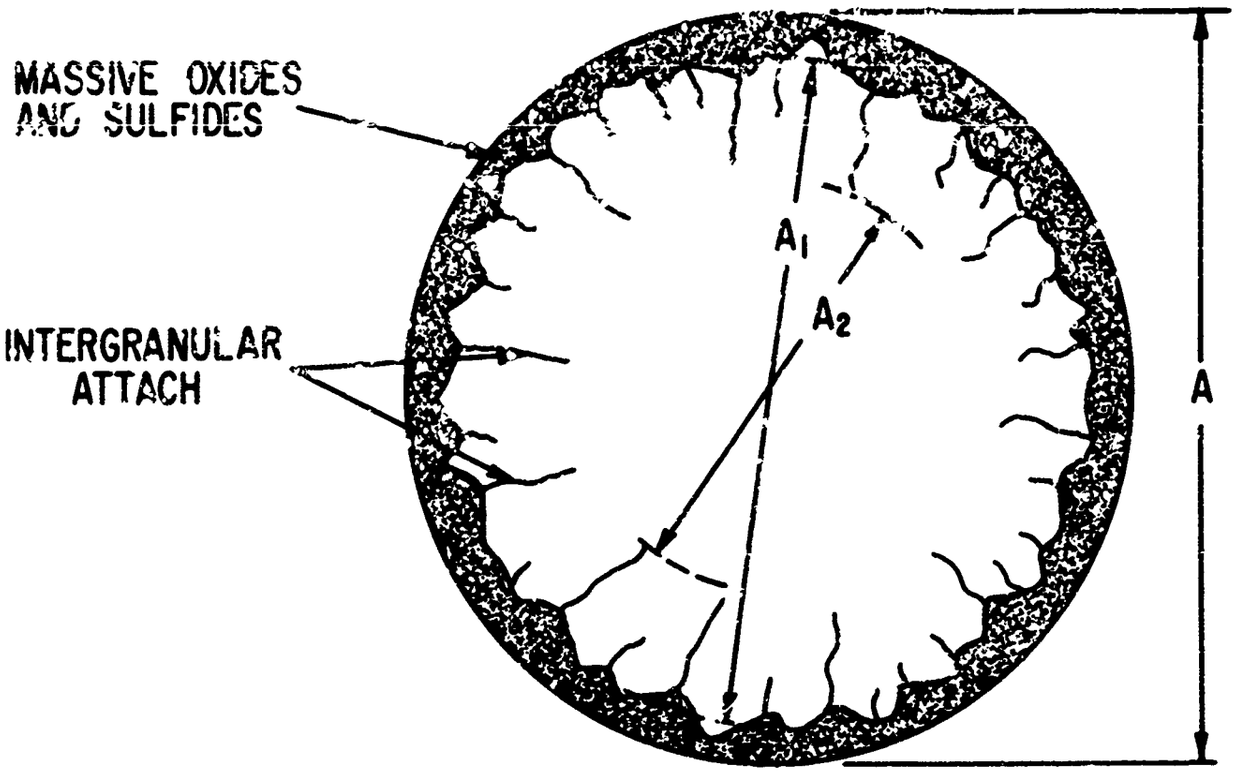

A = Original diameter, measured with a micrometer.

A_1 = Diameter of structurally useful metal, measured at 100X.

A_2 = Diameter of metal unaffected by oxides and sulfides, measured at 100X.

Gross attack: $A-A_1$ averaged loss in diameter due to massive oxides and sulfides.

Maximum attack: $A-A_2$ loss in diameter due to all forms of oxidation and sulfidation.

Fig. 3 Method of measuring hot corrosion attack.

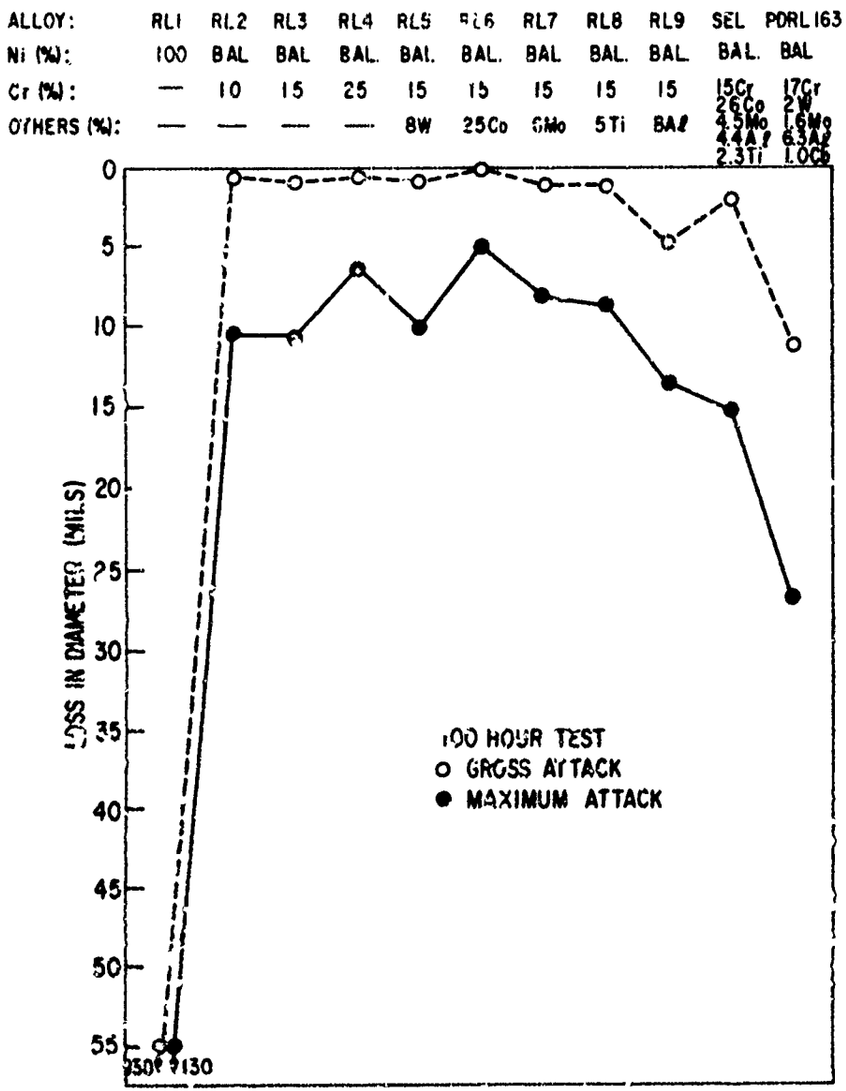

Fig. 4 Hot corrosion data for nickel alloys--1675°F.

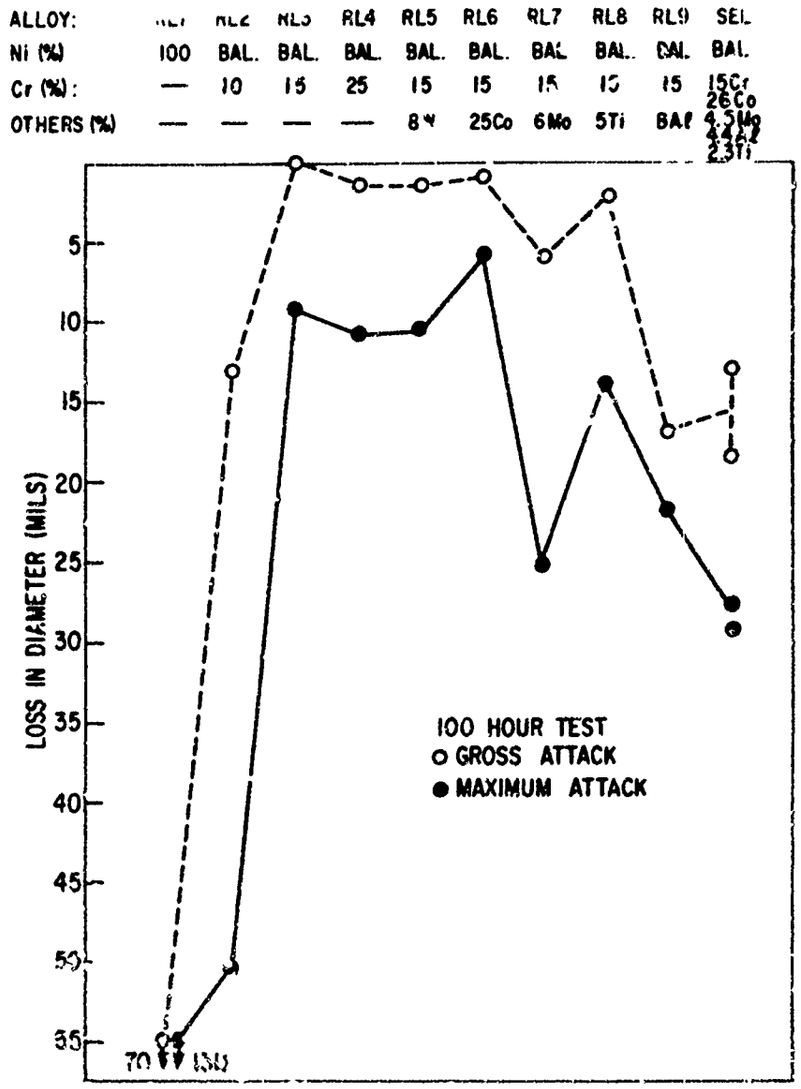

Fig. 5 Hot corrosion data for nickel alloys--1750°F.

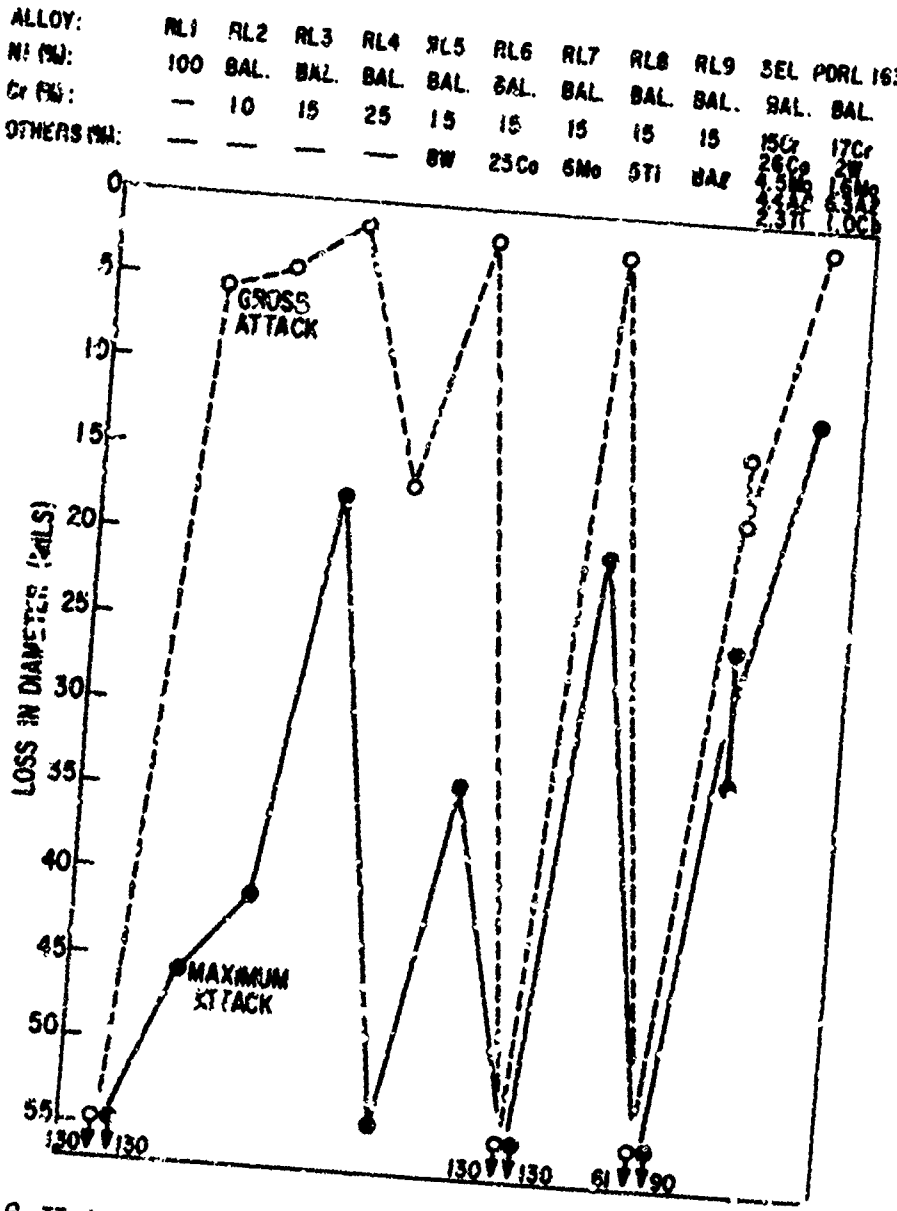

Fig. 6 Hot corrosion data for nickel alloys--
1900°F.

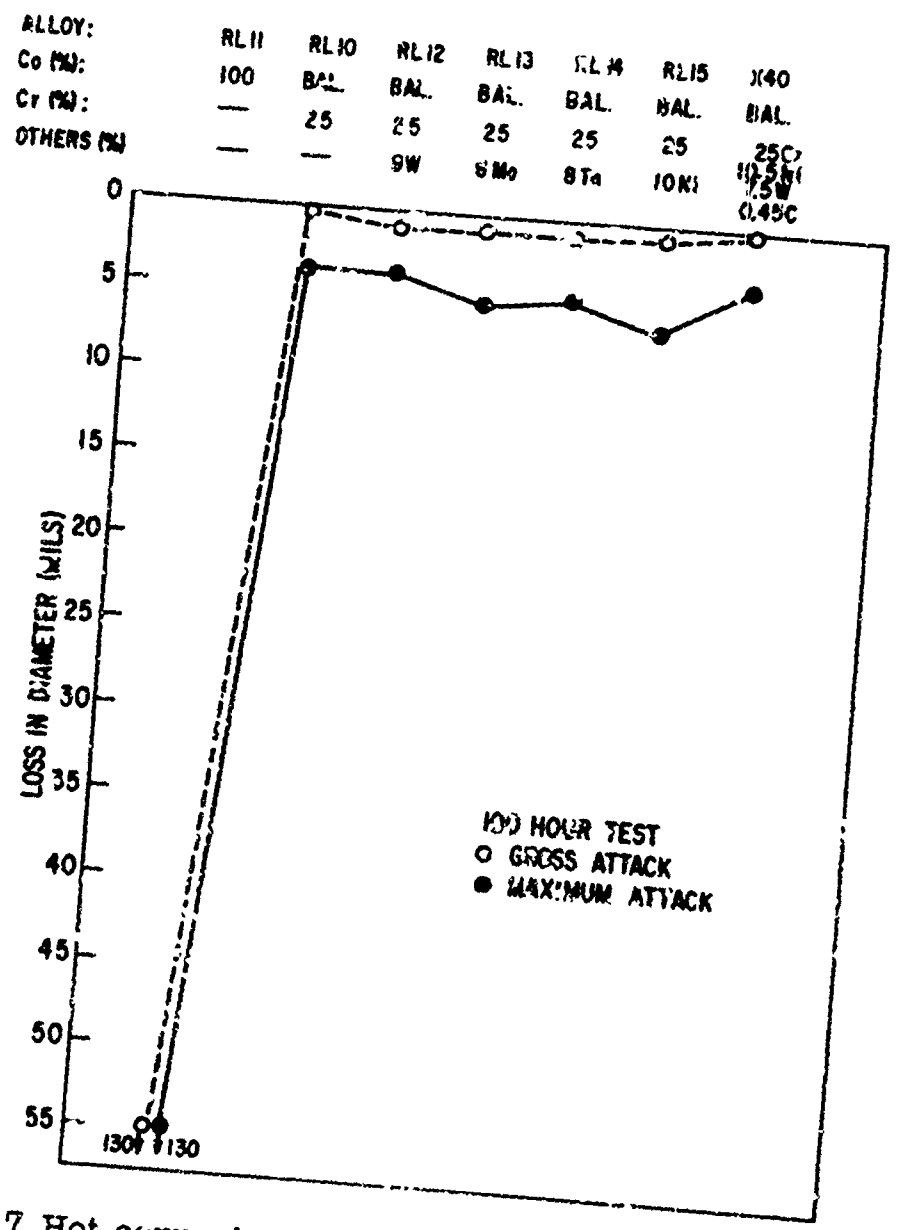

ig. 7 Hot corrosion data for cobalt alloys--
1675°F.

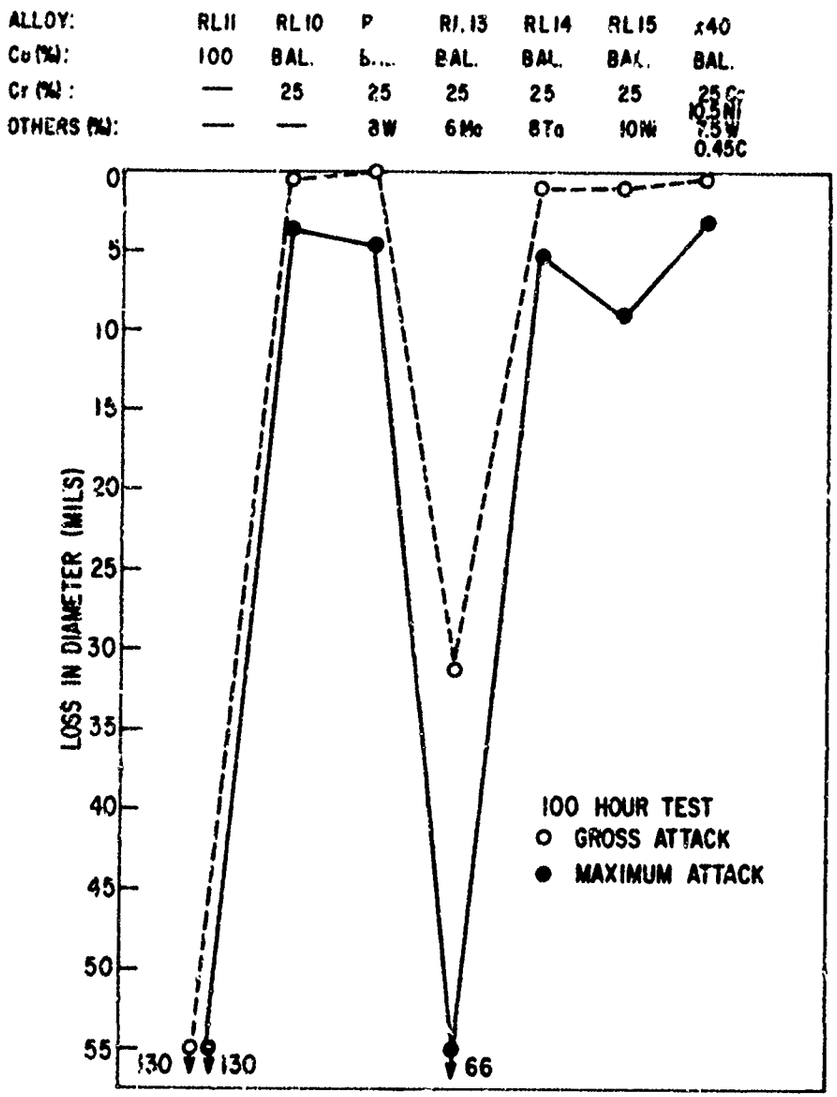

Fig. 8 Hot corrosion data for cobalt alloys--1750°F.

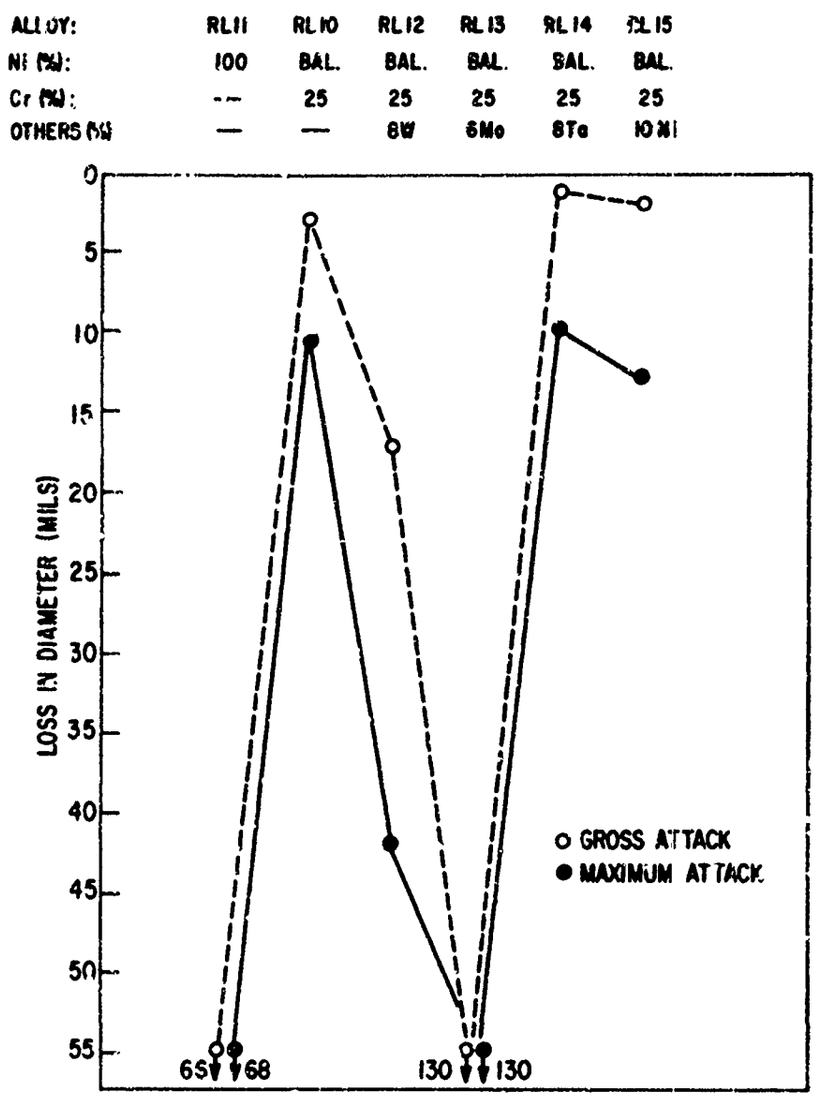

Fig. 9 Hot corrosion data for cobalt alloys--1900°F.

Fig. 10 (RL-1, 1675°F) This microstructure contains considerable amounts of the nickel-nickel sulfide eutectic (light gray). The lighter areas are probably nickel.
Unetched, 250X

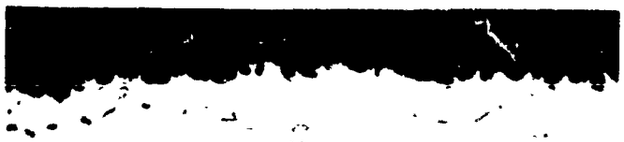

Fig. 11 (RL-3, 1675°F) The subsurface phase is the chromium-rich sulfide. Unetched, 250X

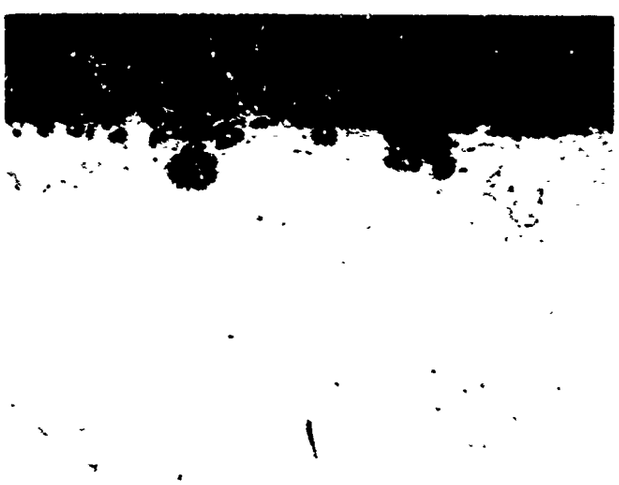

Fig. 12 (RL-5, 1675°F) Note the unusual shape of the oxides (dark gray).
Unetched, 250X

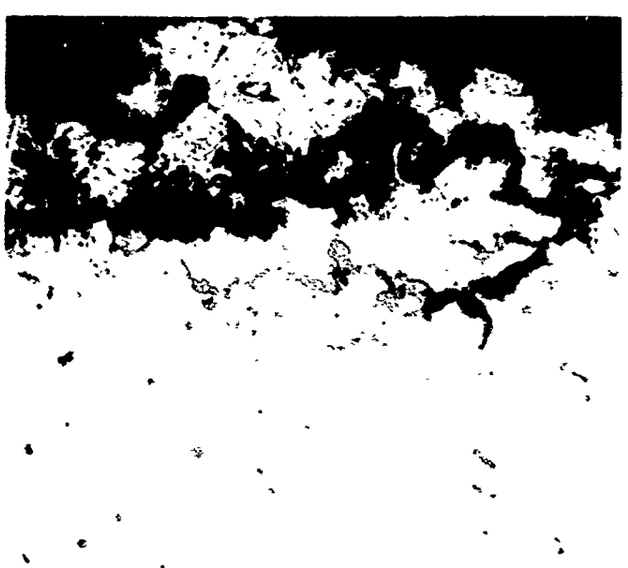

Fig. 13 (SEL, 1675°F) The microstructure shows a large amount of internal oxidation and medium size chromium-rich sulfides (medium gray). Unetched, 250X

Fig. 14 (RL-2, 1750°F) This microstructure has numerous chromium-rich sulfides, including some large ones. Unetched, 250X

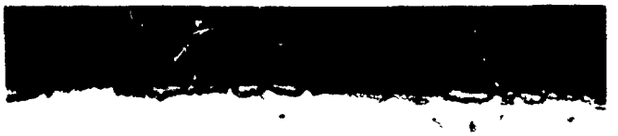

Fig. 15 (RL-3, 1750°F) Note the stringers of long and narrow chromium-rich sulfides (medium gray). Unetched, 250X

Fig. 16 (RL-5, 1750°F) This is an oxide blister with numerous small chromium-rich sulfides in adjacent areas. Unetched, 250X

Fig. 17 (RL-7, 1750°F) The microstructure shows a massive oxidation and small subsurface chromium-rich sulfides. Unetched, 250X

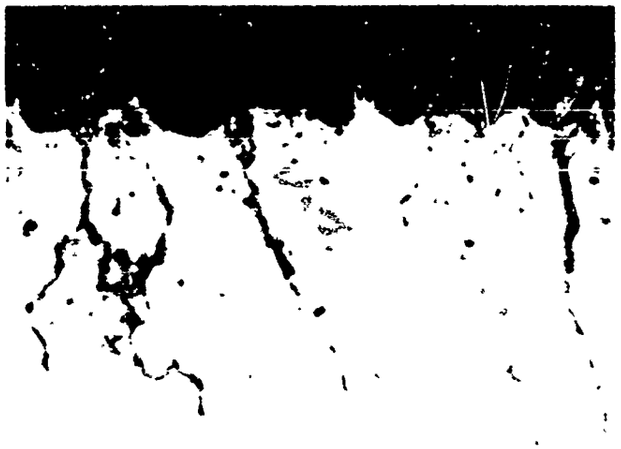

Fig. 18 (RL-8, 1750°F) The subsurface constituents are oxides (dark gray) and chromium-rich sulfides (medium gray). Unetched, 250X

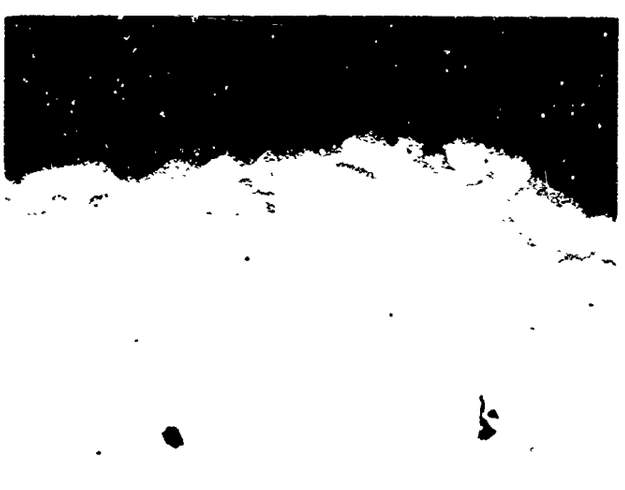

Fig. 19 (RL-9, 1750°F) The medium gray areas are chromium-rich sulfides. Unetched, 250X

Fig. 20 (RL-9, 1750°F) A massive oxidation attack with no visible subsurface phases. Unetched, 250X

Fig. 21 (RL-1, 1900°F) The microstructure is predominantly nickel-nickel sulfide eutectic. The large outlined area is probably nickel. Etchant: glycerine, nitric, acetic. 500X

Fig. 22 (RL-2, 1900°F) There are some oxides (dark gray) and chromium-rich sulfides (medium gray). Between the large chromium-rich sulfide and the oxides there is a stringer of the chromium-rich sulfides and nickel-nickel sulfide eutectic (light gray). Unetched, 250X

(RL-3, 1900°F)

(RL-5, 1900°F)

Figs. 23 and 24 Note the localized penetration of the small chromium-rich sulfides (medium gray). Unetched, 250X

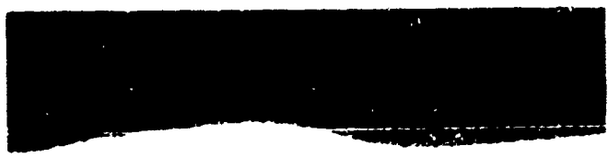

Fig. 25 (RL-7, 1900°F) There is a surface oxidation with no visible subsurface phases. Unetched, 250X

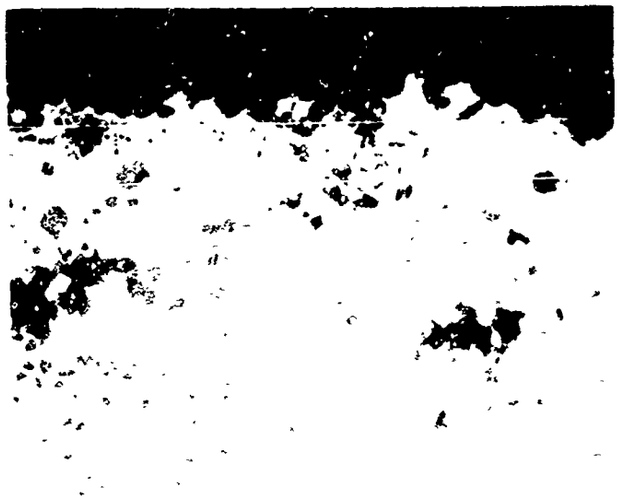

Fig. 26 (RL-8, 1900°F) A dense concentration of chromium-rich sulfides (medium gray). Unetched, 250X

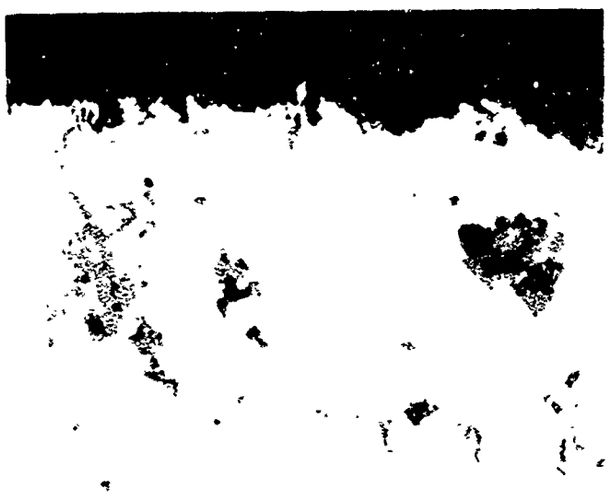

Fig. 27 (RL-8, 1900°F) Two large areas of an unidentified subsurface angular phase (medium gray). Unetched, 250X

Fig. 28 (RL-9, 1900°F) There is a zone of small chromium-rich sulfides near the bottom of the photomicrograph. Close to the surface there are large chromium-rich sulfides surrounded by the nickel-nickel sulfide eutectic (light gray). Unetched, 250X

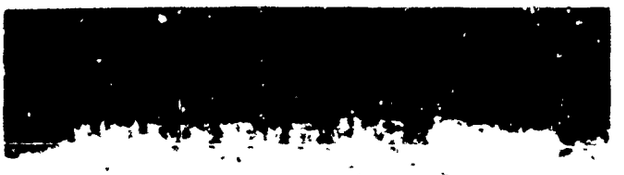

Fig. 29 (RL-10, 1675°F) Small subsurface chromium-rich sulfides. Unetched, 250X

Fig. 30 (RL-11, 1750°F) Microstructure shows an oxide and a constituent that most likely is the cobalt-cobalt sulfide eutectic. Unetched, 250X

Fig. 31 (RL-13, 1750°F) A very fine subsurface network of oxides and chromium-rich sulfides. Unetched, 250X

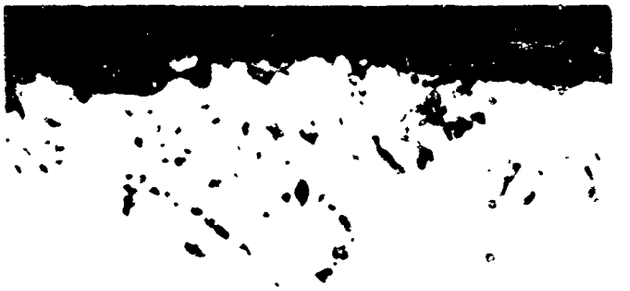

Fig. 32 (RL-15, 1750°F) Subsurface oxides (dark gray) and chromium-rich sulfides (medium gray). Unetched, 250X

Fig. 33 (RL-10, 1900°F) The small subsurface phases are the subsurface chromium-rich sulfides. Unetched, 250X

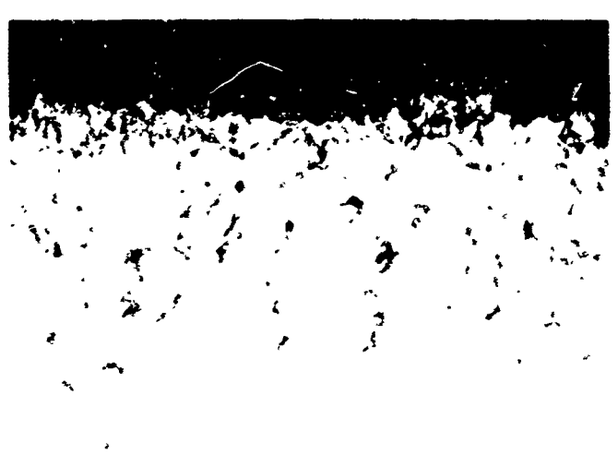

Fig. 34 (RL-14, 1900°F) This microstructure has small subsurface oxides (dark gray) and chromium-rich sulfides (medium gray). Unetched, 250X